# A Direct-Write Thick-Film Lithography Process for Multi-Parameter Control of Tooling in Continuous Roll-to-Roll Microcontact Printing



by

Larissa F. Nietner

B. Eng. Mechanical Engineering
HTWG Konstanz, 2012

Submitted to the Department of Mechanical Engineering
in partial fulfillment of the requirements for the degree of

Master of Science

at the

MASSACHUSETTS INSTITUTE OF TECHNOLOGY

June 2014



Signature redacted

Author.....
Department of Mechanical Engineering
May 20, 2014

Signature redacted

Certified by.....
David E. Hardt
Ralph E. and Eloise F. Cross Professor of Mechanical Engineering
Thesis Supervisor

Signature redacted

Accepted by.....
David E. Hardt
Ralph E. and Eloise F. Cross Professor of Mechanical Engineering
Graduate Officer

# A Direct-Write Thick-Film Lithography Process for Multi-Parameter Control of Tooling in Continuous Roll-to-Roll Microcontact Printing

by

Larissa F. Nietner

Submitted to the Department of Mechanical Engineering
on May 20, 2014, in partial fulfillment of the
requirements for the degree of
Master of Science

# ABSTRACT

Roll-to-roll (R2R) microcontact printing (μCP) aims to transform micron-precision soft lithography in a continuous, large-scale, high-throughput process for large-area surface patterning, flexible electronics and engineered meta-surfaces. Efforts to implement this hybrid process have been limited by the inability to monitor and control the process and the lack of a continuous large-area polymer tool that embodies micron- to nano-scale patterns currently created with wafer-based lithography. Discontinuities arising from a wrapped image carrier, size limitations from silicon wafer sizes, difficulty in achieving uniform stamp thickness, and inability to monitor the contact region, pose challenges in scaling up μCP to R2R processing.

This work examines a new technique to produce seamless cylindrical tools for soft lithography using laser-based maskless lithography for micro-patterning. The process is parameterized and modeled to fabricate novel tooling structurally optimized for microcontact patterning. Positive-tone photoresists SPR 220 and AZ 9260 are examined in their process sensitivity and in their ability to provide tools for scalable μCP.

A fluorescent contact imaging technique is presented on the basis of fluorescent, layered composite PDMS image carriers. By adding fluorescent microparticles to PDMS, the stamp is shown to re-emit UV upon contact with the substrate.

To scale the process for use in large-area applications, a machine design is suggested for a scalable implementation of the examined technique, which has the potential to provide large-scale microstructured tools and thereby facilitate process control and enable scale-up of microcontact printing.

Thesis Supervisor: David E. Hardt
Title: Ralph E. and Eloise F. Cross Professor of Mechanical Engineering

# Acknowledgements

The work in this thesis would not have been possible without the invaluable advice, help, and support of several individuals:

Thank you to Prof. David Hardt for your guidance, support, inspiration, advice, and stirring curiosity.

Thank you to Scott Nill, who has been such a valuable colleague and friend throughout our research. So many of the ideas that went into this project would not have emerged without your help, inspiration, knowledge, enthusiasm and patience. Thank you to Adam Libert for your help and for your hands-on, questioning and undaunted spirit. Thank you, Marcel Thomas and Maia Bageant, for your help and advice on this project. Thank you Joseph Petrzelka and Melinda Hale for the phenomenal achievements and contributions to our lab. Thank you, Paul Tierney, for your support in exploring photolithography. Thank you, Lynne Wilson, for your advice. Thank you to all the graduate students in office 35-135 for the good company, inspiration and support.

Thank you, Birgit Schlaich and Chris Hembry, for being such a good friend for so many years, and for inspiring me to come to MIT. And thank you to my family for your encouragement in spite of the distance. And, particularly, to my brother Alexander – a wise mind.

Thank you especially to all colleagues at KFUPM. It has been a pleasure to collaborate with you through the Center for Clean Water and Clean Energy, and meeting in Saudi Arabia was a wonderful experience.

# Contents

Appendix

# Figures

# Tables

# Chapter 1

# Introduction

Microcontact printing was developed in the early 1990's by Whitesides and Kumar at Harvard University [1]. In this embodiment of the process, polydimethylsiloxane (PDMS) resin is poured over a master template wafer that was patterned using a conventional lithographic process. The cured PDMS stamp is peeled back from the master and inked with alkanethiols. The inked stamp is brought into contact with a gold film substrate, and the alkanethiols transfer to the substrate where contact is made, in a pattern replicate of the master wafer template. These alkanethiols form a self-assembling monolayer (SAM) on the surface of the gold film, which is then used as a resist in a wet etching process. This process was able to reproduce patterns with features as small as 1 μm, and within a year of these results, Whitesides was able to pattern features down to 200 nm in size [2], though with limited feature fidelity. The process was further developed by Biebuyck et al. to reliably cast and print geometry with features below 100 nm [3]. A review of microcontact printing achievements and limitations is available [4], [5].

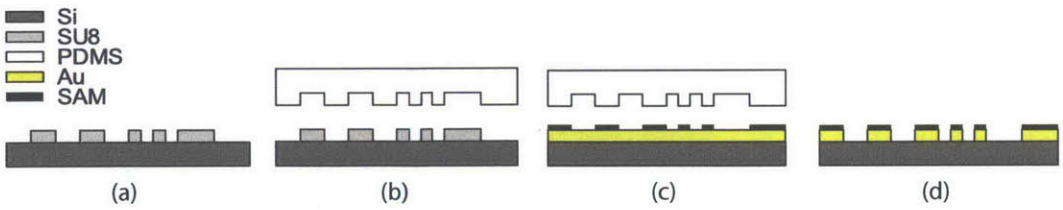


**Figure 1.1: Traditional plate-to-plate microcontact printing process. (a) A master template is formed with conventional lithographic techniques. Typically, this is formed as a pattern of SU-8 photoresist on a silicon wafer. (b) PDMS resin is cast onto the master template. Once cured, it is peeled from the template and shown to have reproduced the template's features. (c) The PDMS stamp is inked with alkanethiols, and brought into contact momentarily with a gold-coated wafer substrate. These molecules diffuse onto the gold surface and self-assemble into monolayer. (d) The SAM acts as a protective mask for when the substrate is etched, leaving just the desired pattern of gold remaining.**

## 1.1 Inks

The purpose of microcontact printing is to reproduce a master pattern on a substrate. A patterned stamp is used to deposit ink onto the substrate where contact is made. Because the printing relies on ink transfer from the stamp to the substrate, the process is highly dependent on characteristics of the stamp, the ink, and the substrate. Compatibility between all three materials is crucial for successful printing.

### 1.1.1 Molecular Inks

Microcontact printing is most commonly performed with self-assembling monolayer (SAM) inks. A self-assembling monolayer is an organized assembly of molecules that form on a surface via adsorption. These single-molecule-thick layers occur when the organic molecules contain a functional head group that has a particular affinity for the target surface. These head groups cause the molecules to self organize and anchor themselves in a single monolayer structured domain on the surface. The head group has an attached molecular chain that forms a tail, with a functional group at the end. These tails also neatly self-organize, protruding from the surface, and the functional groups at their ends can be changed to vary the interfacial properties of the monolayer. The organization of such a layer is depicted in Figure 1.2.

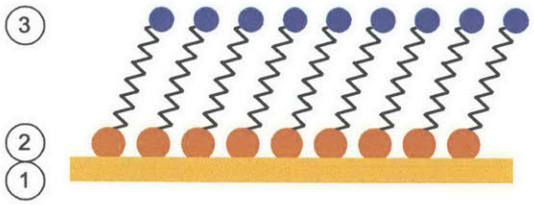


**Figure 1.2: Simplistic representation of SAMs on a gold substrate. Typically, alkanethiols are used in microcontact printing, due to the molecule's head group (2) showing a strong affinity for gold substrates (1). The tails (3) are functionalized to protect the gold substrate from an etching bath, resulting in a selectively etched patterned surface.**

Alkanethiols are specific molecules commonly used to form SAMs. When brought into contact with gold substrates, alkanethiols self-organize into a protective monolayer that can be used to protect the gold from wet etchants. Typically, a PDMS stamp is wetted with a solution of alkanethiols in ethanol or other solvent. This stamp is allowed to dry before being brought

into contact with the substrate, during which time the alkanethiols transfer via a diffusion process. This means that, in most cases, the alkanethiols are deposited only where contact is made between the stamp and the substrate. Once the alkanethiols are on the gold surface, they self-assemble into a monolayer within minutes [6].

The alkanethiols have been shown to quickly transfer to the substrate and reproduce patterns accurately with a stamp contact time of only 1 ms [7]. This is one of the benefits of using SAMs in microcontact printing, as the short requisite contact time allows for high speed printing. Alkanethiols are a molecular ink that transfers via diffusion; there are no fluid dynamics effects that need to be considered. Finally, as alkanethiols diffuse through PDMS, a saturated stamp may allow for multiple prints before having to be re-inked [8]. For these reasons, alkanethiols have become commonly used in the process of microcontact printing on gold substrates.

There are a variety of other molecules that form SAMs on specific substrates, which hold potential for scaling up microcontact printing. Geissler et al. demonstrate eicosanethiols have a similar affinity to alkanethiols for gold, silver, copper, and palladium surfaces [9]. This was used to print metal nanowires on a 1 μm pitch. Lopez and Craighead manufacture surface-relief gratings on a 300 nm pitch via microcontact printing of octadecanethiols onto gold [10]. Delamarche et al. print hexadecnethiols onto copper films in order to achieve a selective etchant mask for TFT LCD gate layers [11]. Jeon and Nuzzo selectively deposit copper onto various substrates using chemical vapor deposition with printed alkylsiloxanes as the SAM mask [12]. These molecules were shown to assemble on substrates of aluminum, silicon, titanium nitride, and their oxides. Glasses, indium tin oxide (ITO), and plasma-modified polymide substrates are patterned with the same process. Octadecyltrichlorosilane is shown to assemble on ITO coated glass, which was used in a process to make OLEDs [13]. Hexadecanephosphonic acid [9] and alkanephosphonic [14], [15] acids are shown to form SAMs on aluminum and aluminum oxide surfaces. This is significant because it might allow for the printing of SAMs onto aluminized PET film substrate in a roll-to-roll microcontact process, rather than having to use alkanethiols on expensive gold film substrate. This aluminum-coated film is made via physical vapor deposition, and is commonly used in a variety of industries.

More information on SAMs and their use in microcontact printing is found in the review paper [16].

### 1.1.2 Liquid Inks

Microcontact printing is also used to print liquid inks. Traditionally in the field of printed electronics, conductive substrates with printed SAM masks are selectively etched to form the desired conductive traces. Instead, conductive liquid inks are directly printed onto non-conductive substrates in the desired trace pattern as shown in Figure 1.3. In the printed electronics industry, PET films have emerged as a common substrate due to their low cost, high clarity, and ease of handling. The use of liquid inks allows for numerous other materials to be used as substrates in the microcontact printing process. Kaufmann and Ravoo provide a review of the use of polymer inks in microcontact printing, as well as a review of the use of polymer substrates in microcontact printing [17].

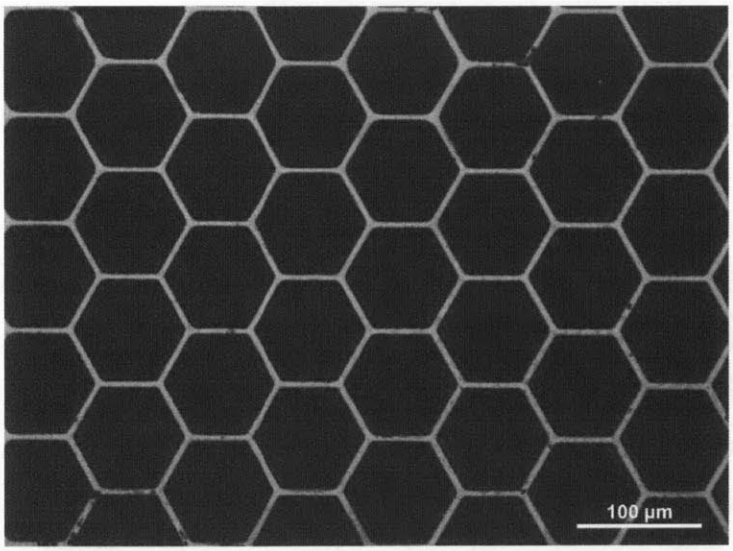


**Figure 1.3: Hale's microcontact printing of liquid ink onto polymer substrate [18].A PDMS stamp was used to transfer Cabot CSD-66 silver nanoparticle ink to a cyclic olefin copolymer substrate. The lines that form the hexagons are approximately 5 µm in width. Such a pattern is discussed in literature for its properties as a conductive grid with a high percentage of optical transmission, potentially useful in photovoltaic cells.**

The low surface energy of PDMS poses a challenge for wetting with most liquid inks. Therefore, the process of printing liquid inks with PDMS stamps is neither as well understood nor as robust as the SAM printing process. There are many important parameters, such as the surface energies of the stamp and the substrate, the composition of the ink, the inking

technique, the geometry of the features, etc. The variables and sensitivities of the liquid ink transfer process are studied in Hale's thesis work [18]. Figure 1.4 depicts some of the results from Hale's work. With a robust model for ink transfer at the micron scale, the direct printing of conductive patterns on polymer substrates could be scaled up into a high-rate manufacturing process.

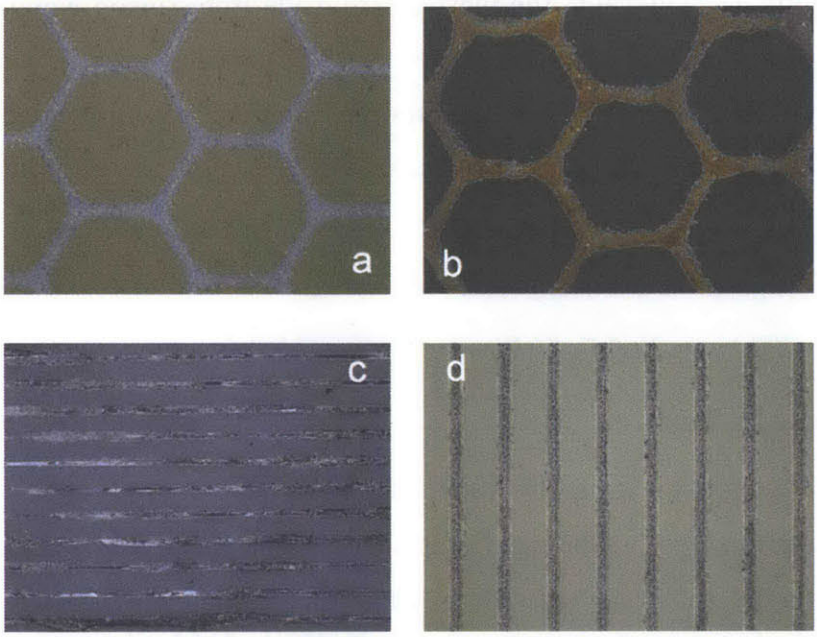


**Figure 1.4: Liquid inks are not as simple to print as SAMs.For example, some of the liquid inks used in Hale's thesis have tendencies to exhibit clumping, which negatively impacts printing results [18]. The Nanomas MES-40 ink used in (a)-(d) is made from 40% solids loading of silver nanoparticles in a mesitylene solvent. (a)-(b) 5 μm line width hex pattern. (c) 20 μm line width (d) 50 μm line width.**

## 1.2 PDMS Stamp Tooling

Typically, the stamps used in the microcontact printing process are cast out of polydimethylsiloxane, a silicon-based organic polymer. Commercially available Dow Corning Sylgard 184 PDMS is a thermoset silicone elastomer that is formed from the mixing of a base and a curing agent. The pre-cured fluid is poured onto a master pattern and is able to closely conform to its geometry. Typically, the masters are made from silicon wafers patterned with the negative of the desired geometry in a conventional lithography process. Drawing a vacuum on this casting helps to degas the liquid and improve results in casting smaller features. As this liquid cures into a solid, the cross-linking process does not cause any significant shrinkage or distortion. These characteristics enable the high fidelity replication of complex geometry with sub-micron features.

### 1.2.1 Conformal Contact

PDMS is also a good material for stamps for microcontact printing because of its ability to make complete contact with substrates with surface asperities. Because SAMs only transfer from the stamp to the substrate where contact is made, complete contact is necessary for reliable feature replication. Petrzelka refers to the ability of a stamp to completely conform to a surface, even over small asperities, as *conformal contact* [19]. Figure 1.5 illustrates this phenomenon. The characteristic of PDMS that makes it good for conformal contact is its high ratio of surface energy to elastic modulus. This ratio is defined as the material radius of curvature [20] which, for PDMS, is on the order of 10 nm. The significant surface energy of PDMS allows the stamp to conform around asperities on this scale, enabling PDMS stamps to make conformal contact with substrates that have a surface roughness of less than 10 nm.

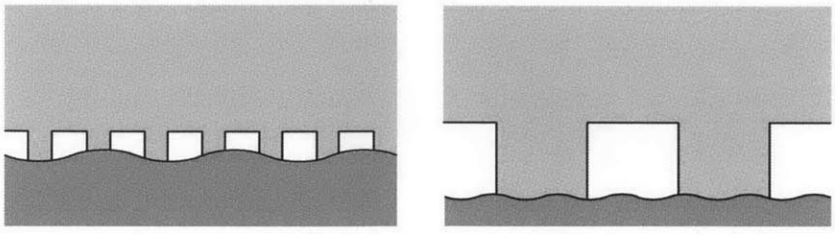

**Figure 1.5: Conformal contact is achieved when the stamp conforms to surface asperities of the substrate [19].**

Though PDMS has several characteristics that make it a good material to use as a stamp, it also has a variety of traits that are problematic. The high ratio of surface energy to elastic modulus can cause elastic collapse, where features spontaneously adhere to each other as shown in Figure 1.6. This effect is pronounced in features closely spaced or with large aspect ratios. PDMS is a soft elastomer, making it very sensitive to contact stresses and allowing it to easily deform. Finally, PDMS is prone to swelling when exposed to organic solvents [21]. This limits material compatibility to select inks and can cause large area deformations that decrease absolute accuracy.

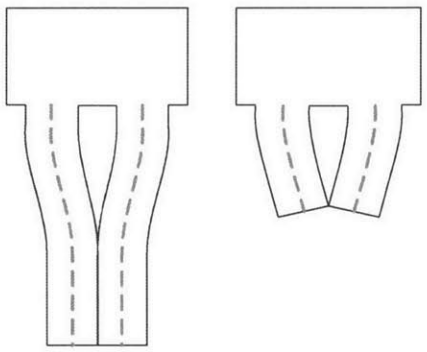

**Figure 1.6: Petrzelka discusses two types of lateral collapse.The high surface energy of the PDMS stamp causes neighboring features to stick to each other [19].**

### 1.2.2 Tool-Related Defects

The success of the microcontact printing process is contingent on the complete and conformal contact of the stamp with the substrate. This requires a great enough print pressure to ensure that there are no gaps between the stamp and the substrate. However, too great a print pressure will lead to stamp defects that can significantly affect the integrity of the transferred pattern. Examples of defects introduced by excessive print pressure include roof collapse, where the roof of the stamp between features bulges outward to make contact with the substrate, and feature buckling, wherein features with large aspect ratios buckle under load. These examples are illustrated in Figure 1.7. Other potential printing defects include sidewall collapse, wherein the sidewalls of the features bulge significantly, and lateral collapse, wherein closely packed features stick to each other due to the large surface energy of PDMS.

Figure 1.16 demonstrates how these modes of stamp deformation can impact the produced product.

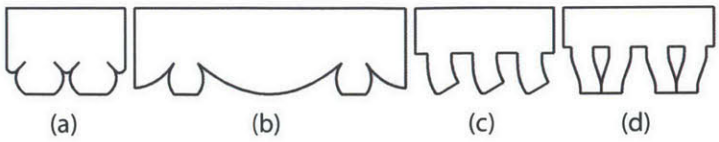


**Figure 1.7: Petrzelka discusses four prominent failure modes of fragile PDMS stamps. (a) bulging features and sidewall collapse (b) roof collapse in sparsely patterned areas (c) buckling of features (d) lateral collapse due to the high surface energy of PDMS [19].**

There have been many approaches to describing the stability of PDMS stamp features [22], [23]. Sharp et al. investigate the theory behind these printing defects and form models that help to guide the stamp design process [24]. Due to the high surface energy and low stiffness of PDMS, microcontact printing stamps are very sensitive to the influence of print pressure and thus often have very narrow process windows for complete conformal contact.

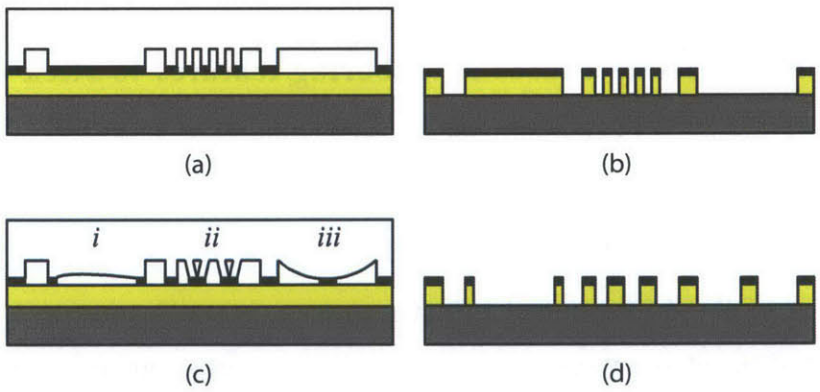


**Figure 1.8: An illustration of how the various failure modes of PDMS stamps can affect the printed results. (a) A stamp in conformal contact without any significant defects (b) A high-fidelity replication of the intended pattern (c) A stamp showing three significant failure modes: (i) air trapping (ii) lateral collapse (iii) roof collapse (d) The printed result from the poor stamp contact is significantly different than the master pattern [19].**

To increase the robustness of the process to these failure modes, materials stiffer than standard PDMS have been used to form the stamp. Schmid and Michel demonstrated the use of a special formulation of hard PDMS that was about four times stiffer than the regular formation, but at the expense of being more brittle [25]. A UV curable hard PDMS formulation

by Rogers allowed for quicker curing times and alleviated thermal shrinkage issues that result from the usual thermal cure process for regular PDMS [26].

The original microcontact printing process by Whitesides experimented with using standard photolithographic plate material, but these were relatively imprecise and only able to pattern features down to 200 μm [1]. Finally, the potential for using block polymer elastomers as microcontact printing stamps was investigated by Trimbach et. al. [27]. These stiff thermoplastics are formed using a hot-embossing process that requires high temperatures and pressures, but can handle 10-15 times the load of traditional PDMS stamps before structural collapse occurs. These stiffer stamps are more robust to structural failure, but they have not been widely adopted in microcontact printing because their high stiffness also results in a decreased ability to achieve conformal contact.

## 1.3 Continuous Tools for Scaling up μCP

Traditionally, tools for microcontact printing are planar. This poses a challenge when scaling up the process to a continuous, roll-based technology. Wrapped stamps have been explored. A novel technique demonstrated the fabrication of seamless PDMS stamps with micron-scale resolution.

### 1.3.1 Flat Stamps

Microcontact printing has traditionally been a plate-to-plate process. In this method, the PDMS stamp is cast from a planar, featured silicon wafer as is seen in Figure 1.9. This plate stamp is then inked and brought into contact with a flat substrate, transferring the ink to that surface as shown in Figure 1.10. Though it has been able to reproduce patterns with great fidelity even at feature sizes of less than 100nm, this plate-to-plate process is inherently limited and does not allow for printing areas larger than the master wafer. A continuous process must be developed to replace this existing method of batch processing to allow microcontact printing to scale to large areas and high rates.

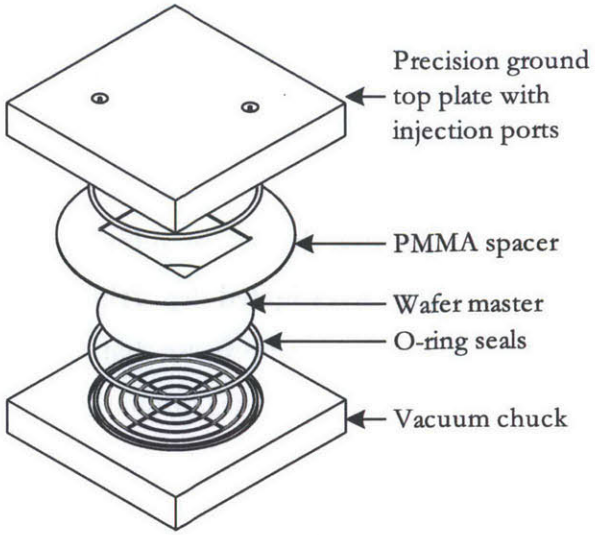


Figure 1.9: The mold created by Petrzelka to cast planar PDMS stamps from patterned master wafers [19].These stamps were used in a plate-to-plate printing setup. As well, some of the stamps formed this way were wrapped around a print roll for roll-to-plate microcontact printing.

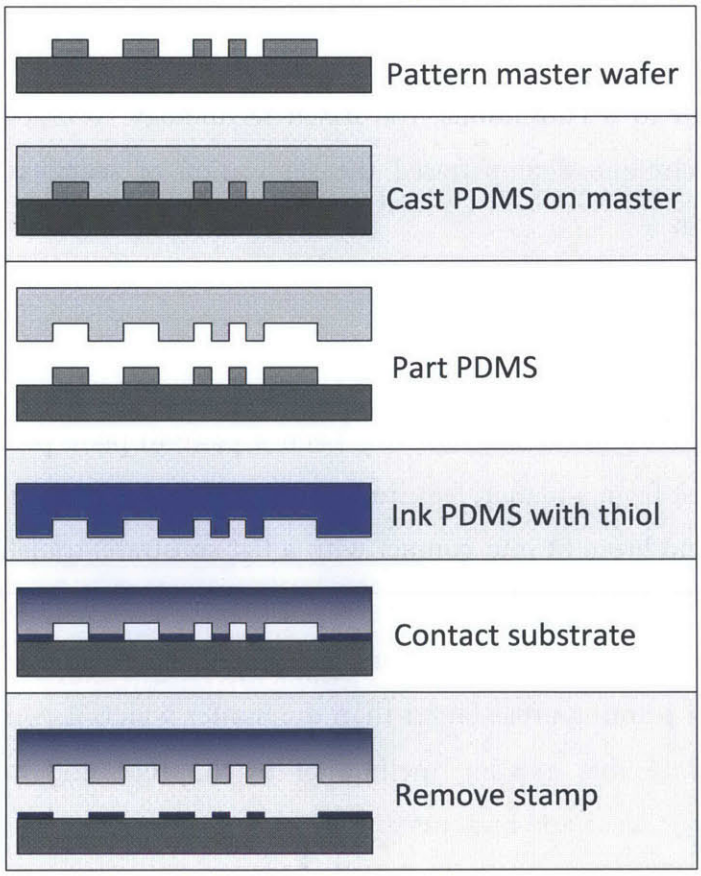


Figure 1.10: A summary of the traditional microcontact printing process [19].

An appropriate continuous manufacturing method to aspire to is roll-to-roll processing. These processes start with a large roll of a thin flexible material, often plastic film. This flexible substrate, called the web, is fed from roll to roll throughout the web-handling machine. Figure 1.11 depicts a large roll-to-roll process used for manufacturing newspapers. A web-handling machine can be designed to have one purpose, or it can have many sequential stations each serving their own purpose, before the finished substrate is finally sliced into sections, rolled up again, or passed on to the next step of manufacturing. The roll-to-roll web-handling method allows for a higher speed and more continuous process compared to the batch processing method, which normally involves a discrete number of sheets in each step of the process. Not only does this lend itself to greater efficiency and make roll-to-roll more economically favorable, but it also helps with improved process control because it has fewer start-stop transients.


**Figure 1.11: Roll-to-roll process on an industrial scale.The ultimate goal of this work is to determine how microcontact printing could be scaled up into a high-speed large-area roll-to-roll manufacturing process, as shown newspaper printing press.**

### 1.3.2 Wrapped Stamps

In order to bring microcontact printing to a roll-to-roll basis, the first challenge is to transform the tooling from flat to round. Xia et al. made the first steps in transferring to a round tool by simply wrapping a flat wafer-casted PDMS stamp around a hand-held roller as shown in Figure 1.12 [28]. Inking this roller with SAMs and rolling it over a flat wafer substrate showed that microcontact printing could be successfully achieved on a roll-to-plate basis. This was a necessary step on the way to continuous manufacturing, and it is requisite to replace the rigid plate substrate with a thin flexible web to make the full transition to a continuous roll-to-roll process.

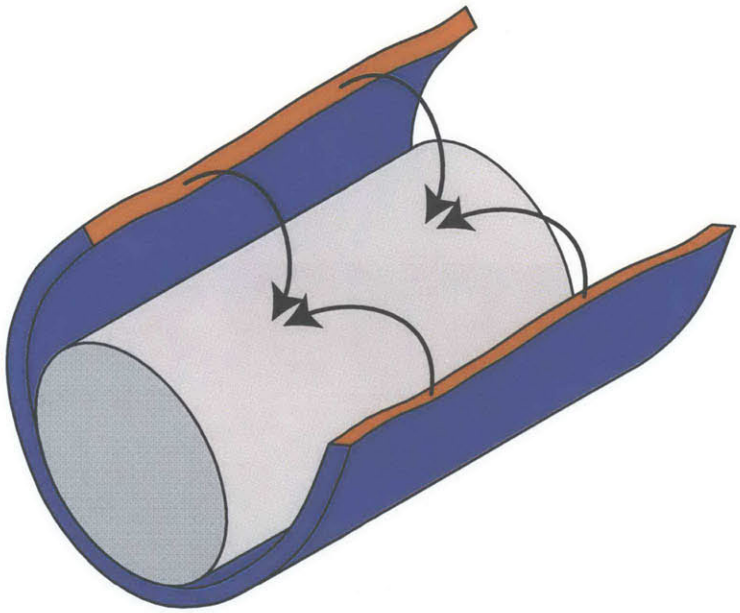

**Figure 1.12: A planar stamp is wrapped around a print roll to enable roll-to-plate microcontact printing. The stamp is often held in place simply by its large surface energy. For more permanent and precise adhesion, the use of cyanoacrylate glue has been demonstrated, and prior art has also plasma bounded PDMS stamps to glass cylinders, as in [29].**

Rogers et al. proposed a process in which a flat PDMS stamp is plasma-bonded to a glass cylinder and printed on a flexible substrate [29], [30]. The Rogers group then worked on porting microcontact stamp-making techniques to a flexographic printing setting by investigating the fabrication of large area stamps [31]. Flat 12" by 12" PDMS stamps were cast with a Mylar backing on a patterned surface, and demonstrated to be able to print features down to 1 μm. These stamps were proposed for printing on flexographic presses with flexible

substrates at high speeds. The marriage of microcontact printing and flexography was referred to as microflexography. However, this printing technique was never tested.

Roll-to-plate and roll-to-roll microcontact printing processes require a cylindrical stamp for the print roll. Machines in the literature use a flat-cast stamp that is then wrapped around a cylinder [28], [29], [31]–[33]. These stamps are typically cast from patterned silicon wafers and then cut down into a rectangle before being mounted on a roll, to give a clean and prismatic stamp profile. However, wafer sizes are limited, so this process will not be able to scale. There are methods for casting larger area microcontact printing stamps [31], but these result in low absolute accuracy and have not been fully developed. In addition, any method that involves the wrapping of a flat-cast stamp around a cylinder will result in residual stress and persistent pattern deformation. Though a stamp can be cut to proper size for wrapping, there will always be a discontinuity at the seam, where the ends of the stamp meet. Such a seam is shown in Figure 1.13. This seam will result in a significant once-per-revolution disturbance that might preclude any reliable printing of micron-sized features. Finally, the stamp accuracy can only be as good as the mounting process. None of the available mounting processes will be sufficiently accurate for mounting of large stamps without causing any pattern distortions or thickness variations.

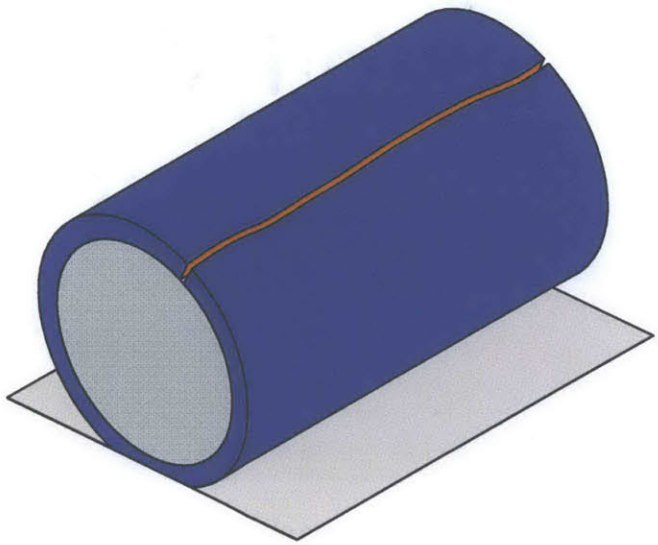

**Figure 1.13: Roll-to-plate microcontact printing has traditionally been accomplished with planar stamps that are wrapped around a print roll. This technique will invariably present a gap or seam where the two ends of the wrapped stamp meet (orange). Such a seam results in a once-per-revolution impulse disturbance to the system, often orders of magnitude greater than the height of the stamp features.**

### 1.3.3 Cylindrical Stamps

A key enabling technology necessary to achieve precision roll-to-roll microcontact printing is the ability to cast a continuous cylindrical stamp and accurately mount it onto a roll. Petrzelka developed a centrifugal casting machine that allows for the casting of continuous cylindrical stamps [19] to address this challenge. These stamps are cast on the inside of a rotating cylinder onto a layer of photoresist that has been patterned by a laser in a direct-write process. These cylindrical stamps have no seam and little feature distortion. The equipment required for and the result of this casting process are both illustrated in Figure 1.14. Not constrained in scale or cost by silicon wafers, yet capable of achieving patterns on the scale of micrometers, this technique has the potential to provide continuous, scalable tools for microcontact printing. This vision was the inspiration for this thesis.

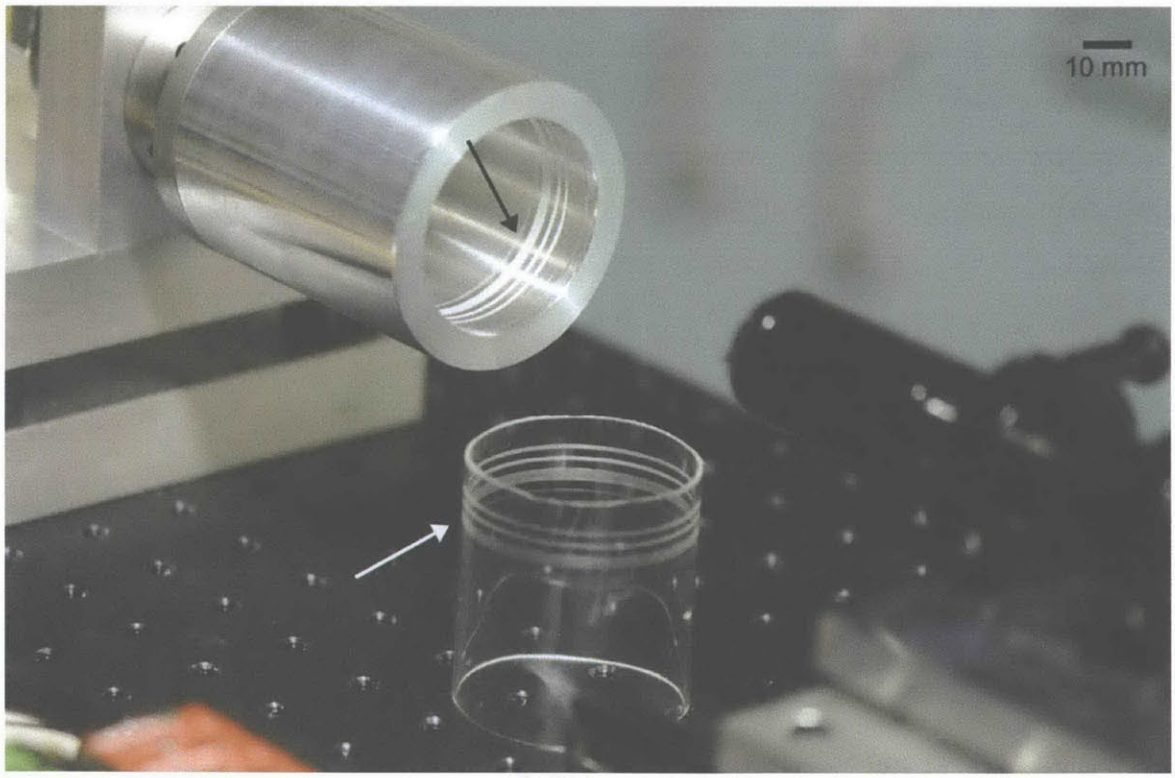


**Figure 1.14: The centrifugal casting machine designed by Petrzelka, and a cylindrically cast stamp [19]. This machine uses a laser to pattern a thin layer of photoresist on the inside of a rotating drum. PDMS resin is then poured into the spinning drum, and the centrifugal force causes the resin to evenly spread throughout the interior surface of the drum. Once the resin is cured, the cylinder is stopped and the stamp is removed. Note the seamless nature of this stamp, and the ability it affords for continuous printing.**

Because the PDMS is so sticky and difficult to slide onto a roll, a special bushing was developed to provide an air cushion for the stamp to slide on over the surface of the roll. When the stamp is in place, the air supply is cut off and the stamp collapses onto the roll as the fluid film dissipates. The bushing is removed from the roll, leaving just the cylindrical stamp mounted in a stress-free state, but fixed in place by the large work of adhesion. A demonstration of this mounting technique is displayed in Figure 1.15.

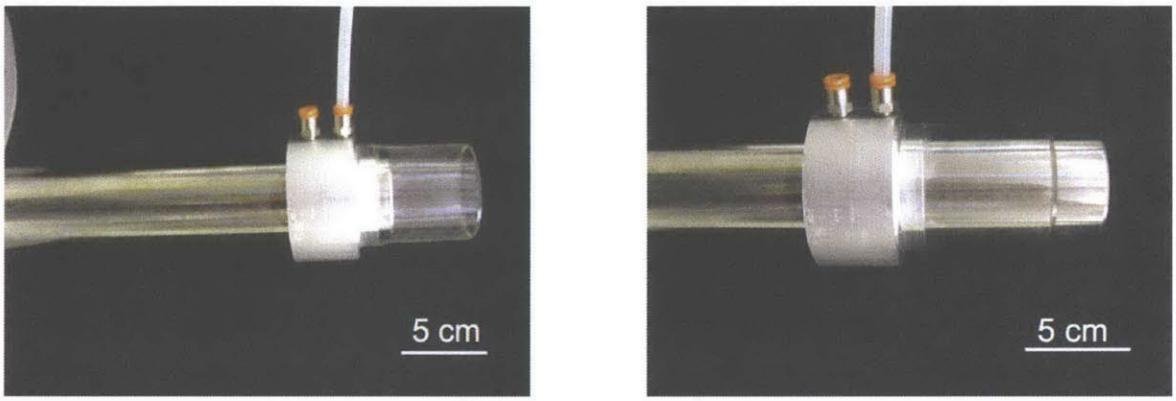


**Figure 1.15: The air bushing designed by Petrzelka to enable mounting of cylindrical stamps on metal rolls [19]. Because of the high surface energy of PDMS, it is too sticky to slide over a metal roll without assistance. This device forms a thin air film cushion between the stamp and the roll, allowing the stamp to be easily slid into place. When the air supply is turned off, the air film collapses and the stamp evenly contracts onto the surface of the roll.**

## 1.4 Roll-Based μCP Processes

To scale microcontact printing into a large-area high-rate manufacturing process, a reliable and repeatable roll-to-roll process must be developed. Three stages are necessary for the scale-up of the microcontact printing process: plate-to-plate, roll-to-plate, and roll-to-roll.

In a roll-based-process, only a fraction of the stamp is engaged with the substrate at any time, and the elasticity of this fraction varies periodically with the rotation of the tool. Various disturbances play a much greater role in the process when increasing the speed.

Consistent quality printing results can be achieved by integrating precision designed and controllable elements into the printing machine. Precision printing machines have been

designed to control and actuate the tool in such a way that defects are reduced. These machines, especially in the manufacturing setting, must allow for the precise control of contact pressure in the print region.

Kendale developed an automated plate-to-plate printing machine, a schematic of which is drawn in Figure 1.16, that used precision actuation of a hard-backed stamp to print onto silicon wafers [34]. By controlling the displacement and special orientation of the stamp plane, it is possible to control the deformation of the stamp features. Similarly, Burgin et al. built a contact aligner that enabled the careful control of the forces exerted on the substrate during the printing process [35]. This printing machine enabled the printing of sub-micron features and suggested that a similar design would work even for larger scale plate-to-plate machines.

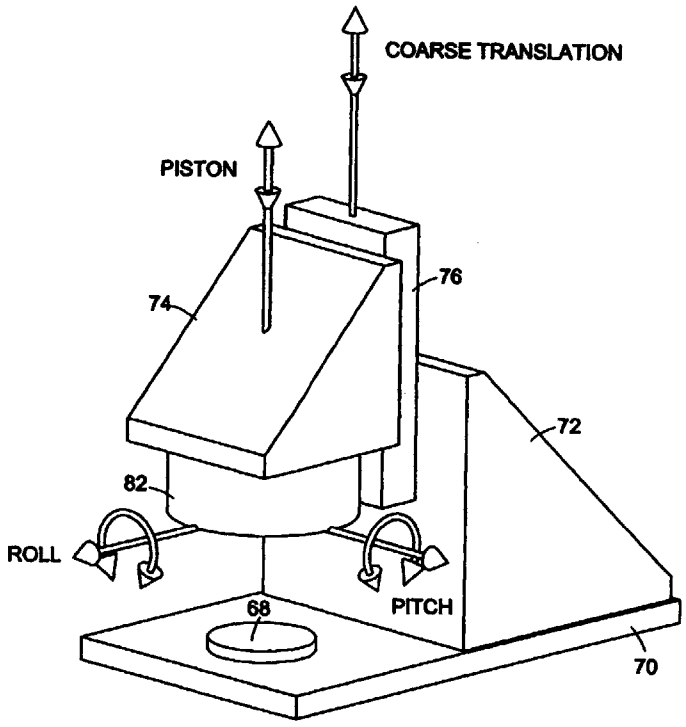


**Figure 1.16: An illustration from the U.S. Patent filing of Kendale's planar microcontact printing machine [36], [37]. This machine precisely controls the roll, pitch, and height of the stamp to enable precise plate-to-plate printing. Though this form of displacement control might work for smaller wafers, it cannot be scaled up to a large area or continuous process.**

Petrzelka built a precision roll-to-plate microcontact printing machine, depicted in Figure 1.17, that enabled control of either the displacement or force boundary conditions on the stamp [36]. This printing process is quite different from plate-to-plate printing, as there is

only a narrow region of stamp-substrate contact at any time. This contact propagates as the stamp is rolled over the substrate. Petrzelka's machine showed that the precise control over the contact forces was a key element to controlling roll-based microcontact printing, and that in-situ inspection of the print region could be a robust form of real-time process control. This precision roll-to-plate printing machine validated the potential for successful roll-to-roll printing.

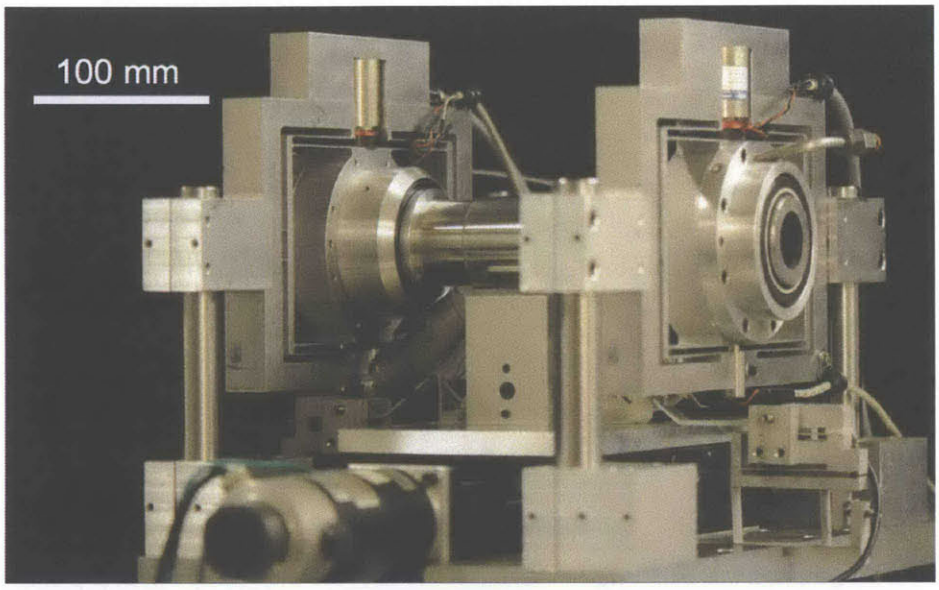


**Figure 1.17: The roll-to-plate microcontact printing machine developed by Petrzelka [19]. This machine utilized parallel kinematic flexure stages to give control over the height and tilt of the print roll. A linear positioning stage below the print roll was designed to carry a wafer or glass microscope slide substrate. An optical prism could be mounted on the linear positioning stage, allowing for real-time in-situ visualization of the contact region between the round stamp and flat substrate.**

To investigate the feasibility of roll-to-roll microcontact printing, Stagnaro developed a web-handling machine for the continuous printing of alkanethiols on gold foil [32], depicted in Figure 1.18. This pilot-scale machine was possibly the first to combine the material system and printing methods of microcontact printing with the roll-based processing techniques used in the manufacturing industry. It demonstrated the successful printing of etch-resistant SAM patterns with 10 μm features at speeds of up to 400 feet per minute. These results show the potential for high speed roll-based microcontact printing. However, the machine was limited in its ability to control force at the contact region. The print force was indirectly controlled by

manually adjusting micrometer heads, which compressed a compliant layer of foam on the impression roll against the print head. This gave little ability to control the contact between the stamp and the substrate, which would prevent this machine from being able to print more intricate and fragile patterns. The use of a planar casted stamp limited the repeatability of the printing, as the mounting process was dependent on the operator skill [33].

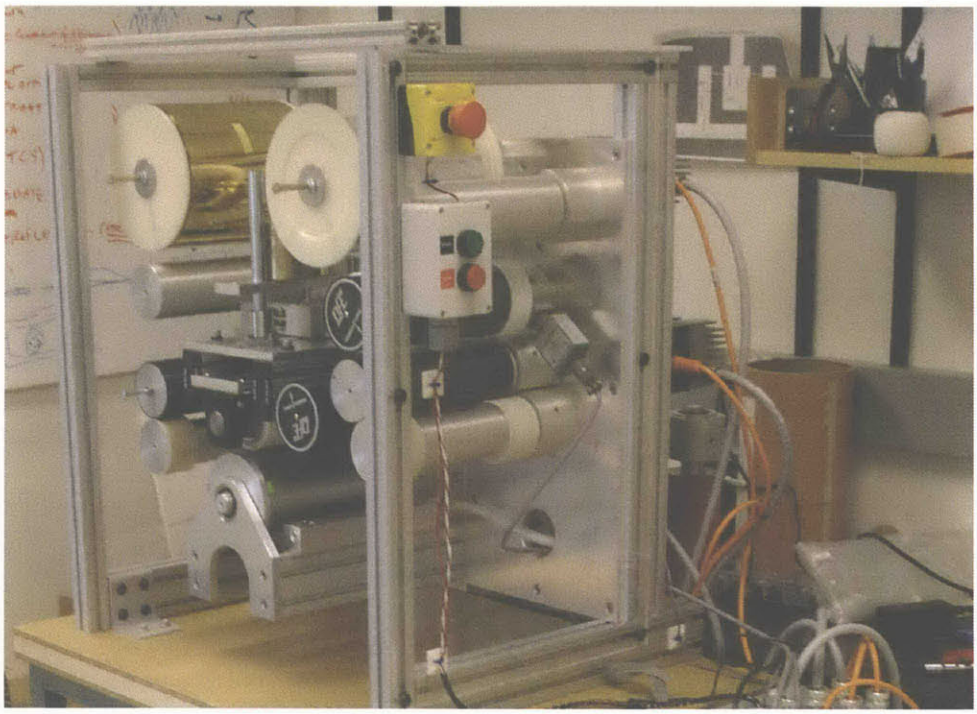

**Figure 1.18: The roll-to-roll microcontact printing machine developed by Stagnaro. This machine achieved successful pattern transfer at web speeds of up to 400 feet per minute, but also demonstrated the need for a precision print head and a continuous stamp.**

Baldesi continued work on this project and created a precision positionable print head for Stagnaro's roll-to-roll microcontact printing machine [38]. This print head was designed to have actuation in five axes, allowing for the precise setting of the print head location relative to the impression cylinder. However, the positioning was achieved through manual adjustment of micrometer heads. This design, shown in Figure 1.19, was an improvement over the original print head and allowed for the stage to be set in the proper location at the beginning of each print run. However, Baldesi concluded that automated actuators and a closed-loop controllable print head would be necessary for any further development of the process.

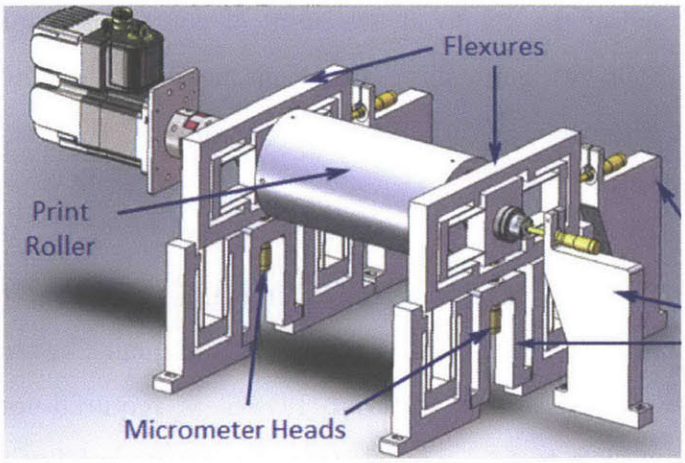


**Figure 1.19: The print head developed by Baldesi [38]. The print roll is supported by parallel flexure stages with micrometer positioning. This gave manual control over five degrees of freedom, but it was determined that an active closed-loop controllable print head would be necessary for future roll-to-roll microcontact printing machines.**

In the course of their work investigating the failure modes of PDMS stamps, Sharp et al. present methods for observing the stamp and the contact pattern during deformation using an inverted microscope shown in Figure 1.20 [24]. This laid the groundwork for directly observing stamp behavior in situ.

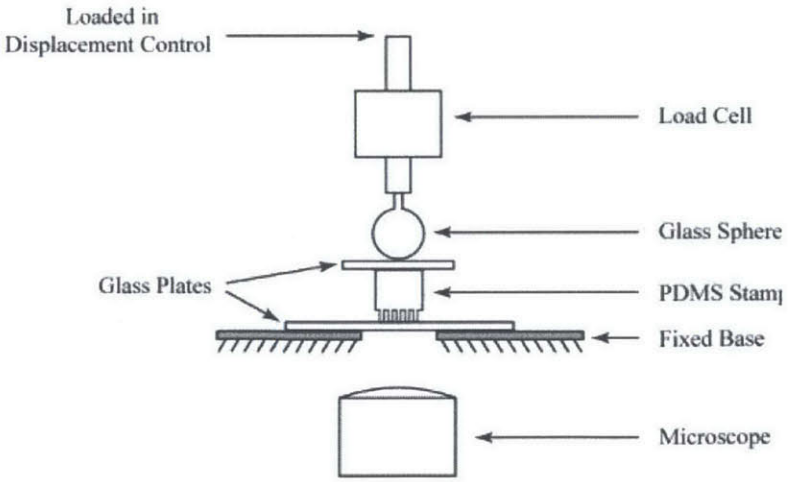


**Figure 1.20: Sharp et al. present a method of in situ observation of stamp deformation. The system utilizes an inverted microscope to view the contact. The stamp is placed pattern-side down and loaded through a glass sphere to permit coaxial illumination. Redrawn with permission from Effect of Stamp Deformation on the Quality of Microcontact Printing: Theory and Experiment. Sharp et al. Copyright 2004 American Chemical Society.**

The idea for imaging the stamp at the point of contact is employed by Petrzelka to evaluate different methods for controlling the print head in a roll-to-plate configuration. Furthermore, the work suggests that direct sensing and control of the contact may be a viable method for scalable process control.

In summary, roll-to-roll machines for microcontact printing bear great, untapped potential. Two critical parameters are stamp compliance and quality control.

The compliance of the stamp material, PDMS, is required for sufficient substrate contact, but it gives occasion to tool-related defects, such as bulging or buckling of stamp features. Herein lies the greatest challenge for the scale-up of microcontact printing. Since all efforts to actively actuate the print head through impedance control rely on a constant pattern fill factor and compliance to work with a constant print force, the scope of active print head actuation is inherently limited. Therefore, a method needs to be developed that allows for the provision of mechanically optimized stamps for roll-based microcontact printing.

Furthermore, to scale up microcontact printing, a method needs to be developed to inspect the result of the print, or the patterning process itself, in line.

## 1.5 Conclusion

Roll-to-roll microcontact printing seeks to scale up high-resolution microcontact printing, making it applicable to a wide range of large-scale patterning processes. To make this technology viable, tools need to be provided which are not only large enough to enable a high throughput, but also allow continuous fabrication. Simultaneously the fine feature generation that allows microcontact printing to resolve below a single micron is to be leveraged towards overcoming the challenges of contemporary microcontact printing.

Optical maskless lithography has achieved resolution below the micron-scale. Even though a variety of systems are available, they are predominantly limited to flat substrates, such as silicon and glass wafers, and to a substrate diameter of 300 mm or less.

It is possible to create seamless, cylindrical PDMS stamps by a centrifuge-based, cylindrical laser direct write lithography system. This method has been proven, in a first iteration, to have the potential to solve the challenge of implementing a more efficient

manufacturing process for tools for large-scale microcontact printing. To harvest this potential, a robust process needs to be defined over a wide range of desired applications, which is capable of creating tools that minimize any disturbance in the consequent printing process.

# Chapter 2

# Prior Art in Tool Fabrication for Microcontact Printing

PDMS stamps for microcontact printing are traditionally cast on silicon wafers. Their high resolution and feature fidelity faces a trade-off in scalability. A technique based on centrifugal casting seeks overcome this limitation.

## 2.1 Flat Stamp Fabrication

A unique advantage of microcontact printing is the capacity of PDMS to replicate sub-micron geometries. However, the conventional method of casting PDMS against a flat patterned surface creates several limitations when applied to R2R printing geometries. The desired stamp is cylindrical, and thus a flat stamp must be wrapped on a cylindrical mandrel and joined at the seam.

### 2.1.1 Procedure: Wafer-Based Casting

Stamps for microcontact printing are currently cast on patterned wafers [39]. Commercial lithography equipment is available to create arbitrary patterns of sub-micron resolution on silicon wafers. After lithographic patterning, a pattern can be etched into the silicon wafer to create a PDMS master (Figure 2.1). More commonly, the lithographic pattern on the wafer serves as the master [40]. The wafer may be placed in a petri dish and submerged in PDMS. A vacuum forming method is preferred, because it provides a uniform stamp thickness and releases trapped air that leads to material heterogeneity.

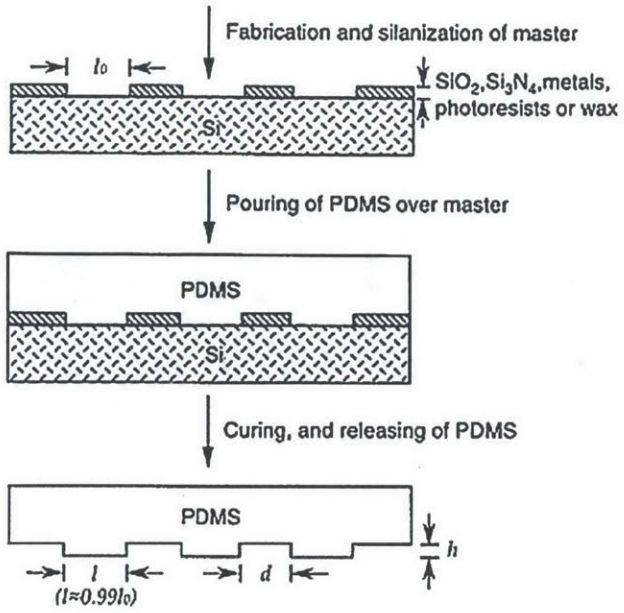


Figure 2.1: PDMS stamp fabrication for microcontact printing. The PDMS stamp is produced by casting on a wafer patterned with photoresist. The photolithography step determines the stamp feature geometry .

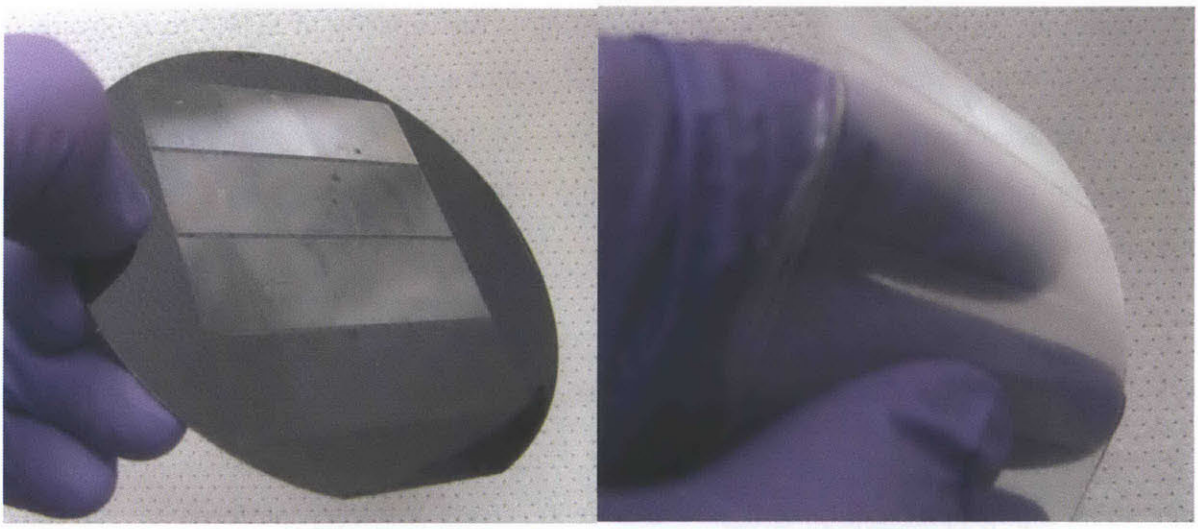


Figure 2.2: Patterned wafer (a) and PDMS stamp fabricated thereby (b) [19].

### 2.1.2 Challenges Posed by Wafer Limitations

Advantages of this technique are the outstanding resolution and fidelity of the elastic material, which allow microcontact printing to reproduce patterns in sub-micron resolution.

However, as the method relies on wafers as substrate, it presents obvious limitations in scalability. The finite repeat length renders the technique unsuitable for production of large-area patterned surfaces.

## 2.2 Fabricating Continuous Tools

To overcome the limitations presented by wafers, a technique has been proposed that is based on centrifugal casting of the master and the PDMS stamp into a cylinder. It has been proven viable to recreate stamps with a uniform thickness and micron-scale patterns of high fidelity.

### 2.2.1 The Key to Scalability

Roll-to-roll microcontact printing promises to significantly increase throughput over plate-to-plate microcontact printing and permit new applications. In roll-based microcontact printing, a PDMS stamp is wrapped around a printing roll. The finite wafer size limits the scale-up of microcontact printing. Furthermore, as the stamp is wrapped around a roll, the discontinuity caused by the seam adds a periodic disturbance to the process.

### 2.2.2 A Proposed Concept

To overcome this limitation and allow for a robust consequent printing process, a technique has been proposed in which the wafer substrate is replaced by a rotating cylinder [41]. The centrifugal nature of this setup allows for smooth deposition of a planarizing layer, the deposition of a uniform thickness photoresist layer, and after patterning the photoresist, centrifugally casting the stamp material. As this technique does not use silicon wafers as a substrate for the cast, it is not constrained in scale or cost by wafer-based processing equipment. Moreover, as is the case with a silicon master, several stamps can be created from the same pattern without notable quality loss.

### 2.2.3 Procedure

The method explored by Petrzelka and Hardt [41] comprises the following steps (see Figure 2.3)

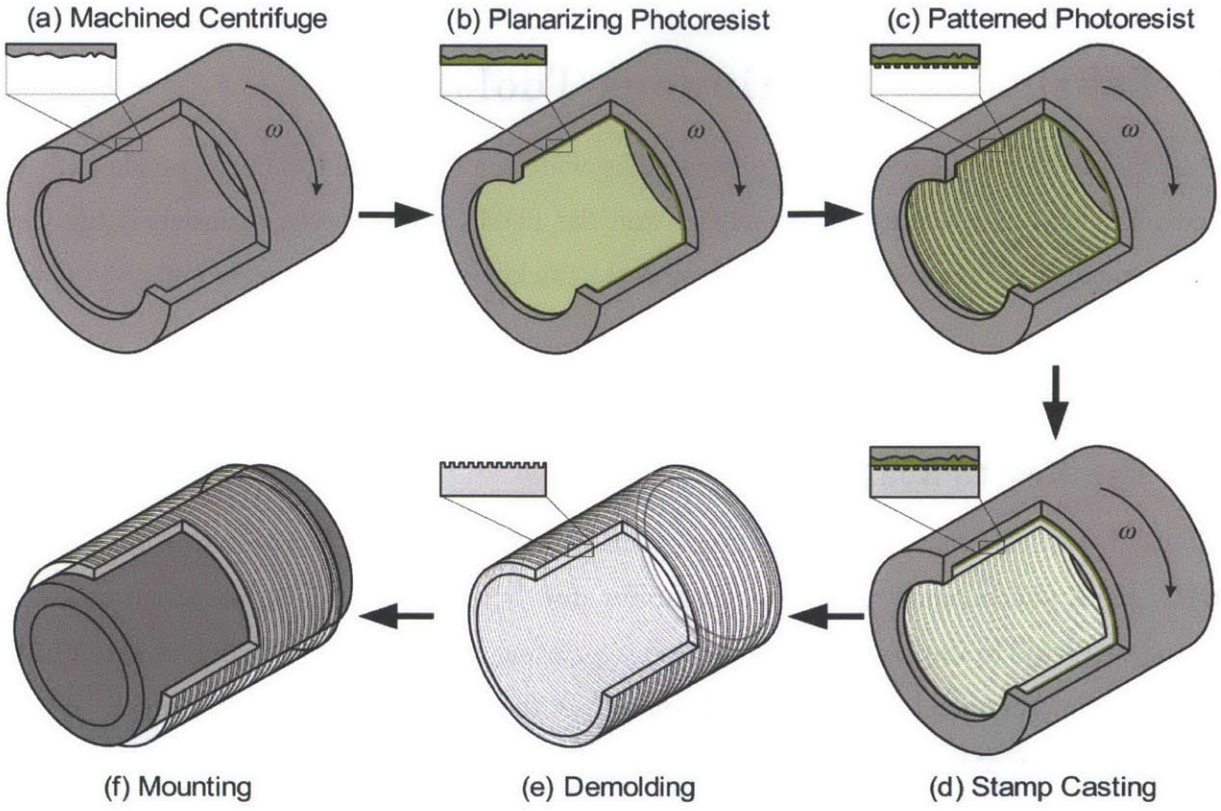


**Figure 2.3: Stamp making process steps in the centrifugal apparatus. The drum surface is smoothened and centered with a planarizing layer of negative photoresist. Another layer of photoresist creates the patterned master, into which the PDMS tool is cast [41].**

a. A machined centrifuge drum serves as basis for the mold.
b. A layer of photopolymer is centrifugal-cast into the drum to create a planar surface.
c. An additional layer of photoresist is applied and patterned to create a mold (master) with micron-sized cavities. The patterning step determines the overall geometry of the produced features on the stamp.
d. PDMS is cast into the mold to produce the stamp
e. The stamp is demolded from the centrifuge.

The stamp is mounted on the printing roll using a film of compressed air.

A prototype has been built which proves the viability of the process. Initial experiments show a 2 μm runout and a taper of 340 μrad [19].

### 2.2.3.1 Planarizing Layer

Photolithography is usually performed on planar, smooth silicon surfaces. To obtain a smooth cylindrical surface and to compensate for minimal eccentricity of the drum, the surface of the drum is fully covered with a layer of a photopolymer prior to patterning. A negative photoresist is chosen to make it resistant to the processing steps required for the subsequent deposition and structuring of the patterning layer.

To apply the layer, the drum is first cleaned with acetone and allowed to dry. Then a solution of 0.5 – 1.0 ml SU-8 2015 (Microchem) and 5 – 7 ml SU-8 thinner (cyclopentatone) are mixed using a stirring rod and introduced to the centrifuge using a syringe, while the drum spins at a speed of 50 rad/sec (8 rev/sec). Care is taken to not introduce air bubbles in the solution during mixing. The drum is then accelerated to 300 rad/sec (48 rev/sec) over a period of 5 sec. Given a solids fraction of 63% in SU-8 2015, the volume introduced to the drum spreads out to an average film height of 34 μm (for 0.5 ml SU-8 2015) to 67 μm (for 1.0 ml) after evaporation of the solvent. The solvent is evaporated by heating the centrifuge to 95 °C and baking the photoresist at this temperature for 60 minutes. The final height of the planarizing layer can be approximated through to the solids fraction of the photoresist, but additional shrinkage arises from thermal expansion and cross-linking [42]. It should be noted that the coefficient of thermal expansion (CTE) of aluminum ($24 * 10^{-6}$/K) is much closer to that of SU-8 ($50 * 10^{-6}$/K) than the CTE of silicon ($2.3 * 10^{-6}$/K).

The remaining solid layer is cross-linked during near-ultraviolet LED flood exposure with a wavelength of 405 nm, using three modules of 20 mW optical power each. The lights are translated along the length of the drum at a rate of 5 μm/sec, while the drum spins at the same speed of 300 rad/sec (48 rev/sec).

The layer of SU-8 is cross-linked while baking it again at 95 °C for 15-60 minutes, depending on its thickness. It is then heated o 150-200 °C for 15-60 minutes to ensure adhesion to the aluminum drum.

### 2.2.3.2 Patterning

In Petrzelka's work, two photoresists were considered to form the patterning layer: SU-8 [19] and SPR 220 [41], the former a negative resist and the latter a positive resist.

The photoresist was prepared and introduced as described in 2.2.3.1. It was found that a volume of 0.5 ml SU-8 2015 leaves a final layer thickness of 33 μm. The resist was exposed with a laser emitting a wavelength of 405 nm, which requires a higher exposure dose than specified for 365 nm wavelength for SU-8, given the much high higher transmittance of the resist at the higher wavelength. In initial experiments, the laser was focused on the resist film using optics (see 2.2.4) while rotating the drum at 300 rad/sec (48 rev/sec) for 8 to 20 seconds per axial position, writing lines on a 50 μm pitch. After exposure, the photoresist is baked at 95 °C for 60 minutes and developed in SU-8 developer (Microchem) once cooled.

To explore the precision of the process, a positive resist, SPR 220, was also used in initial trials. SPR 220 remains highly sensitive at a wavelength of 405 nm, which is ideal for the chosen laser. To form a patterning layer, 0.1 ml SPR 220-3.0 (Dow Corning) were thinned with 5 ml of 2:1 ethyl lactate (Sigma Aldrich) and anisol (Sigma Aldrich). The mixture was inserted into the drum at a spinning speed of 50 rad/sec (8 rev/sec). The drum was then accelerated to 300 rad/sec (48 rev/sec) and the mixture centrifuged for 60 seconds before baking it to 115 °C until all solvent is evaporated, while aerating it with compressed air.

Once cooled down to 25 °C, the photoresist layer was exposed with aforementioned laser and focusing optics at an energy level of 200 $mJ/cm^2$, corresponding to 50 ms per rotation for a 12 μm beam diameter.

The exposed film is developed for 60 seconds under a stream of MF24A developer (Dow Corning) and rinsed with deionized water.

After casting one or multiple PDMS stamps on the patterning layer, the layer of SPR 220 can be removed using organic solvent (such as acetone), leaving the planarizing layer intact. On the contrary, SU-8 leaves a permanent patterning layer.

### 2.2.3.3 PDMS Stamp Centrifugal Casting

To create the stamp, a volume of 10 ml PDMS (Sylgard 184, Dow Corning) was mixed at the recommended 10:1 ratio of base and curing agent before it is degassed under vacuum for 10 minutes to remove air bubbles. The PDMS is then inserted into the drum rotating at 50 rad/sec (8 rev/sec) and centrifuged for 5-10 minutes to equilibrate the layer thickness of the viscous material.

The spinning centrifuge was then heated to 65 °C for 60 minutes to crosslink the PDMS. Once cooled, the created PDMS stamp is removed from the drum and rinsed with ethanol.

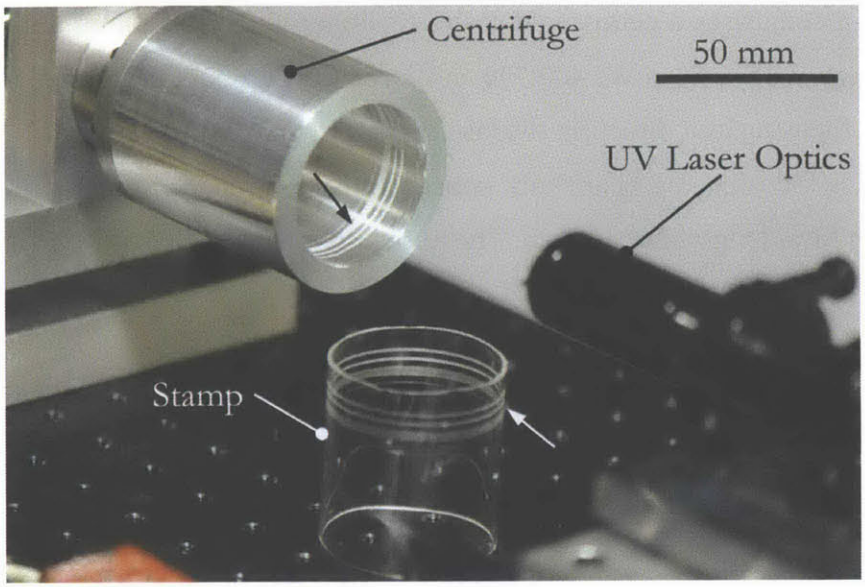


**Figure 2.4 The cylindrical stamp after removal from the centrifuge [19].**

### 2.2.4 Apparatus

For these initial trials a proof of concept machine was developed and was also used for the subsequent experiments in this thesis.

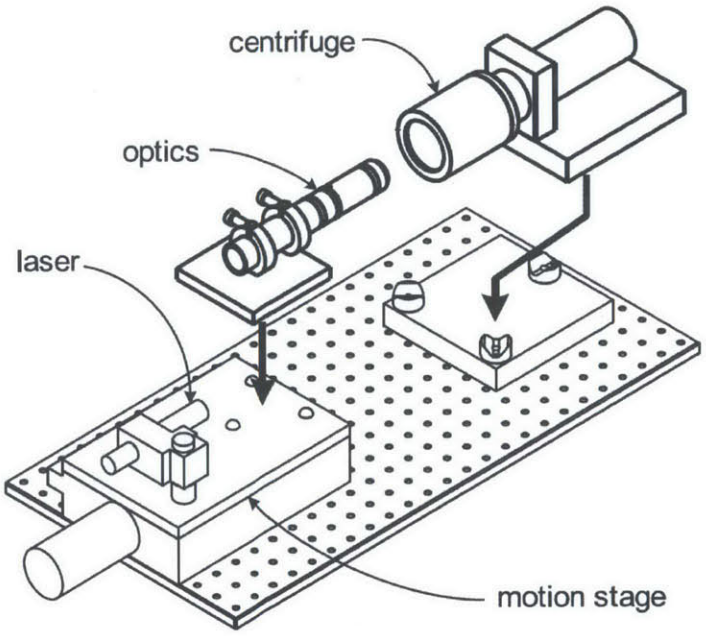


**Figure 2.5: A proof of concept of the apparatus that allows for investigating the process in detail. It comprises the centrifugal casting cylinder (top right) as well as the laser mount and a detachable optics assembly [41].**

The setup comprises a centrifugal caster (cylinder with Ø 52.8 mm and length 60 mm) and a linear stage with a 80 mW, 400-700 nm laser (to be operated at 405 nm) and simple optical tools for focusing and directing the laser beam (NA = 0.08).

The optics focusing the beam to a concentrated spot comprise a simple plano-convex lens with 75 mm focal length and a prism. The optics are depicted in Figure 2.6.

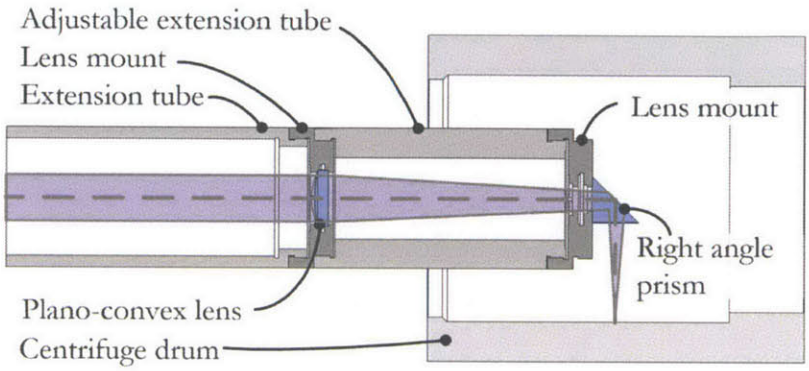


**Figure 2.6: Focusing optics [41].**

### 2.2.5 Results

The precision of the created patterns and surfaces in the photoresist is measured through the PDMS stamp cast on them, since PDMS replicates surfaces at nanoscale resolution. The topology of each surface is measured with a white light interferometer (Zygo). The SU-8 planarizing layer achieves a surface roughness of about 20 nm RMS, while the SPR 220 coating achieves about 10 nm RMS. The drum runout is reduced from 15 μm to 2 μm through the planarizing layer.

In the SU-8 pattern, an exposure time of 15 seconds per axial position, corresponding to an exposure dose of 6.25 MJ/cm$^2$ at a wavelength of 405 nm, which is not well-absorbed by the photoresist. An exposure of 10 and 20 seconds per axial position, thus a variation in exposure dose of 25 % increase or decrease, led to an over- or under-exposure, respectively. In each exposure level, the geometry of the created features varies in width and sidewall angle, as depicted in Figure 2.7. The low photoresist absorption at the laser wavelength, disturbances caused by the bearings and substrate reflection may be major factors contributing to the roughness of the feature edges.

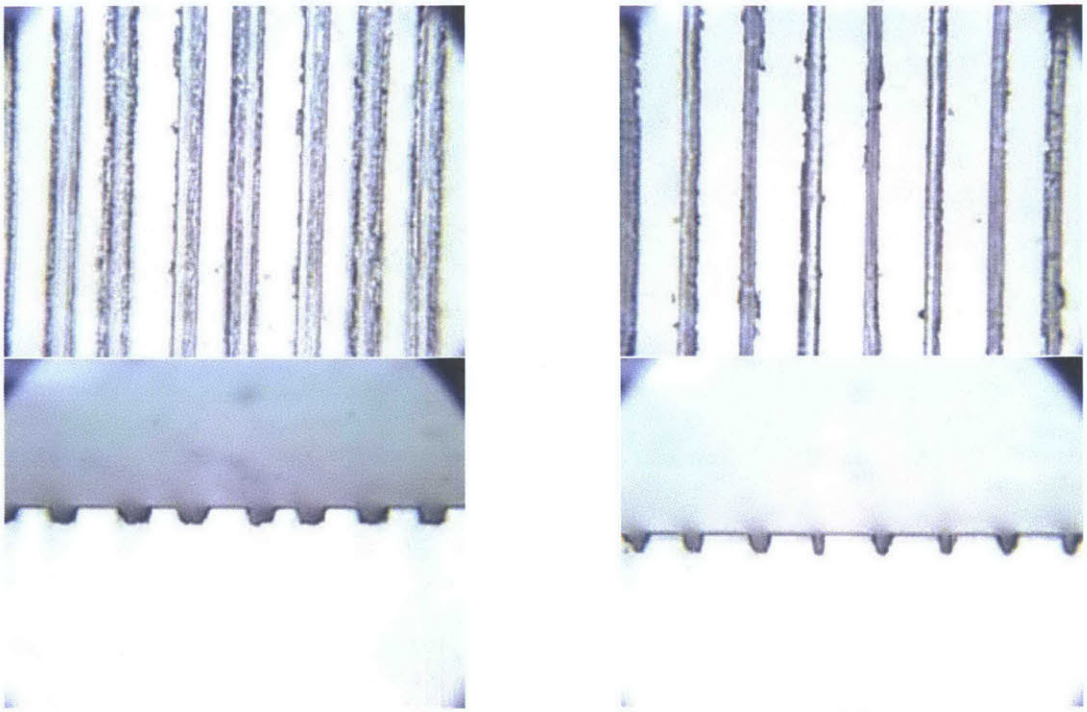

(a) (b)

**Figure 2.7: The quality of the features created by patterning SU-8 is characterized by rough edges and varying width dimensions [19].**

By contrast, feature sizes of 10 μm width and height were achieved in the SPR 220 patterning layer. Feature edges are significantly smoother than with SU-8. Feature edges exhibit a radius of about 1-2 μm, and the repeatability of these results produced by this process is not further investigated.

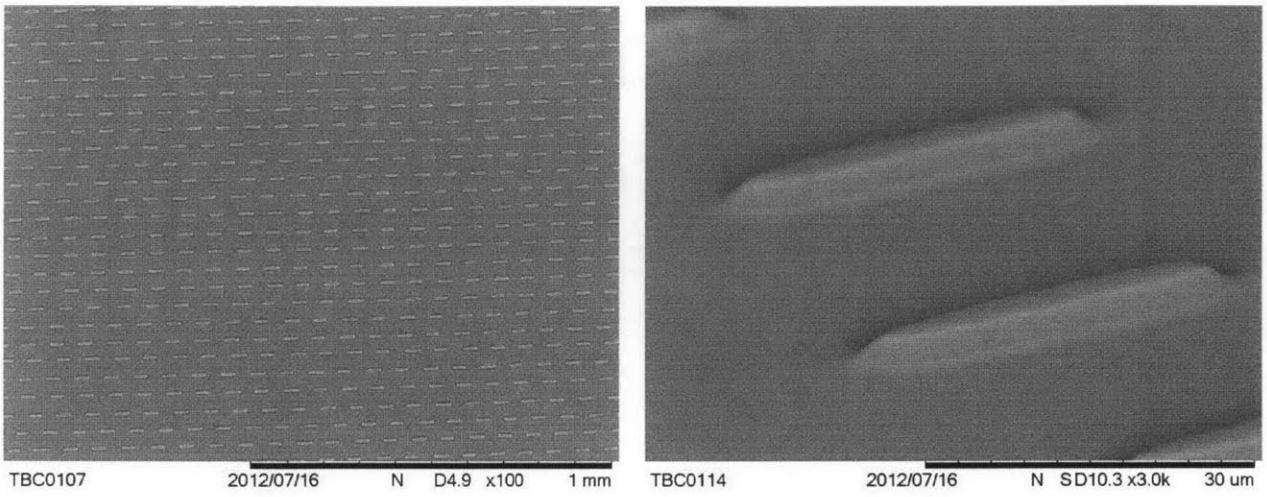


**Figure 2.8: Feature sizes of 10 µm and smooth edges were achieved with SPR 220 [41].**

Given an aspect ratio of about 1:1, the smooth topology, and a resolution on the order of few micrometers, it is worth investigating the repeatability and limits of the feature fidelity with SPR 220 and similar positive photoresists as patterning layer materials.

### 2.2.6 Conclusion

Although the initial feasibility study of the novel technique presents promising results. Analysis is required on the robustness and the dimensional limits of the process. Moreover, additional potential can be exploited by exploring other degrees of freedom presented by the process in order to improve the consequent printing process, foremost the morphology and accuracy of the resulting print stamp features.

The work presented here examines the photolithographic process in this novel setup. It develops a detailed process model around the unexplored field of intra-cylindrical laser direct write lithography on thick resist film. It determines the robustness of the process towards the variation of the process factors such as exposure intensity; resist film thickness and writing speeds. Furthermore, the cylindrical casting method of PDMS for creating functional stamps for microcontact printing is extended to enable real-time contact imaging in R2R µCP through the developments of multi-layer fluorescent stamps.

# Chapter 3

# Thick-Film Laser Direct-Write Lithography Process Model

The geometry of the tool determines the quality of the print in microcontact printing. By optimizing the stamp feature geometry, possible errors in the subsequent printing process can be greatly reduced. The critical step in creating the geometry of the tool is the photolithographic patterning. The patterning layer serves as the master that the PDMS tool is cast into, and PDMS has been shown to replicate surfaces with nanoscale precision. Therefore, The shape of the stamp features negatively replicates the shape of the patterning layer.

The patterning is done with photolithography. Traditionally, photolithography is used to selectively pattern bare, oxidized or metal-coated silicon wafers for subsequent etching. As such, the vertical geometry of the photoresist is of limited importance, if the resolution is maximized and the thickness is sufficient to withstand the etching process. Steep sidewalls are preferred in certain etching processes. Thus, high aspect ratios, i.e. a thick film and great lateral resolution, are usually preferred. The technique investigated in this work, however, aims to fabricate a cross-sectional geometry that replicates stamp features favorable for printing. The sidewall angle and edge radius are the most important properties that can be used to increase the performance of the fabricated stamps in the microcontact printing process. To ensure the robustness of this photolithographic process, it is important to understand both the physical properties of the light source and the chemical properties of the photosensitive material shaped by it.

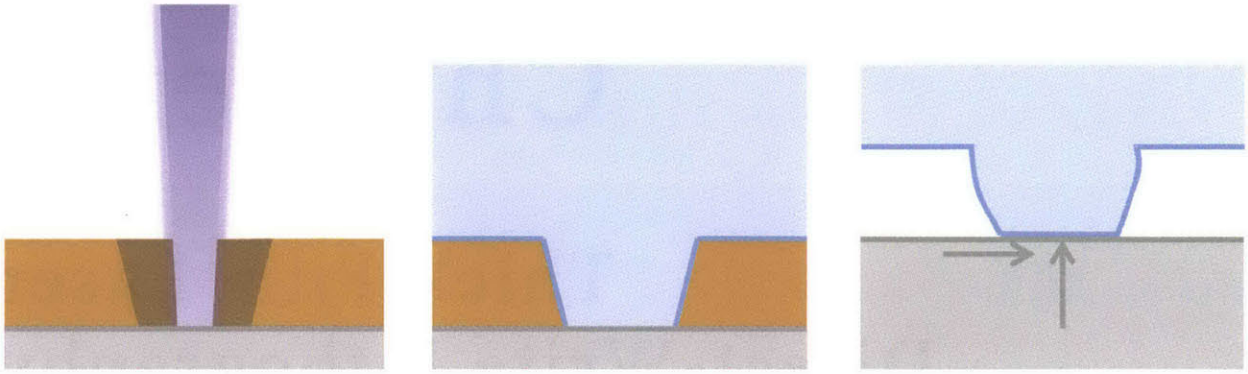


**Figure 3.1: Motivation for investigating intra-cylindrical laser direct write lithography. The patterning step (a) determines the shape of the stamp feature, since the lithographic pattern serves a master for the centrifugal casting of the PDMS stamp (b). In the printing process (c), the stamp has to withstand normal pressure with the substrate required to transfer ink, and minimal lateral torque from transmitting force to the passively driven print roll, capillary forces and van-der-Waals interactions with adjacent feature surfaces.**

## 3.1 Motivation

Microcontact printing achieves a fine resolution and high speeds as a result of the high compliance of its stamp material, PDMS. As seen in 1.2.2, the flipside of the ease of conformity is an increased susceptibility to feature collapse, buckling and other error modes. An optimization of the features' cross-sectional geometry can reduce the susceptibility to errors while providing for the necessary compliance for conformal contact. An optimized feature cross-section can therefore contribute to the robustness of the printing process.

An overview of common error modes is presented in Figure 3.2.

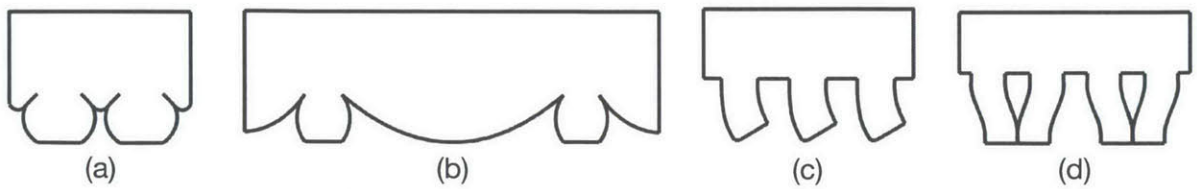


**Figure 3.2: Error modes in microcontact printing. (a) Sidewall collapse. (b) Roof collapse. (c) Buckling. (d) Lateral collapse [19].**

### 3.1.1 Reduction of Defects

The most common errors are illustrated in Figure 3.2 and Figure 3.3. The underlying factor for these error modes is the features' mechanical resistance against variation in printing force, against van-der-Waals interactions and against capillary forces [43], where the material's elasticity is required for ensuring conformal contact with the substrate [44].

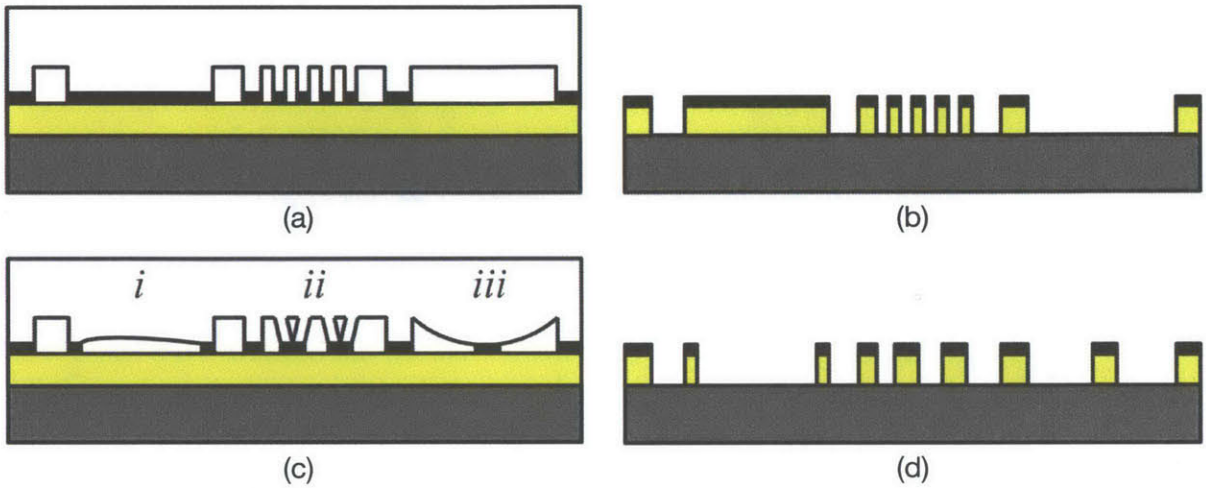


**Figure 3.3: Defect formation through tool elasticity. Local variation in printing force and surface energy effects can cause mechanical deformation of the stamp. (a) Ideal contact and (b) resulting pattern transfer; (c) imperfect contact and (d) resulting pattern. Defects include air entrapment (i), lateral feature collapse (ii), and roof collapse (iii) [19].**

These defects can be avoided by optimizing the geometry of the stamp features. Due to its compliance, PDMS tools have been found to collapse or sag for feature aspect ratios greater than ≈2 or less than ≈0.05 [40].

### 3.1.2 Control of Ink Deposition

The low surface energy of PDMS, combined with its high compliance, provides good conformal contact with the substrate. Importantly, a low surface energy repels the ink, making it difficult to control the volume of the deposited ink [45]. If a radius is present between the flat top and the sidewalls, or if the top of the stamp is rounded, an excessive amount of ink may be deposited as ink is also supplied from the feature sidewalls. In flexography, this phenomenon is well researched.

Figure 3.4 illustrates the effect of the feature topology on the printing result and shows that flat tops significantly improve the resolution of the print [46]. Since PDMS is even more compliant than the material used for conventional flexography plates, the conclusion can be derived that in microcontact printing, stamp features with a flat top and minimum edge radius may significantly contribute to a consistently high fidelity of the print conducted with said stamp.


(a) (b)

**Figure 3.4: In flexography, flat tops can achieve a higher resolution than peak tops. The peak compresses upon substrate contact, which promotes ink transfer from the feature sidewalls. (a) Conventional digital plate with a 7% dot (percentage referring to area coverage). (b) Flat-topped dot plate with 2% dot. The flat top features significantly improve the fidelity of the print. Resolution in both cases: 102 lpi (lines/inch) [46].**

### 3.1.3 Repeatable Fabrication

Furthermore, as a Design-for-Manufacture approach is applied, the robustness of the tool fabrication process can be improved. By finding optimal parameters for minimizing variation in the process and thus increasing its resistance to potential disturbance, the stamps fabricated are most consistent in their properties, which further improves the robustness of the subsequent microcontact printing process.

## 3.2 Fundamentals of Photolithography

The basic determinant of feature shape in the centrifugally cast tools is the shape of the exposed and developed photoresist. To understand the limitations of this process, and in particular the implications of direct laser writing, the following review of photolithography is presented.

Photolithography, "printing with light", is the process of patterning a surface by first fully covering the substrate with a light-sensitive polymer material, known as photoresist, and then partly removing this photoresist following selective exposure with light of a given wavelength. Depending on the type of photoresist, the material properties of the polymer are changed such that it remains either in the exposed or in the unexposed regions and is removed in the other using suitable chemicals. The pattern can be created by use of a 1:1 mask in direct contact with the layer of photoresist, optical imaging of the mask, or serial exposure using a scanned narrow beam light source. To former two determine the pattern a priori with the mask geometry, while the latter creates a pattern via the trajectory of the scan pattern.

### 3.2.1 History

The history of optical lithography dates back to the early 1960s, when contact printing was developed to as a manufacturing technology for the integrated circuit (IC) which was invented in 1958 [47]. In contact printing, a mechanically created, selectively translucent mask was placed directly on the substrate, typically a wafer - first germanium, later silicon - patterned with photoresist. As this technique was prone to defects, it soon evolved to proximity printing, as the mask was placed at a few micron distance to the substrate [48]. Contact printing and proximity printing laid the foundations of photolithography, and ultimately of printed electronics.

### 3.2.2 Photoresist

The development of photolithography was made possible through the development of photosensitive resin in 1935 and 1940 [49]. Although very different in their respective behavior, the two types of material both undergo property changes under the influence of light

that critically affect the material's solubility. In 1935, polyvinyl cinnamate, the first negative photoresist, was created by Louis Minsk of Eastman Kodak [50]. The material was characterized by its ability to polymerize upon irradiation with ultraviolet light. Only 5 years later, Oskar Suess developed the first diazoquinone-based, positive-tone photoresist at Kalle & Co AG, which was later acquired by Hoechst AG [51].

The characteristic of positive vs. negative photoresist is further illustrated in Figure 3.5.

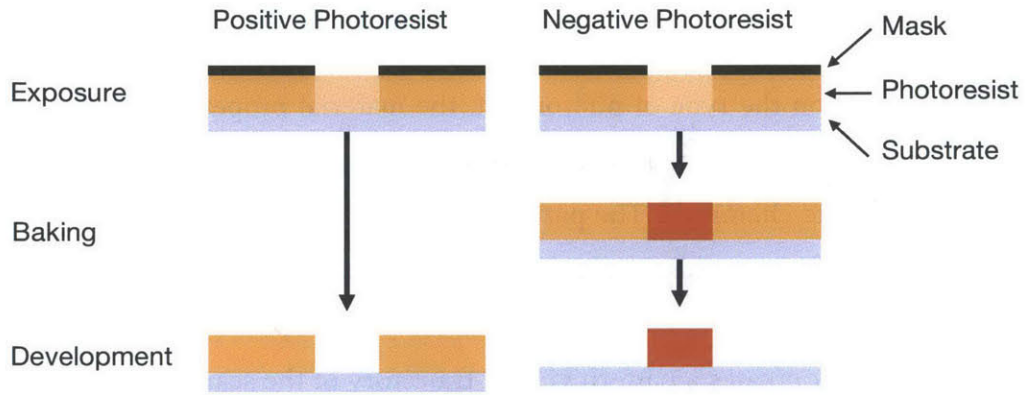


**Figure 3.5: Positive vs. negative photoresist. Positive photoresist will dissolve in exposed areas, negative photoresist will crosslink in exposed areas.**

To date, diazoquinone is the photoactive chemical in most positive photoresists for the g-, h- and i-line[i], such as AZ 9260 and SPR 220. In the exposure process of a typical positive-tone photoresist, diazonaphthoquinone (DNQ), the diazo-derivative of naphthoquinone, forms a ketene upon irradiation with light in the UV range around 300 to 450 nm [52]. This reaction, which is also known as Wolff rearrangement[ii], converts DNQ into a ketene and thus leaves a nucleophilic C=O group, which readily reacts with ambient water, forming base soluble carboxylic acid. The chain of reactions is illustrated in Figure 3.6.

---

[i] Certain common illumination wavelengths in photolithography are derived from the spectral lines of mercury (Hg): 436 nm (g-line), 405 nm (h-line) and 365 nm (i-line).

[ii] In a Wolff rearrangement (discovered in 1902), a $\alpha$-diazocarbonyl compound is converted into a ketene under the loss of di-nitrogen, induced by light or heat irradiation.

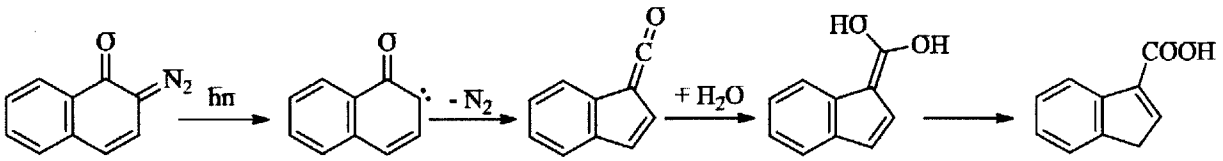

**Figure 3.6: Chain of reactions in typical positive photoresist. A Wolff rearrangement lets diazoquinone form ketone upon exposure - the mechanism in most positive-tone photoresists. The nucleophilic nature of the ketene attracts ambient water. Resulting from this addition: C(O)OH , base soluble carboxylic acid [52].**

DNQ is used in combination with novolac resin to inhibit the resin's solubility in aqueous base developer. The ketene formed upon exposure, however, reacts with ambient water following the exposure into a base soluble indene carboxylic acid. Thus, a pattern is formed of the exposed areas in a positive photoresist, which are dissolved during the development step.

Chemically amplified resist contains acid-sensitive groups and an additional compound, which releases acids upon ultraviolet exposure. During a post-exposure bake, these acids diffuse and catalyze the fragmentation of the respective functional groups. Chemically amplified resist is prone to shot-noise and is usually applied in the deep-UV regime, when a lack of photoresist sensitivity requires a more efficient reaction.

### 3.2.3 Light Sources

Originally, mercury (Hg) lamps provided the near-UV light required for photoresist exposure. In comparison to other non-laser light sources, mercury lamps emit very bright light and their emission spectrum reaches the deep-UV region [53]. The spectral lines of Hg lamps - 436 nm (g-line), 405 nm (h-line) and 365 nm (i-line) - have defined photolithography standards to date.

The development of the excimer laser in Russia in 1970 opened the door to a new kind of optical lithography [54]. Excimer lasers extended the wavelength spectrum of the laser technology into the UV range. Soon after invention, a variety of wavelengths and intensities could be generated using different gas media, such as Krypton Fluoride (KrF) and Argon Fluoride (ArF) [55]. In 1980, Kantilal Jain, of IBM Almaden Research Center, applied the

excimer laser technology to the production of IC chips and created excimer laser lithography. His patent includes an optical setup to incorporate a laser as the light source for a projection lithography system [56].

The first metal vapor lasers were created in the 1960s, beginning with the helium-mercury laser, one of the first laser types ever developed. Experimenting with different gain media, the helium-cadmium (He-Cd) laser originated as a pulsed laser [57]. Its inventors, Silfvast and Fowles, explored a variety of possible wavelengths for the He-Cd laser, and Silfvast managed to build the first continuous-wave He-Cd laser after he had joined Bell Labs in the late 1960s [58]. As the cadmium ion excitation lines of 325 nm and 441.6 nm fall into the sensitivity spectrum of certain photoactive materials, the He-Cd laser remains important for photolithographic applications.

The size, cost, maintenance and thermal aspects present disadvantages to the use of metal vapor and excimer lasers in photolithographic applications.

Diode lasers, also known as semiconductor-based solid state lasers, enabled the rapid development of the CD and DVD technology, beginning in the 1980 [59]. When diode lasers were installed in lithographic systems, they proved to allow for compact, low-cost photolithography [60].

Solid state lasers, such as the neodymium-doped yttrium aluminum garnet (Nd:YAG) laser, are rarely used for UV applications, as they naturally emit light in the IR spectrum. However, passive Q-switching of the Nd:YAG crystals allows for the production of UV light with applications in deep UV lithography [61].

### 3.2.4 Commercial Equipment

Since the capabilities of the lithographic production processes determine the resolution and the performance of semiconductors, production-scale photolithographic equipment has largely been developed by semiconductor producers, such as Hewlett-Packard, IBM or Samsung, in collaboration with suppliers of optics, lasers, actuation and process chemistry. Moreover, a number of suppliers provide high-performance, lab-scale equipment. In the following, examples are given for industrial laser direct write lithography system suppliers.

One of the prominent suppliers of laser lithography systems is Heidelberg Instruments GmbH. The German company was founded in 1984 through the merger of a variety of laser,

optics and imaging startups. Today, their focus is on maskless lithography systems, with wavelengths of 363 to 442 nm, for direct write applications and the production of photomasks. Laser sources are solid state diode lasers and, occasionally, high power gas lasers for applications that require high intensities. Their machines are specified to accept substrates up to 200 mm x 200 mm for resolutions down to 0.5 μm and are equipped with components for autofocus, alignment and grayscale exposure management [62]. Their largest machine, currently, supports substrates of up to 1.4 m x 1.6 m and is capable of producing structures down to 1 μm.

Silicon Valley based Optical Associates Inc. (OAI) builds a broad range of equipment for UV exposure, imprint and PV metrology, including laser direct write systems. Their current high-end maskless laser direct write lithography system manages substrates up to 400 mm x 400 mm and is specified to produce a laser spot diameter anywhere between 0.5 μm and 100 μm. Its absolute precision is given as 1 μm for a stage travel resolution of 40 to 100 nm. Its repeatability is specified within 100 nm.

Intelligent Micro Patterning LLC filters and focuses a mercury lamp beam onto the substrate. Using mercury lamps, their systems are capable of broadband exposure in the g-, h- and i-line. They claim sub-μm feature generation, but do not specify the intensity of the beam. However, they offer cylindrical, rotating substrates with diameters of 1 mm to several inches. The resist film is created on the cylindrical substrate via dip coating.

ASM Lithography, headquartered in the Netherlands, uses plasma sources to create extreme ultraviolet (EUV) light with a wavelength of 13.5 nm and uses 20 W ArF lasers to create deep-UV light with a wavelength of 193 nm. ASML utilize immersion lithography to create numerical apertures up to 1.35, allowing for a specified minimum resolution of 40 nm with a 193 nm light source.

E-beam direct write lithography equipment suppliers include eAISC, Advantest and Mapper. Carl Zeiss in Aalen, Germany, are known to supply specialty optics for photolithography.

Nanoscribe GmbH, a German spin-off that was founded at Karlsruhe Institute of Technology in 2007, develop high-resolution 3D printers and high-resolution photoresist. With their proprietary photoresist they claim to achieve 150 nm resolution with two-photon polymerization.

MIT's spin-off LumArray applies a parallel laser direct writing process by splitting a deep-UV excimer beam into up to 1000 separately intensity-modulated beams.

Canon released photolithographic equipment with a substrate size of 9 m by 11.6 m.

## 3.3 Process Theory

In general, the photolithographic process encompasses the following steps:

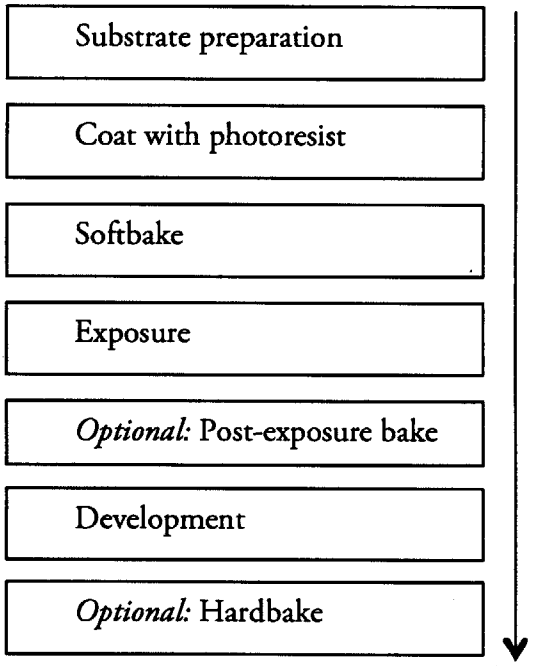


To prepare the substrate, often an adhesive coating or anti-reflective coating is applied. Untreated silicon surfaces may not provide for proper adhesion of the photoresist.

The resist, comprising photoactive compound (PAC), resin and solvents, is then applied via spin coating. Photoresist suppliers usually give values for the expected residual layer thickness as a function of the spin speed, and in many cases, the formulation names represent the expected film thickness for a given spin speed.

The photoresist is then baked to remove solvents and solidify the film. The rigid resist film is then selectively exposed with light of a certain wavelength that the PAC is sensitive to.

A second bake is sometimes needed to trigger a catalytic reaction, to diffuse products of the reaction caused by the exposure, or to enhance adhesion to the substrate.

During development, dissolvable material is washed away to reveal the pattern created during the exposure process. In the case of positive photoresist, the exposed resist has reacted to be dissolvable by the developer.

To improve adhesion to the substrate, a hard-bake is often performed following development.

### 3.3.1 Processing Mechanisms

The photolithographic process is made up of multiple steps, most importantly the coating of the substrate, baking to remove solvent, the selective exposure, and the development which leaves the eventual pattern.

#### 3.3.1.1 Photoresist Coating

In conventional photolithography, the resist film is applied via spin coating.

In the case of centrifugal laser lithography, the layer of photoresist is applied to the inside surface of a cylindrical drum. It can be shown that for centripetal acceleration much greater than gravity and a fluid layer of height $h$ much smaller than the drum diameter $2r$, the circumferential pressure gradient is the product of the fluid density $\rho$, the centrifugal acceleration $r\omega^2$, and the gradient of the variable thickness $h(x)$ of the fluid film [19]:

$$\frac{\partial p}{\partial x} = \rho r\, \omega^2\, \frac{dh}{dx} \tag{3.1}$$

where $\omega$ is the angular velocity, $r$ is the radius of the drum, and $x = r\psi$ is the circumferential distance with $\psi$ being the angular displacement about the axis of the drum. The fluid film profile $h$ then follows a decaying sinusoidal solution with wavelength $\lambda_f$:

$$h(x,t) = \bar{h} + e^{-t/\tau_f} \cos\left(2\pi \frac{x}{\lambda_f}\right) \tag{3.2}$$

where $\bar{h}$ is the height of the uniform free surface approached by all values $h(x)$ with increasing time $t$. Equally, the fluid flow rate $Q$ must be related to the instantaneous change in the same height profile. For a dynamic viscosity $\mu$ it can be concluded that:

$$\frac{dh}{dt} = -\frac{dQ}{dx} = -\frac{d}{dx}\left(\frac{\rho r\omega^2}{3\mu}\frac{dh}{dx}\bar{h}^3(x)\right) \tag{3.3}$$

Applying the solution to $h(x,t)$ found earlier and solving for the asperity decay time constant in the fluid layer $\tau_f$ gives:

$$\tau_f = \frac{3\mu\lambda_f^2}{4\pi^2\rho r\omega^2\bar{h}^3} \tag{3.4}$$

A sinusoidal unevenness would thus decay with a time constant $\tau_f$.

It can further be shown that for a small leveling error $\epsilon_{axis}$, the free surface will exhibit a taper $\epsilon_{fluid}$ that is much smaller than the leveling error if the centripetal acceleration is much greater than gravity ($g$):

$$\epsilon_{fluid} = \frac{\epsilon_{axis}g}{\omega^2 r} \tag{3.5}$$

To reduce the time to reach equilibrium, $\tau_f$ can be reduced by reducing the kinematic viscosity. This can be achieved by the addition of solvents with a lower viscosity. Furthermore, the effective height of the fluid film is increased by the addition of such a solvent, which further reduces the time constant for equilibration. Since the viscosity of photoresist, which proportionally affects the time constant, increases exponentially with its solids content, and given the average film thickness reciprocally enters the time constant to the power of three, the process of casting a layer can be greatly accelerated through the addition of solvent.

In conventional spin coating, the centrifugal force vectors are parallel to the flat substrate. As the drum is a finite closed system and the force vectors are perpendicular to the substrate, the final thickness of the resist depends on the initial resist volume and the solids content.

With the drum being a cylinder with radius $r$ and therefore circumference $2\pi r$, and lengh $l_z$, and the photoresist being of volume $V$ and solids content $\beta$, the final average height $\bar{h}$ can be predicted as follows:

$$\bar{h} = \frac{V}{\beta * 2\pi r l_z} \tag{3.6}$$

This can be used to calculate the necessary volume of resist for a particular resulting thickness $\bar{h}$.

### 3.3.1.2 Soft-Bake

To evaporate solvent in the photoresist and stabilize the film, it needs to be thermally treated prior to exposure. Two factors limit the maximum temperature of this baking process. The control of the baking temperature must not exceed the boiling point of the solvent to limit the solvent gradient and prevent the topmost layer from solidifying while the bulk of the resist is still liquid. Otherwise the diffusion of the remaining resist can lead to the formation of trapped bubbles and the topology is characterized by "wrinkles". Furthermore, a high temperature over a long time will decompose the photoactive compound, which affects the rate of development during exposure [63].

Figure 3.7 shows how the resist looses its optical sensitivity when baked too hot.

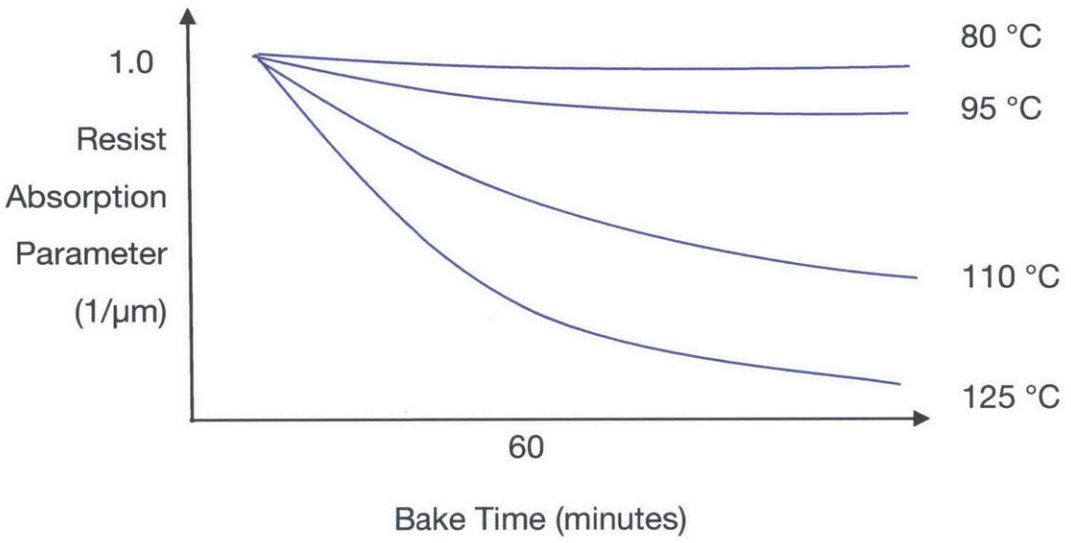


**Figure 3.7: Effect of prebake temparature on the sensitivity of the resist. Above 80 °C, a long duration prebake drastically diminishes the sensitivity of the photoresist, leading to potential burning effects [64].**

The nucleophilic reaction of the DNQ-ketene requires water to be present. In thin resist films, ambient humidity is sufficient. Thick films of photoresist need a certain water content throughout to provide for the supply of $H_2O$ molecules. As the prebake leaves the resist dry, an additional rehydration time is necessary for thick films.

### 3.3.1.3 Optical Exposure

UV light irradiation chemically changes the photoresist and makes positive resist soluble in aqueous base developer, as explained previously. Diazonaphthoquinone (DNQ) inhibits the solubility of novolac resin in aqueous base developer. A Wolff rearrangement, that is triggered by UV irradiation, transforms photoresistive DNQ into a ketene. The latter reacts with ambient water to form a base soluble indene carboxylic acid. Thus, the selective UV exposure creates a pattern in a positive photoresist to make the exposed regions dissolvable during the development step.

The Wolff rearrangement in DNQ is caused by light with a wavelength between 300 and 450 nm. Depending on the individual resist chemistry, the sensitivity to different wavalengths across the spectrum varies. Important marks are the g-, h- and i-line. A typical sensitivity curve (SPR 220) is shown in Appendix A.3.

The exposure curve of photoresists is usually nonlinear and ideally shows threshold behavior. The more pronounced this mechanism, the higher the "contrast" of a resist. A high-contrast resist does not form a feature below a given energy dose, and then shows a steep curve in the relationship of energy dose to formed feature, until the saturation point is reached.

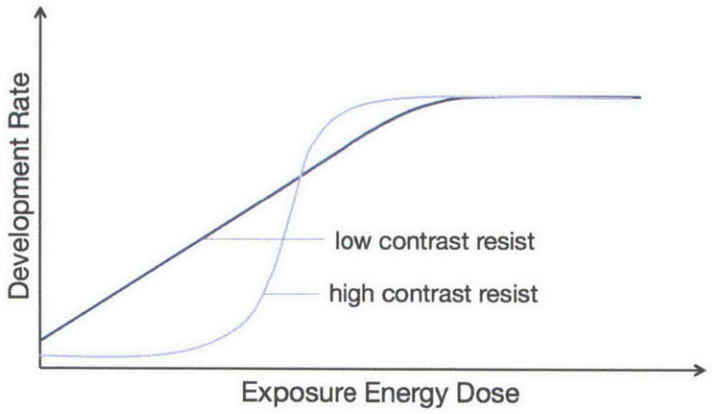


**Figure 3.8: Development rate per dose for exemplary photoresists.**

Since the irradiation has to pass through the resist film, which has a given absorbance, a thicker resist film will require a higher energy per unit of surface area to trigger the photochemical reaction throughout the full layer thickness. The total required irradiation usually increases at a proportionally growing rate with an increase in resist thickness. This exponential relationship represents the integral of the proportional absorbance in each infinitesimal layer of material.

In a diffraction-limited system (i.e those with focusing transmission optics), the distribution of the incoming light will set a limit for the achievable resolution [65]. In direct write systems, the width of the laser beam presents the limit for the achievable line width. To account for the differences in resist photochemistry and illumination system quality, the optical resolution criteria, minimum pitch between features $p$ and depth of focus $2z_R$, are often extended by coefficients $k_1$ and $k_2$ [66], [67]:

$$p = \frac{k_1 \lambda}{NA} \tag{3.7}$$

$$2z_R = \frac{k_2 \lambda}{(NA)^2} \tag{3.8}$$

where $\lambda$ is the wavelength and NA is the numerical aperture. Typical values are $k_1 \approx 0.4$ and $k_2 \approx 0.7$ [68]. Interference lithography and other specialty lithography techniques pass the diffraction limit and achieve sub-wavelength resolution, but are constrained to repeating patterns [69].

If the substrate is reflective, the incoming light often not only penetrates the resist, but also reflects off the substrate, causing further exposure of the photoresist. Often, the wave characteristics of the UV beam lead to interference of the incoming and the back-reflected light beam. This standing wave effect can cause a rippling surface on the feature sidewalls. Specialty anti-reflective coatings (ARC) have been developed to overcome this effect that work either by applying them underneath or on top of the resist layer. Where bottom anti-reflective coatings (BARC) can help eliminate standing waves that affect feature side walls [70], top anti-reflective coatings (TARC) can reduce the amplitude of the resist swing curve if the thickness is appropriately chosen for providing destructive interference inside the coating [71]. To a certain extent, a post-exposure bake helps diffuse the exposed DNQ and flatten out possible ripples on the topology. Excessive post-exposure bake can undesirably affect the feature shape and round off the feature edges.

#### 3.3.1.4 Post-Exposure-Bake

Although usually not necessary, some photoresist manufacturers recommend baking after exposure. This will diffuse the photoactive compound and provide a smooth topology. In

addition, the so-called post-exposure-bake (PEB) improves adhesion between the resist and the substrate.

The reaction with ambient water, which is part of the photolithographic process, requires a rehydration time of up to 30 minutes depending on the thickness of the resist.

#### 3.3.1.5 Development

The development step creates the pattern from the exposed and thus locally chemically modified photoresist. Physically, dissolvable material is washed away. Developers are usually basic aqueous solutions, with organic amines such as tetramethylammonium hydroxide TMAH or inorganic salt such as potassium hydroxide [72].

A variety of methods have been developed to submerge the resist film on wafers. Traditionally, coated wafers were placed in large beakers. Automated in-line processing uses equipment similar to spin-coaters. In spin development, the developer is poured on the rotating wafer. In spray development, the developer is sprayed on the rotating wafer as a fine mist, which gives more uniform developer coverage. In puddle development, the developer is poured on a stationary wafer, which does not move throughout the development time. Specialty developer formulations are available for each of these methods [73].

The development step is usually followed by a rinse and agitation in DI water.

### 3.3.2 Resist Formulation

To allow for different film thicknesses, various resist formulations are available. For thicker resist films, the production of nitrogen during the exposure process is critical, as bubbles will form as a result. Ambient water is not as ubiquitous as for thin films. As a trade-off, thick-film resists require a much higher exposure dose as thin-film resists.

SPR 220 is recommended for film thicknesses of single micron. The range for AZ 9260 is given with 5 μm to 25 μm.

## 3.4 Modeling

To derive a robust patterning process, the laser irradiation distribution and photoresist sensitivity to such an irradiation were synthesized into a model for both the photoresist chemistry and physics during the exposure process. To better understand the patterning process and the subsequent experiment, it is useful to develop a model of the patterning process. This model comprises a characterization of the light source (in this case a focused laser) and how that interacts with the photopolymer resist. The components of the model include a model of the energy absorption of the photoresist and a model for the intensity and distribution of the incoming laser energy. These two are combined to predict the regions within the resist that will be developed after a specified exposure dose and distribution.

### 3.4.1 Photoresist Modeling

The key input to the photoresist is the "exposure dose" which is given by the product of the light intensity $I$ and the exposure time $t$:

$$E(x) = I(x) \cdot t \tag{3.9}$$

where $E(x)$ is the exposure dose at a depth $x$ after exposure time $t$.

For positive photoresist, exposure will allow the resist to dissolve upon development, whereas for negative resist the opposite is true.

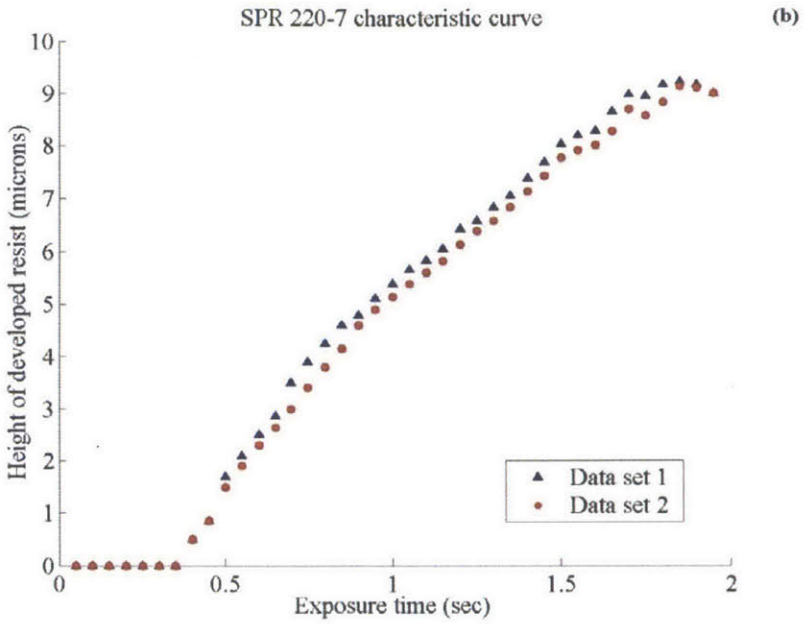


**Figure 3.9: Contrast curve for SPR 220-7.0. With increasing depth, the absorption increases, reducing the steepness of the contrast curve [74].**

Resists are engineered to react non-linear to exposure. This is often called the "contrast" of the resists, and refers to a threshold type behavior (see 3.3.1.3). In general, the contrast curve of a positive photoresist can be divided in three regions:

a. No reaction below a certain energy threshold
b. After threshold is reached, material reacts until saturated
c. If resist is saturated ("bleached" or dose to clear), it will be removed completely upon development

Some positive photoresists show "dual-tone" behavior, i.e. when applying energy larger than an additional threshold greater than the necessary dose to clear, the resist solubility decreases again. In dual-tone lithography, this mechanism is exploited to increase resolution by creating two narrower trenches with a single pass of the exposure source utilizing the Gaussian distribution of the beam. In such a case, this behavior is enhanced by adding a negative-tone sensitizer to the positive-tone DNQ-novolac resin [75], such as hydroxymethyl-melamine [76] or 4-4'-bis(azidophenyl)sulfone [77].

In a positive photoresist, the resist thickness remaining per exposure dose is determined by the contrast of the resist process, $\gamma$. The resist contrast can be defined as the slope of the function that describes the remaining resist thickness $d_r$ normalized by the initial

and total thickness $d_c$ in relation to the proportional exposure dose $E/E_c$ on a logarithmic scale [66], [71]:

$$\frac{d_r(E)}{d_c} = \gamma \, ln\left(\frac{E}{E_c}\right) \tag{3.10}$$

$$\therefore \gamma = \ln\left(\frac{E}{E_c}\right)^{-1}\left(\frac{d_r(E)}{d_c}\right) \tag{3.11}$$

for exposure doses up to $E_c$, the dose to clear, which will completely remove the resist. High-contrast resist is characterized by a steep slope and thus nearly threshold conditions for feature formation. This allows for steep sidewalls even with Gaussian irradiation. In so-called gray-scale lithography, exposure dose below dose to clear allows for a varying depth.

The Dill model [78], named after the IBM engineer who first started modeling lithography, defines parameters A, B and C to model the exposure of the photoresist. Parameters A and B, refer to the absorption of the unexposed and bleached resist, respectively. Parameter C refers to the rate at which the resist is exposed. During exposure, the photoactive component reacts to its bleached products. In that process, the absorption coefficient of the resist changes. The absorption coefficient is made up of the resin, the sensitizer or photoactive compound, its exposure products and solvent or moisture content. During the exposure process, the concentration of these substances changes. To simplify modeling, Dill developed a model that finds an absorption coefficient for the bleached resist, B, a coefficient for the difference in absorption between unexposed and bleached, A, and a coefficient to describe how the composition changes upon exposure, C.

The parameters A and B, unless provided in the resist data sheet, can be calculated from the absorption coefficients of the unexposed and exposed resist [64]:

$$A = \frac{1}{d}\ln\left(\frac{T_\infty}{T_0}\right) = \alpha_{unexposed} - \alpha_{exposed} \tag{3.12}$$

$$B = \frac{1}{d}\ln\left(\frac{T_\infty}{T_{12}}\right) = \alpha_{exposed} \tag{3.13}$$

where $d$ is the depth into the resist, $T_0$ is the transmittance of the unexposed resist, $T_\infty$ is the transmittance of the exposed resist and $T_{12}$ is the transmittance of the air-resist interface [64]. From Equations (3.12) and (3.13) it can be seen that A is the exposure-dependent part of

the resist absorption parameter, whereas B is the exposure-independent part. To express the time- and location-dependent absorption of the resist, the parameter $M$ is introduced which marks the remaining fraction of photoactive material or dissolution inhibitor. $M$ is 1 for the completely unexposed resist, and decreases towards 0 as the exposure progresses.

The absorption / attenuation coefficient for any time and location is then:

$$\alpha(x,t) = AM(x,t) + B \tag{3.14}$$

According to Beer-Lambert's law [80], the transmission through the partially exposed material until a given depth $d$ can be calculated as follows [64], [80]:

$$T(d,t) = \exp\left(-\int_0^d \alpha(x,t)dx\right) \tag{3.15}$$

Given Equation (3.14) above, this gives:

$$T(d,t) = \exp\left(-\int_0^d (AM(x,t) + B)\,dx\right) \tag{3.16}$$

The intensity at any depth into the material can then be expressed as:

$$I(d,t) = I_0 * \exp\left(-\int_0^d (AM(x,t) + B)\,dx\right) \tag{3.17}$$

$M(x,t)$, the fraction of remaining photo-initiator, is a function of the cumulative intensity experienced at any location. It admits the following differential equation:

$$\frac{\partial M(x,t)}{\partial t} = -I(x,t)M(x,t)C \tag{3.18}$$

A solution to this first order differential equation can be found as:

$$M(x,t) = \exp\left(-\int_0^t I(x,t)C\,dt\right) \tag{3.19}$$

The standard exposure rate constant is the third Dill parameter. C can be approximated as follows [64], [81]:

$$C = \frac{A+B}{AT_0(1-T_0)T_{12}}\frac{dT}{dE}\bigg|_{E=0} \tag{3.20}$$

$T_{12}$ can be calculated through the refractive index, $n_{resist}$:

$$T_{12} = 1 - \left(\frac{n_{resist}-1}{n_{resist}+1}\right)^2 \tag{3.21}$$

The refractive index of positive photoresist at 405 nm is typically around $n_{resist} \approx 1.7$, so that $T_{12}$ is typically around $T_{12} \approx 0.93$.

### 3.4.2 Laser Modeling

The laser irradiance of a diode laser is approximated with a Gaussian distribution [61], [82]. For a longitudinal coordinate z and a transversal coordinate r, the irradiance $I$ can the be described by

$$I(r,z) = I_0 \left(\frac{\omega_0}{\omega(z)}\right)^2 e^{-\frac{2r^2}{\omega^2(z)}} \tag{3.22}$$

with $\omega^2(z) = \omega_0^2 \left(1 + \left(\frac{z \cdot \lambda}{\pi \cdot \omega_0^2}\right)^2\right)$.

The width of the beam, $2\omega_0$ at the focal point, is defined as the distance between the two locations with an irradiance of $\frac{I_0}{e^2}$ across the transverse of the beam, where the irradiance in the center of the beam equals $I_0$.

An alternative definition of the beam width is the "full width at half maximum" (FWHM). For a Gaussian beam [82],

$$FWHM = \frac{\sqrt{\ln 2}}{\sqrt{2}} * 2\omega = 0.589 * 2\omega \tag{3.23}$$

Equally,

$$2\omega = 1.699 * FWHM \tag{3.24}$$

The two definitions of the beam with, $2\omega_0$ and FWHM, are illustrated in a simulation generated in Mathematica, in Figure 3.10.

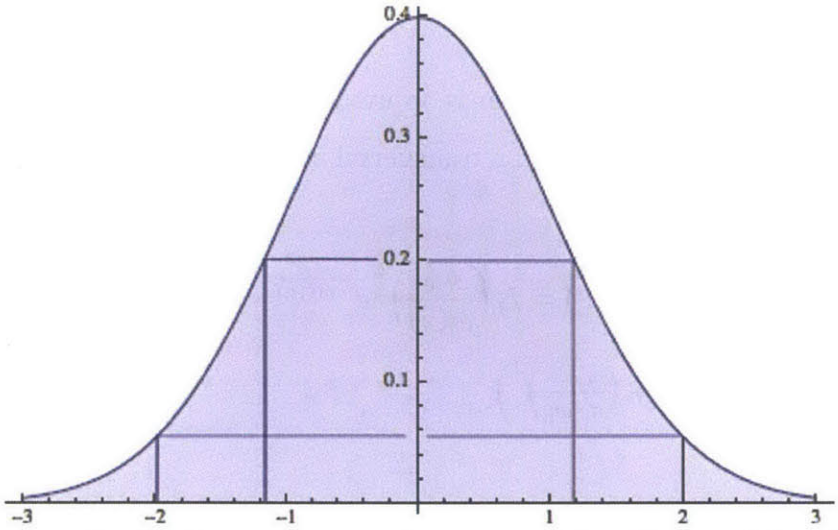


**Figure 3.10: Standards for Gaussian beam width. The width of a Gaussian beam can be described by $2\omega_0$ or by its full width at half maximum (FWHM), with a relation given by $2\omega = 1.699 * \mathbf{FWHM}$ [83].**

At the focal point, the beam width $\omega$ equals the beam waist, $\omega_0$, and to either side of the focal point the width extends hyperbolically, as described in Equation (3.22).

The wavelength $\lambda$ proportionally determines the beam waist $2\omega_0$ that can be achieved at a given angle of divergence $2\theta$:

$$\omega_0 = \frac{\lambda}{\pi\theta} \tag{3.25}$$

Therefore, the smaller the wavelength $\lambda$, the smaller the beam waist.

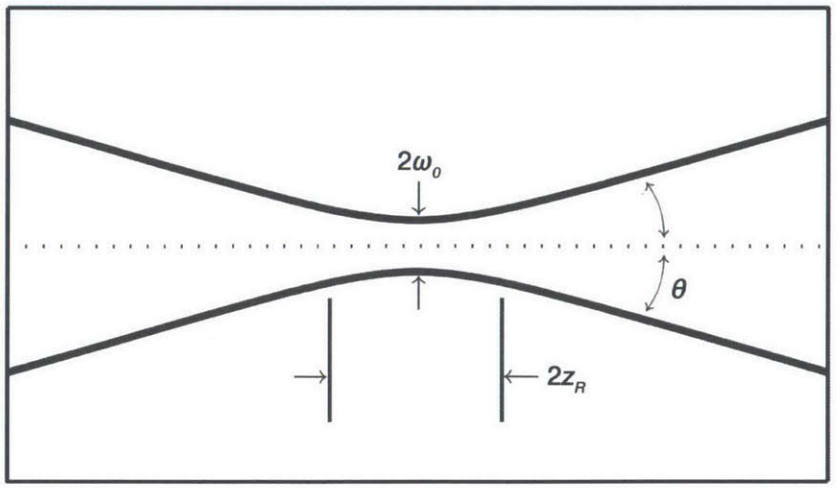


**Figure 3.11: The Rayleigh length, $2z_R$, relates to the beam waist and to the numerical aperture. For a beam waist of 5 µm, NA of 0.04 and a wavelength of 405 nm, the Rayleigh length is 194 µm.**

The confocal parameter or depth of focus of a beam describes the distance between the two point on either side of the focal point where the beam cross section is twice the value at the focal point, and therefore $\omega$ is $\sqrt{2}\,\omega_0$, or $\omega^2 = 2\omega_0^2$. The distance between this position and the focal point can then be described with the following expression:

$$z_R = \frac{\pi\omega_0^2}{\lambda} \tag{3.26}$$

This dimension is known as the Rayleigh length of the beam and is illustrated in Figure 3.11. Thus, for a given wavelength, an increase in the numerical aperture decreases the minimum spot size but also decreases the Rayleigh length.

As the maximum intensity is given with $I_0(z) = I_0\left(\frac{\omega_0}{\omega(z)}\right)^2$, the intensity at either side of the Rayleigh length is half the intensity at the focal point. For parameters typical of the work described here, for a wavelength of 405 nm and a beam waist $\omega_0$ of 5 μm, the Rayleigh length $z_R$ is 194 μm. The change in intensity, simulated using Mathematica, is displayed in Figure 3.12.

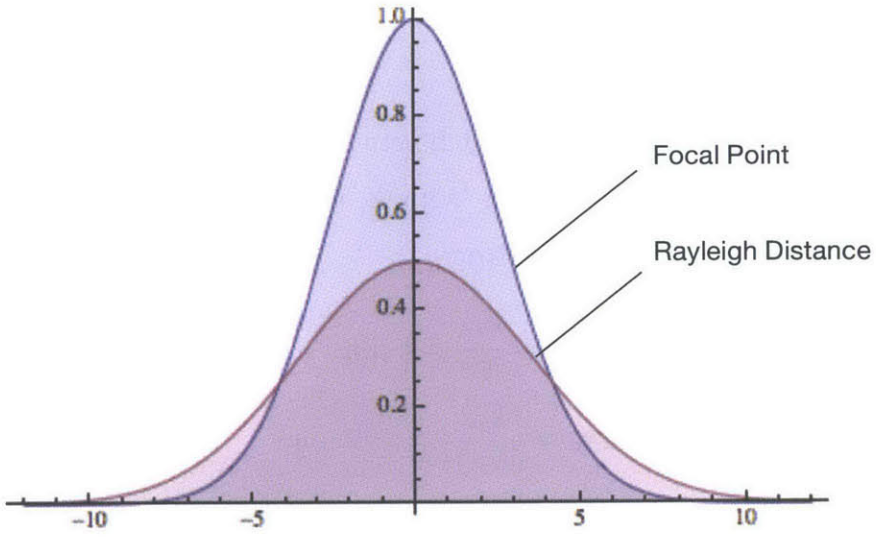


**Figure 3.12: Change in intensity from focal point to Rayleigh distance. The Rayleigh Length marks an extension in diameter by $\sqrt{2}$ and a reduction in maximum intensity by 1/2. For the parameters in this work, the diameter extends from 5 μm at the focal point to 7 μm at the Rayleigh distance.**

The absolute integral of the irradiation across the profile of the beam, $\iint_{-\omega}^{\omega} I(r,z)\,dr$, is constant for any position along the beam, z, for ideal conditions, as the laser power travels with the beam. Therefore, the local irradiation at the center of the beam is significantly higher at the focal point than to either side of it. This mechanism is illustrated in Figure 3.13.

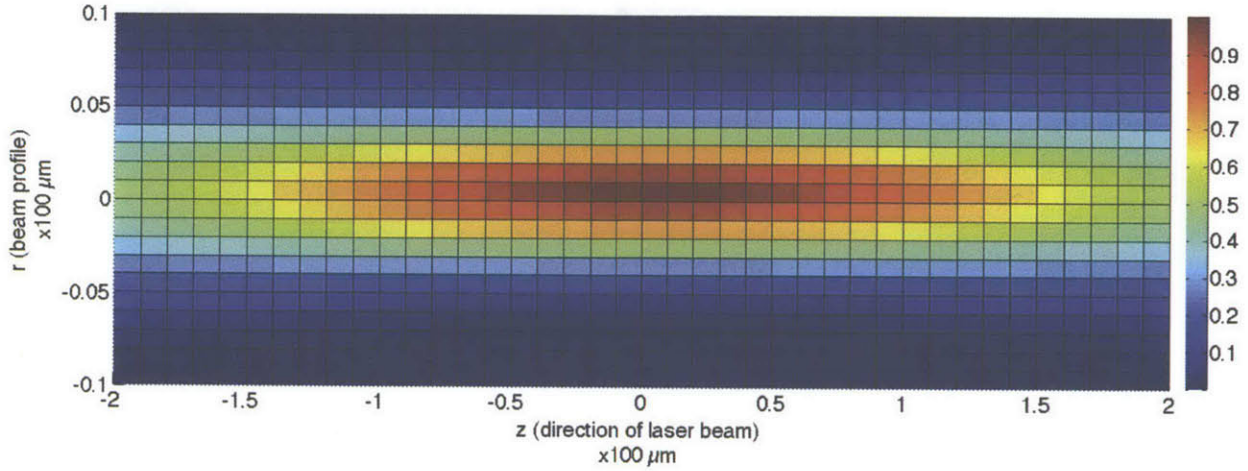


**Figure 3.13: Gaussian beam waist with irradiation distribution around the laser focal spot. Parameters are a wavelength of 405 nm and a beam waist $\omega_0$ of 5 μm. The simulation shows a range of 20 μm across the beam profile r (ordinate) and 400 μm across the length of the beam, z (abscissa).**

The resolution criteria, minimum pitch between features $p$ and depth of focus $2z_R$, can be approximated for thin films of resist. With $k_1 \approx 0.4$, $k_2 \approx 0.7$, the numerical aperture $NA = \frac{3mm}{75mm} = 0.04$ and wavelength $\lambda = 405\ nm$:

$$p = \frac{k_1 \lambda}{NA} = 4\ \mu m \tag{3.27}$$

$$2z_R = \frac{k_2 \lambda}{(NA)^2} = 177\ \mu m \tag{3.28}$$

These values approximate the limits for thin films of resist.

To account for factors that affect the ideal dimensions of the beam, the so-called beam quality factor, also known as beam propagation factor $M^2$describes the relationship between

the beam waist radius, the half-angle beam divergence and the wavelength of the beam [82], [83]:

$$M^2 = \frac{\theta \pi \omega_0}{\lambda} \tag{3.29}$$

Even though optical correction can help compensate, the asymmetry of diode lasers has en effect in its applications. The circularity can be quantified as follows:

$$f_{circularity} = \frac{4\pi A}{P^2} \tag{3.30}$$

with area A and perimeter P. For an elliptical beam with an area of $\frac{\pi}{4} d_1 d_2$ and a perimeter simplified to $\frac{\pi}{2}\sqrt{2d_1^2 + 2d_2^2}$, this can be roughly approximated as

$$f_{circularity} \approx 2 * \frac{d_1 d_2}{d_1^2 + d_2^2} \tag{3.31}$$

## 3.5 Analytical Simulation

Combining the model for the exposure and resist reaction mechanisms, a numerical model can be derived. This model can then be used to simulate different resists, laser beam width and focus and overall dose.

The maximum intensity of the laser beam can be estimated if the absolute optical power and the width of the laser beam are known, as the laser power equals the integral of the intensity over the cross-section of the beam. Given the shape of the beam is Gaussian; the total power is given by:

$$P = I_0 \int_{-\infty}^{\infty} e^{-\frac{2r_x^2}{\omega_x^2}} d\, r_x \int_{-\infty}^{\infty} e^{-\frac{2r_y^2}{\omega_y^2}} d\, r_y = \frac{\pi}{2} I_0 \omega_x \omega_y \tag{3.32}$$

Solved for

$$I_0 = \frac{2P}{\pi \omega_x \omega_y} \tag{3.33}$$

The system to be modeled is described by the following parameters:

**Table 3.1: System Specifications**

| Specification | Value |
|---|---|
| Laser beam waist, $\omega$ | 5 μm |
| Wavelength, $\lambda$ | 405 nm |
| Power, P | 80 mW |

Assuming a symmetric beam with $\omega_x = \omega_y = 5\,\mu m$ and given a laser power of $P = 80\,mW$, Equation (3.33) gives a peak intensity of $I_0 = 103 * 10^3 \frac{W}{cm^2}$, which is the basis for simulating the beam profile.

The Dill model A and B parameters for SPR 220 resist are given in the manufacturer's data sheet. For AZ9260, the absorption coefficients for unexposed and exposed resist can be extracted from the absorption curve given. Alternatively, they can be measured [64], [78].

The optical sensitivity parameter C can be approximated using the slope of the transmittance curve [65], [82]:

$$C = \frac{A + B}{AT_0(1 - T_0)T_{12}} \frac{dT}{dE}\Big|_{E=0} \tag{3.34}$$

$T_0$ and $dT/dE|_{E=0}$ can be extracted either from a basic measurement of the resist transmittance, as seen in Figure 3.14, or from an interpolation of provided exposure energy examples (see Appendix A.3).

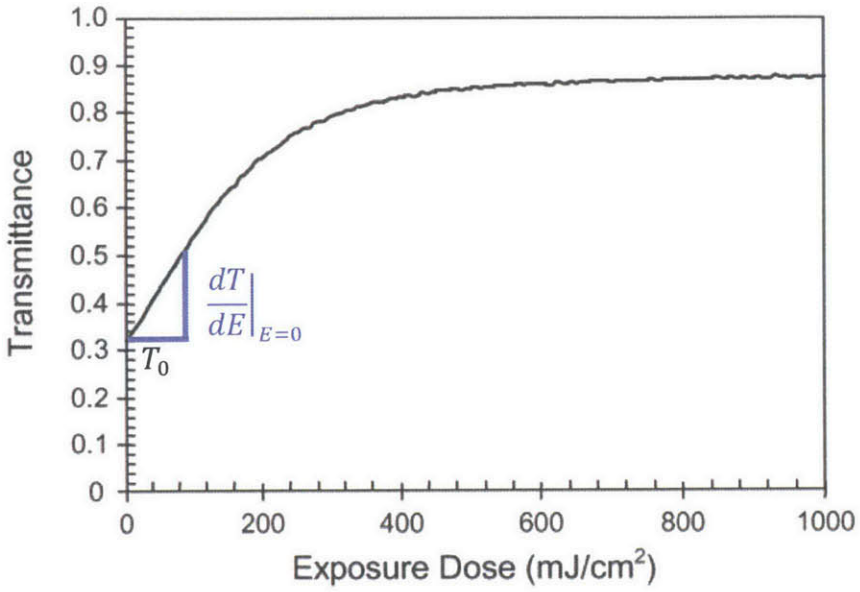


**Figure 3.14: A typical example for a transmittance curve for a positive photoresist, from which characteristic parameters can be extracted [65].**

Accordingly, the following values were determined for the two photoresists used:

**Table 3.2: ABC Parameters for Simulating the Exposure Process**

| Parameter | SPR 220 | AZ 9260 | Units |
|---|---|---|---|
| A | 0.71 | 0.36 | $\mu m^{-1}$ |
| B | 0.02 | 0.01 | $\mu m^{-1}$ |
| C | 0.017 | 0.005 | $cm^2/mJ$ |

A simulation is generated using MATLAB to investigate the accuracy of both the Dill model and the determined parameters.

To model vertical laser irradiation at the focal plane, the intensity is described as a function of the lateral distance to the beam axis. The axial change in focus is neglected since the system described has a very small numerical aperture of 0.04, corresponding to a depth of focus in the photoresist of 177 μm (see Equation (3.28)), which exceeds the investigated film thickness by a factor of 10.

The photoresist is modeled as a mesh. Two matrices are created to simulate both the intensity acting on each mesh interval and the remaining photo-initiator in each lateral and

vertical mesh interval over a given number of time intervals. In a construction of nested loops, the photochemical process was simulated over time. In each time-discrete iteration, the transmittance through all the material covering a given mesh interval was integrated using the cumulative of the overlying intervals' photo-initiator concentration, following Equation (3.16). Factored with the irradiation intensity as a function of the lateral position of the mesh interval, the intensity present at each element of the mesh is calculated as described in Equation (3.17). This intensity, stored in a matrix for each lateral and vertical mesh interval, yields to a change in photo-initiator concentration determined by Equation (3.19).

As the Gaussian beam is most intense at its center, its nonlinear propagation through the photoresist bleaches the material in the center of the beam, before a similar amount of energy as accumulated in the surrounding material. This leads to somewhat tapered feature sidewalls. By contrast, flat-top profile beams can be created using beam-shaping or are native to certain kinds of lasers. However, they do not usually reach the resolution of a focused Gaussian beam. Masking the beam through an aperture of a certain shape would introduce non-uniform diffraction patterns to the beam profile.

Cross-sectional maps of remaining photo-initiator-concentration determined with this simulation for different time intervals are shown in Figure 3.15 for SPR 220 and Figure 3.16 for AZ 9260. As can be extracted from the results of the simulation, the Gaussian nature of the beam can be leveraged to create features of a certain desirable structure and geometry.

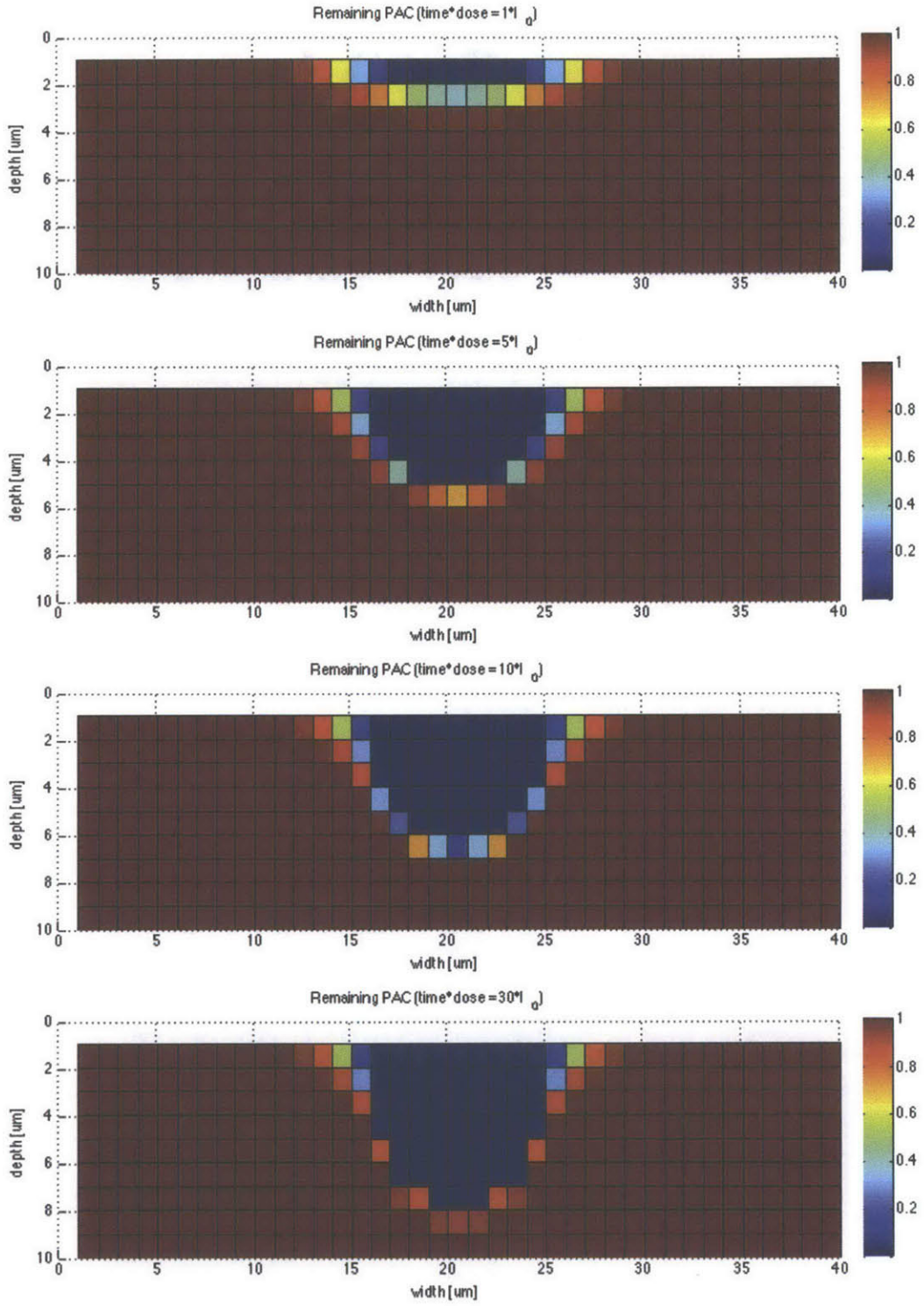


Figure 3.15: Result of the simulation for SPR 220. Exposure durations $t = t_0 + 1, t_0 + 5, t_0 + 10$ and $t_0 + 30$ in 0.1 msec intervals for a beam with a waist of 5µm and 80mW laser power. The simulation predicted round sidewalls and edges as the energy propagates deeper into the material. In the graphs, the concentration of remaining photoactive compound is shown by color.

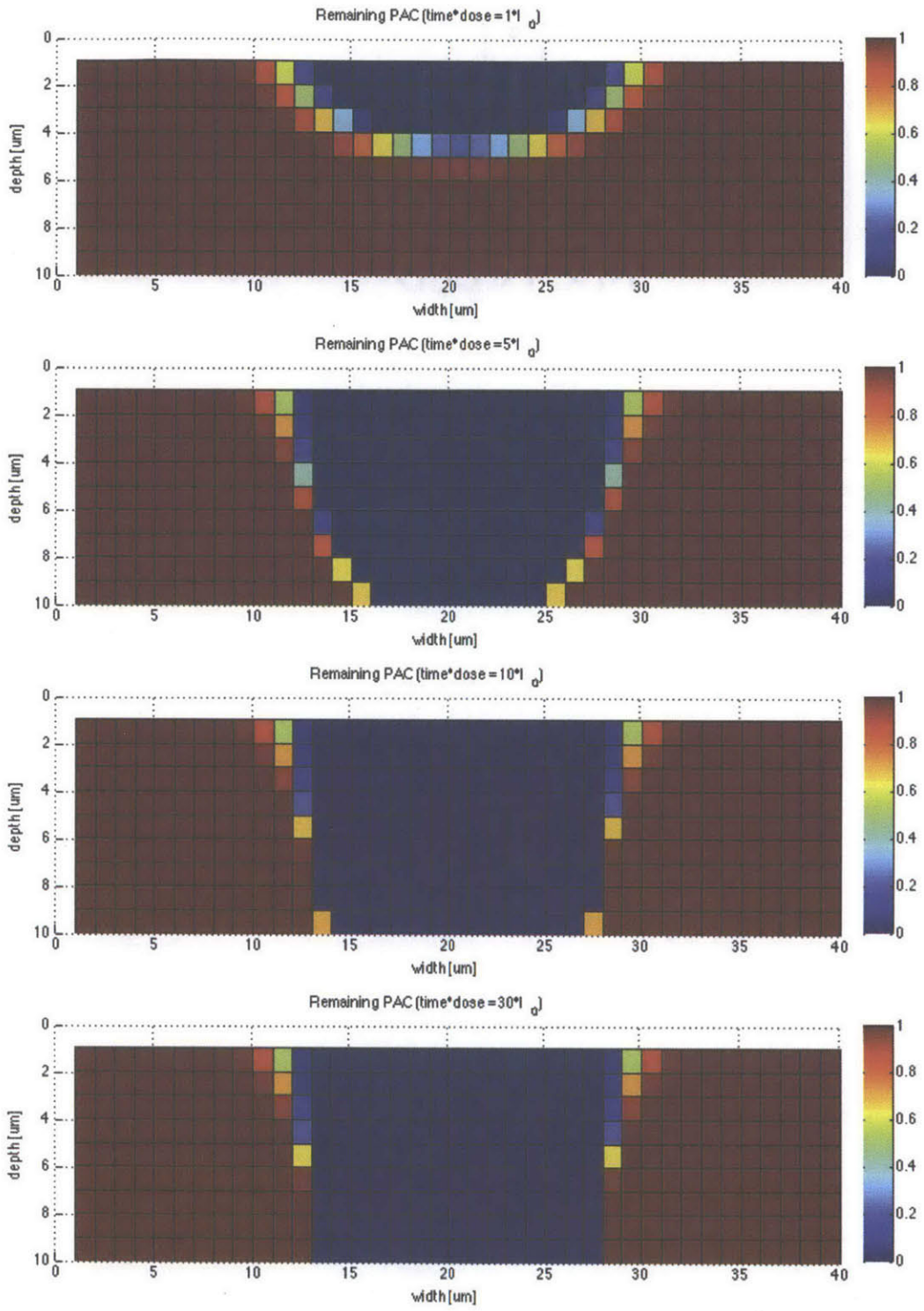


Figure 3.16: Result of the simulation for AZ 9260. Exposure durations $t = t_0 + 1, t_0 + 5, t_0 + 10$ and $t_0 + 30$ in 1 msec intervals for a beam with a waist of 5µm and 80mW laser power. The simulation showed nearly straight sidewalls, as the low absorption attenuates light less significantly when passing through the material.

## 3.6 Conclusion

An introduction was given to photolithography as a means of patterning flat surfaces with micro- to nanoscale resolution. A model was presented to describe the photocuring mechanism experienced by the material upon irradiation. A Gaussian beam was modeled as an exposure distribution. Parameters were derived for exemplary positive photoresists. The exposure process was modeled for both photoresists, using said Gaussian beam as a theoretical means of irradiation. An analytical simulation shows theoretically achievable geometries for different energy levels.

# Chapter 4

# Cylindrical Thick-Film Structure Fabrication

The theoretical projections demonstrate a great potential for versatile stamp feature fabrication. To enable large-scale, continuous microcontact printing, not only the laser-lithographic process needs to be understood, but also it needs to be paired with a scalable tool fabrication process.

In the following, the laser direct-write lithography process that was modeled in Chapter 2 is applied to the cylindrical photolithographic apparatus. A system model is created and a framework of experiments is constructed to validate and characterize the lithographic process in the unexplored context of this cylindrical apparatus. The results of these experiments are extracted to yield information about the limits, the sensitivity to certain parameters and the versatility of the process, as well as the performance of the apparatus with regard to the creation tools that enable the scale-up of a robust roll-based microcontact patterning process.

## 4.1 Laser Direct-Write Lithography for Seamless Tools

To create a viable and scalable process for fabricating continuous tools that allow for a robust and scalable microcontact printing process, the photolithographic process model needs to be verified using the centrifugal casting system. The following set of experiments was proposed to verify the analytical results extracted from both the concept centrifugal photolithography tool fabrication process, which is essentially a non-planar substrate, and from the advanced investigation into laser-lithographic cross-sectional geometry generation.

The direct lithography process allows for more degrees of freedom than classic photolithography with a mask. In addition to the size and intensity of the laser beam, which affects the size of the formed features, its vertical focal position affects the geometry of the formed features. As sidewall angles are affected, this shift critically affects the stamp features' stability, i.e. their resistance to buckling, and thus the robustness of the printing process with the produced tool.

## 4.2 System Architecture

The simulation in the previous chapter assumes ideal conditions. The photolithographic process is sensitive to certain parameters. Based on these, the weak points of the experimental apparatus are determined to design experiments for investigating the process.

### 4.2.1 System Model

The exposure physics discussed in 4.1 contribute most significantly to the final result of the patterning process. The unusual substrate, which differs substantially from much more common silicon wafers, presents an unexplored factor to the system, both in mechanical and optical aspects.

The final feature geometry depends not only on the exposure energy distribution and dose, but also on the thermal and chemical processing of the photoresist prior to and following the exposure process. As mentioned in 3.3.1, the baking temperature and the duration the material experiences an elevated temperature can impact the sensitivity, partly decompose, or provide the material with insufficient reactant for concurrent or subsequent process steps.

A chart summarizing process variable interrelations is depicted in Figure 4.1.

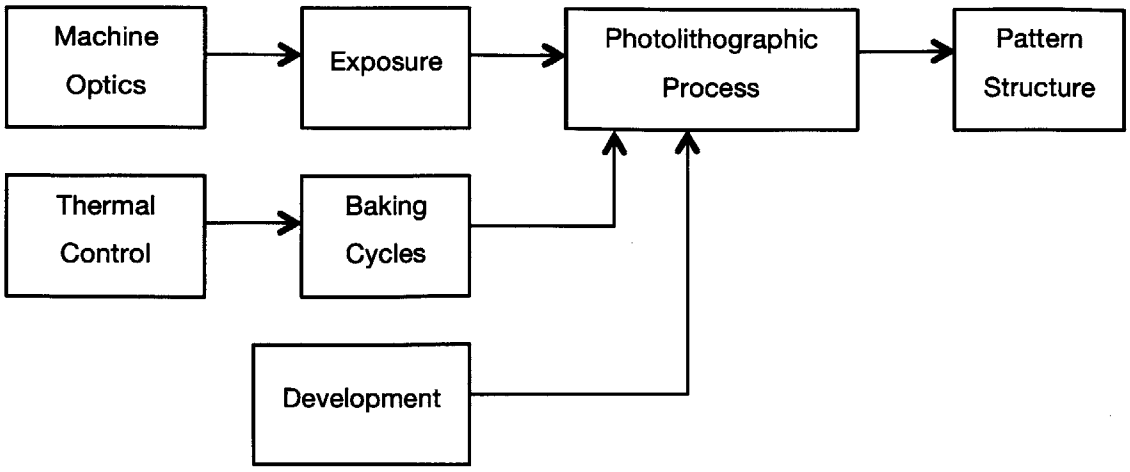


**Figure 4.1: Block diagram of important process mechanisms and potential sources of variation. The optics of the machine determines the exposure. Viable control is required to control baking and development, which affect the sensitivity of the resist. The photolithographic process, which is subject to all these variables, determines the final structure of the created pattern.**

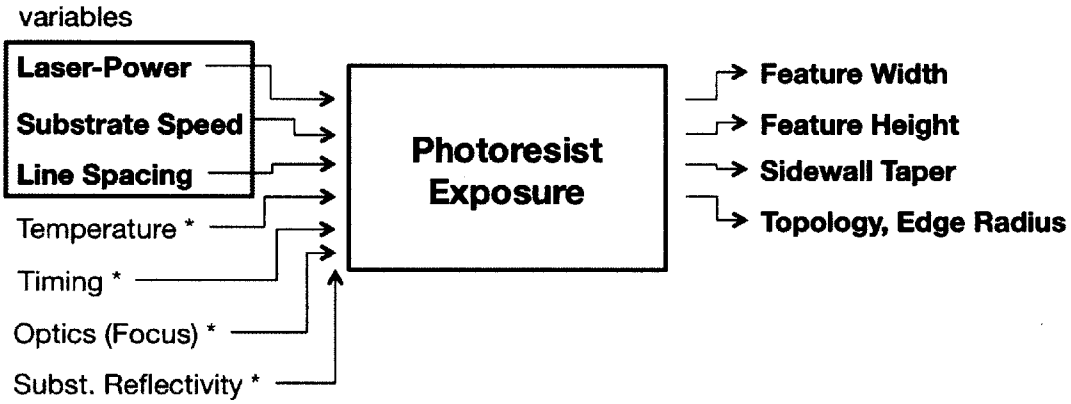


**Figure 4.2: Process variables in the photolithographic process. The conducted experiments examine the effects of laser power, substrate speed and line spacing on the resulting feature geometry and dimensions.**

This work examines the boundaries and the sensitivity of this patterning step to process parameters such as exposure dose, exposure rate, film thickness and substances used (see Figure 4.2).

Exposure mechanics as reviewed in the previous chapter, are the prominent factor in the formation of the features. The exposure dose is the energy that the resist receives at the wavelength that it is sensitive to. It is made up of the time integral of the laser irradiation at a

location. For a beam that moves relative to the substrate at a constant speed $v$, the cumulative exposure along an infinitesimal section of the path of the laser over the substrate is given by:

$$\int_w E = \frac{P}{v} \tag{4.1}$$

where $P$ is the laser power and $E$ is the exposure energy.

As the marginal edges of the Gaussian shape of the beam are non-zero, they can add to the exposure energy when nearby another line or feature. Since the product of the chemical reaction that takes place in the photoresist upon exposure is maintained over time, the 'tails' of the Gaussian beam have an effect on adjacent exposed regions. This effect is also known as the proximity effect. Since both Gaussian functions in each location add up, the sum of the energy introduced to the substrate between them is higher than just one marginal edge of the Gaussian beam alone. In effect, this can increase the minimum feature size and limit the minimum spacing between exposed regions.

### 4.2.2 Error Budget

The apparatus used to verify the robustness of the lithographic process incorporates a simplified version of a laser-lithographic system, paired with a horizontally oriented cylindrical centrifugal casting base. For the patterning step, a linear stage is used to position the laser and optics parallel to the axis of rotation of the drum, while incremental rotation of the drum is used for positioning in the radial direction. The laser is fixed on the stage and can be manually adjusted in both its height and angle relative to the axis of motion of the stage for initial alignment. The optics, comprising a lens and a mirror, and the centrifuge, driven by a motor, are mounted on three-ball kinematic couplings. The structural loop is shown in Figure 4.3.

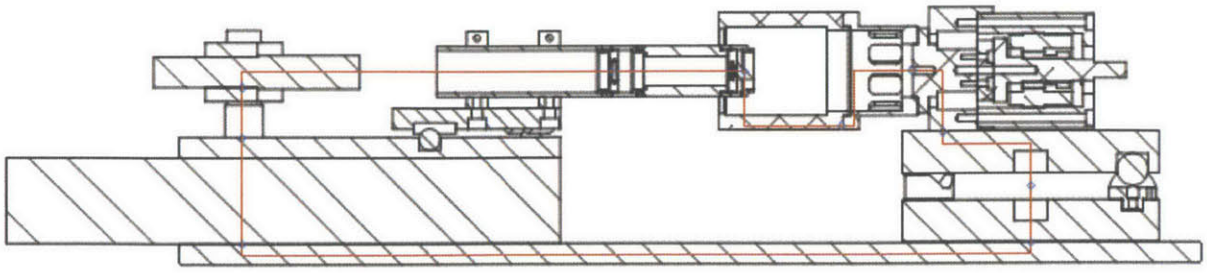

**Figure 4.3: The structural loop of the apparatus. Interfaces (illustrated above) present eminent sources of error.**

Although no additional load is generated during the process, even small displacements may significantly affect the precision of the process. During the cast of the layer of photoresist, a taper or eccentricity of the drum would introduce great thickness variations. The underlying layer of floor-exposed photoresist prevents such failure.

To further ensure uniform exposure, the focal range needs to be in the same vertical position with respect to the drum. No auto-focus system is included in the concept apparatus, thus no closed-loop control accounts for errors in focus. Therefore, the trajectory of the stage has to be parallel to the lower section of the drum. Error modes are illustrated in Figure 4.4.

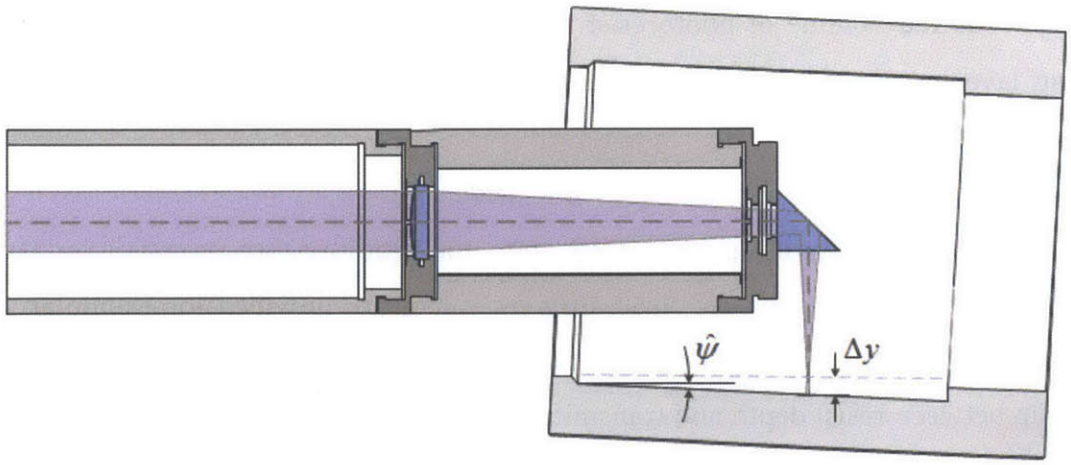


**Figure 4.4: Influence of alignment of focus. A deviation in the position of the drum can affect the focal point to the beam relative to the layer of resist inside the drum.**

Since the optics are not mounted directly to the laser, but separately on a three-point kinematic coupling on the same linear stage, a deviation of the position of the optical components from the actual path of the beam cannot be fully prevented. The most likely consequence of such a displacement is unanticipated optical effects, notably spherical aberrations, which can result in a focal shift.

The high transparency of the SU-8 planarizing layer may introduce further variation by allowing reflection of the laser beam on the reflective aluminum drum interface.

## 4.3 Design of Experiments for Thick-Film Patterning

To explore the boundaries of the photolithographic process in the apparatus and to verify the parametric model, experiments were constructed with varying exposure dose, substrate speed, and film thickness using two different positive-tone photoresists.

### 4.3.1 Approach

A series of experiments were carried out to characterize the cylindrical patterning process. To inform these experiments the model developed above was used to determine the range of layer thickness and energy levels to be investigated.

The required volume of photoresist for obtaining an average film thickness $\bar{h}$ of the patterning layer can be calculated with the surface area of the drum, $2\pi r l_z$, and the solids content of the resist, $\beta$:

$$V = \bar{h} * \beta * 2\pi r l_z \tag{4.2}$$

The exposure dose is approximated from the requirements provided by the resist manufacturer. For SPR 220 and AZ 9260, discrete values are provided for exemplary typical thicknesses, which can be mapped to an exponential function, due to the exponential relationship between resist depth and transmitted irradiance.

As shown in 3.3.1.3, the relationship of depth of penetration and exposure dose can be described using the following expression:

$$\frac{d_r(E)}{d_c} = \gamma \ln\left(\frac{E}{E_c}\right) \tag{4.3}$$

where $d_r(E)/d_c$ is the fraction of the remaining unexposed resist depth, $E/E_c$ is the delivered portion of the energy dose necessary to render the full thickness of the resist dissolvable, and $\gamma$ is the gradient of their relationship on a logarithmic plot, known as the contrast of the resist.

For SPR 220 and AZ 9260, the relationship of exposure energy dose and thickness of dissolved resist for a specified development time was determined using energy dose values given by the photoresist manufacturer [85], [86]. A plot is shown in Figure 4.5.

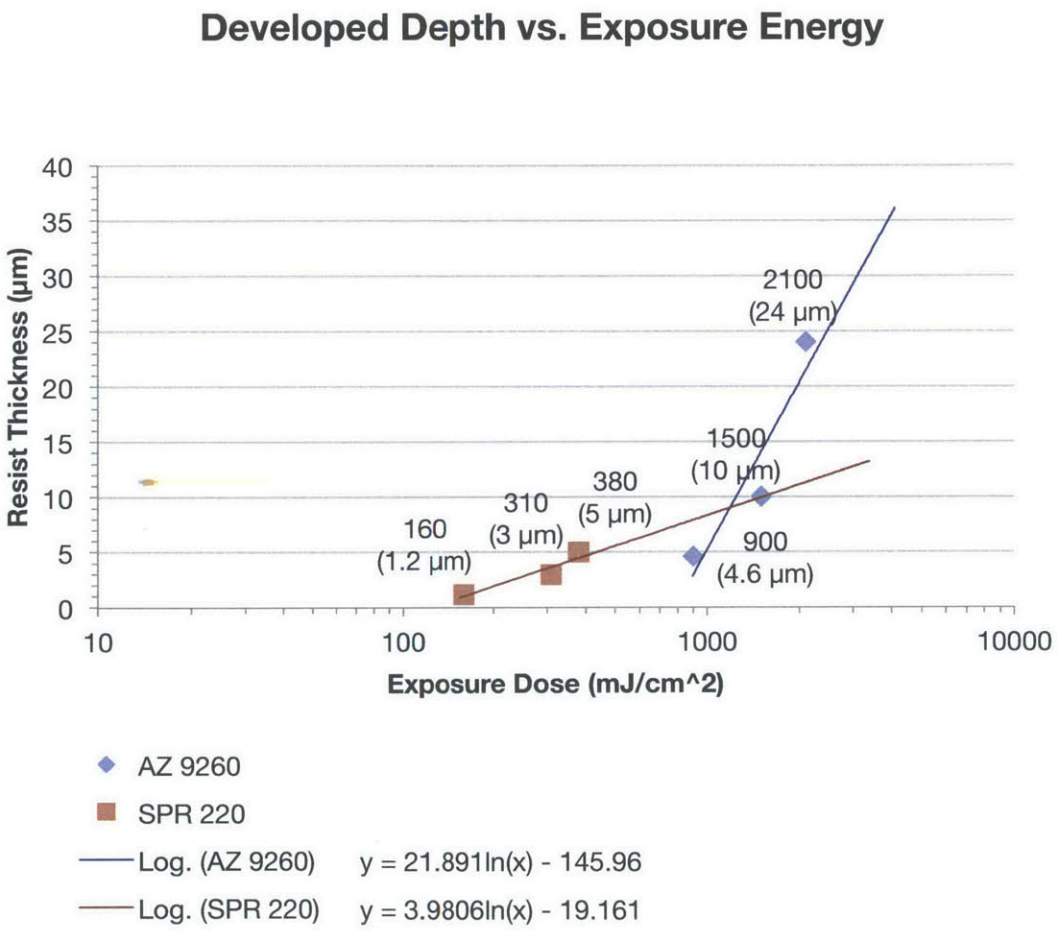


**Figure 4.5: Photosensitivity and model of SPR220 and AZ 9260. Extracted from data given in the manufacturers' data sheets [85], [86].**

### 4.3.2 Procedure

All experiments were conducted in a setup consisting of a centrifugal casting drum, a thermal management system, and a linear stage with interchangeable optics, ventilation and LED exposure modules. The drum, 52.8 mm in diameter and 60 mm in length, is designed for rotational speeds up to 400 rad/s. The optics module comprises a lens and a mirror to focus the laser beam on the inner surface of the drum. The thermal management system consists of a heat gun directed at the drum and a fan adjacent to the motor and bearing housing of the centrifuge. A non-contact temperature sensor is pointed at the drum to control the temperature. The setup is shown in Figure 4.6.

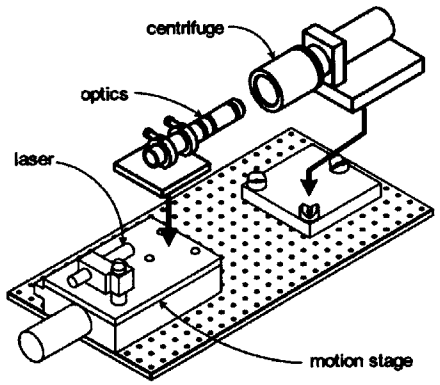


**Figure 4.6: The experimental setup. It contains the centrifugal drum, a laser with optics, and an LED for flood curing (replacing the laser optics) as well ventilation for cooling (reproduced from Figure 2.5 for convenience) [41].**

The drum's inner surface was bare Aluminum with a 5 – 15 μm planarizing layer of SU 8. The SU 8 planarizing layer withstands organic solvents and does not degrade notably. Thus, it could be reused over several experiments without a loss in quality.

The general operating procedure for the photolithography experiments is conducted as follows:

a. Clean surface using acetone and dry.
b. Insert solution of photoresist and solvent and spin for the liquid to spin out evenly.
c. Still spinning, evaporate solvent and softbake. A ventilating module consisting of a fan and a tube is mounted on the linear stage and moved inside the centrifuge to create a high-velocity air flow surpassing the resist film.

d. Cool down and allow for rehydration.
e. Expose the photoresist selectively using aforementioned laser and optics (see Appendix A.2).
f. Optional: Post-exposure bake.
g. Develop under a stream of developer. Immediately agitate in DI water. Use compressed air to dry.
h. Cast degassed PDMS. Spin, then cure PDMS under heat.
i. Remove the cast cylinder and examine longitudinal sections under an optical microscope.

For numeric values, see Appendix A.1.

Variations are introduced in (1) exposure dose, (2) exposure rate and (3) photoresist volume to find a general method for parameter selection to achieve a desired, arbitrary pattern.

### 4.3.3 Table of Experiments

The purpose of this work is to find how the exposure speed, resist thickness and laser power affect the resolution limits for a given resist in the centrifugal lithography apparatus to examine the boundaries of such a technology in enabling a scale-up of microcontact printing.

The experiments were designed to account for possible shortcomings of the machine for repeating the process. For example, the diode laser power was kept constant to avoid temperature dependent power fluctuations. Accordingly, the substrate speed was varied to vary the dose.

To account for the errors of the system, in particular axial variations in the machine geometry, the speed was varied in intervals (sections) along the length of the drum. Continuous lines were chosen maximize the comparability of results and to facilitate their extraction, as illustrated in Figure 4.7.

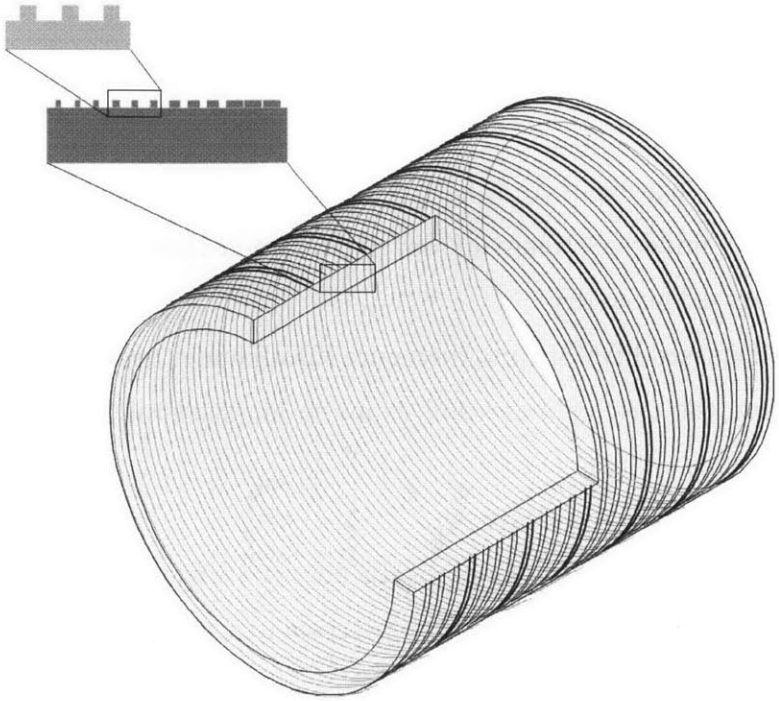

Figure 4.7: For any resist film thickness, the experiment comprised multiple line arrays (sections) with different substrate speeds. Each speed was applied for 3 rotations.

For the two resists, this approach led to the experiments summarized in Figure 4.8.

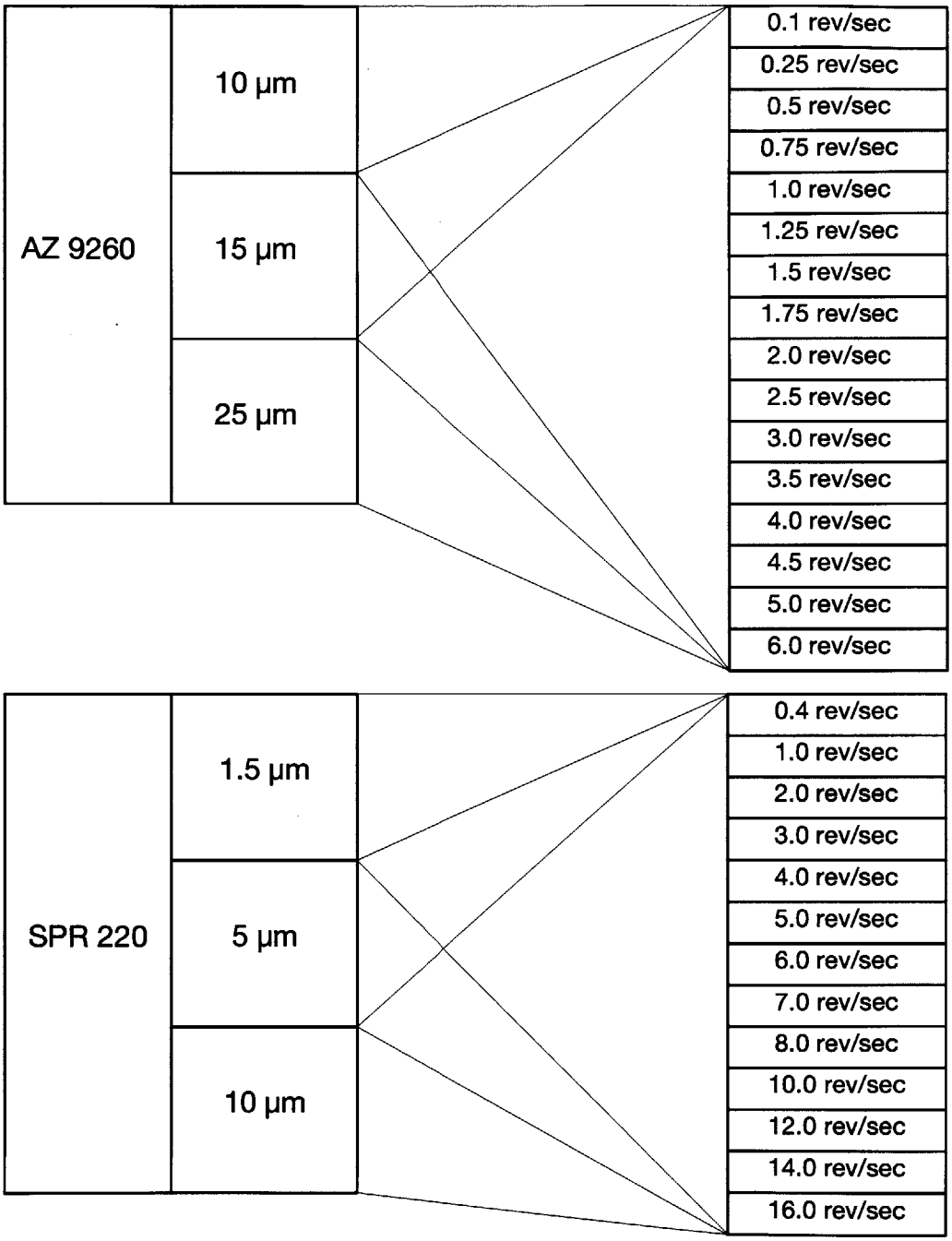


**Figure 4.8: Proposed experiments. For each photoresist film thickness, lines were written at a range of speeds. SPR 220 is more photosensitive than AZ 9260 and requires around thrice the exposure dose for achieving the same depth of penetration.**

Each of the different speeds was written on the resist for three complete, non-overlapping rotations of the tool. In an experiment with 15 different speeds, this resulted in 45 separate circumferential features. In turn, this set of 45 lines was repeated at 10 different axial locations along the cylinder evenly spaced from the inner, cantilevered end to the outer end of the drum. In this way, both the effect of exposure and machine precision effects could be evaluated.

## 4.4 Feature Formation Results

The experiments were conducted following the protocol in Appendix A.1 for SPR 220 and Appendix A.2 for AZ 9260.

The geometry of the produced lines was then measured via centrifugal-cast PDMS, using a white light interferometer and optical microscopy. The cast parts were sectioned longitudinally using a razor blade at three evenly space angles, as shown in Figure 4.10. The sectioned tools were then placed in an optical microscope (LW Scientific) and projected on a CCD camera (9.6 pixel/μm using a 40x objective). For each feature on the tool, the root width and top width were measured, along with a maximum feature height and sidewall angle. These quantities are illustrated in Figure 4.10.

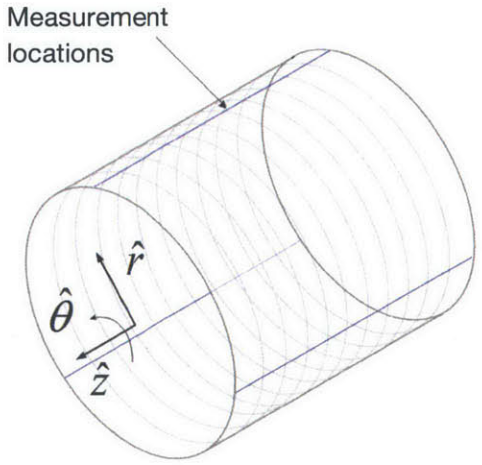


**Figure 4.9: The line cross-sections were measured by longitudinally sectioning the PDMS stamp in three slices.**

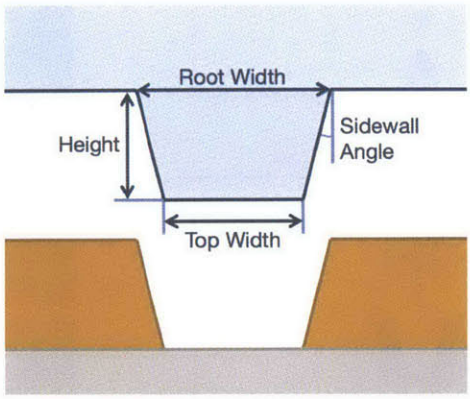


**Figure 4.10: Nomenclature for the interpretation of the experimental results.**

A white-light interferometer (Zygo) was used to investigate the topology of the created pattern and to verify the thickness of the pattern.

### 4.4.1 Medium Contrast Resist (SPR 220)

SPR 220 (Dow Corning) is a general-purpose thick-film positive photoresist. The experiments were conducted with SPR 220-3.0 with a medium viscosity, thinned with a 2:1 solution of ethyl lactate (Sigma Aldrich) and anisole (Sigma Aldrich). Following exposure, the pattern was developed using MF-24A developer (Dow Corning).

Early experiments conducted with SPR 220, following the procedure described previously, revealed that SPR 220 has no clear exposure cutoff. A range of exposure intensities was found for which there was a feature, but it was insufficiently developed. The erased material, which translates to a feature in PDMS in the stamp-casting process, was round and could not reach the underlying layer of SU 8.

SPR 220 also showed considerable effects of dual-tone behavior or burning upon over-exposure. Once a threshold exposure dose is reached, the state of the material turned from soluble to insoluble again, showing a "dented" topology in the resulting stamp. Finally, the exposure of SPR 220 was not fully time invariant. If exposure happened faster, the required energy per surface area was reduced.

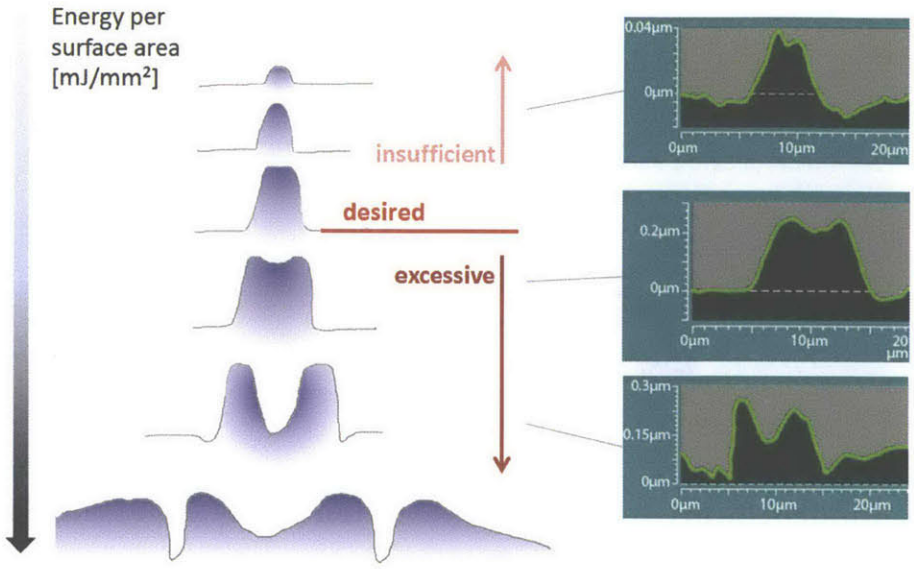


**Figure 4.11: Change in feature cross-section for SPR 220 feature formation for varying exposure energy levels.**

The experiments confirmed that for increasing substrate speed and thus decreasing energy dose, the width of the produced feature decreases. Below a certain threshold energy dose, the cross-sectional shape of the formed feature did not reveal a flat top with distinct edges to the feature sidewalls, but instead a round feature. The height of the feature did not immediately decrease, indicating that the SU 8 layer was still reached.

Figure 4.12 shows the result of an experiment with different substrate speeds and a film thickness of 5 µm, extracted from all angular drum positions for three evenly spaced sections. The data points each represent the mean value for each given speed.

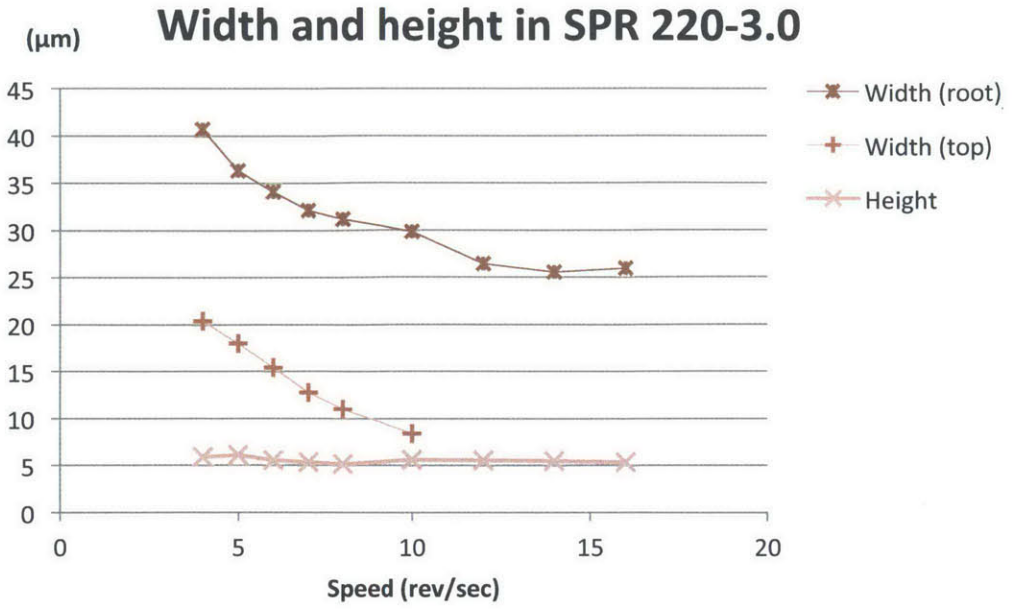


Figure 4.12: Width and height of features formed in SPR220 (thickness: 5 μm). Burning or dual-tone effects were visible at speeds lower than 10 rev/sec, creating a narrow process window.

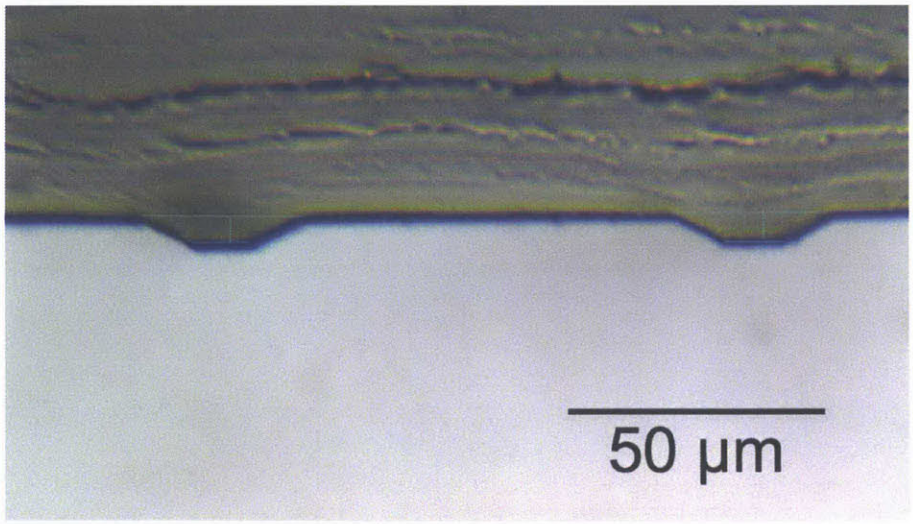


Figure 4.13: A typical stamp created with a SPR 220 pattern. Cast into the resist photoresist master the stamp replicates its pattern and serves as an intermediate in evaluating the photolithographic process. With SPR 220, straight but highly angled sidewalls were formed. The image above shows the features formed for 8 rev/sec. At the printing side, the feature of the stamp has a width of 11 μm at a total height of 5.1 μm.

### 4.4.2 High Contrast Resist (AZ 9200)

AZ 9200 is a high-contrast thick-film photoresist, recommended for film thicknesses between 5 μm and 25 μm. Its Dill A and B values are given with 0.37 and 0.01 respectively. The resist was chosen since it is known to produce a good contrast and precise edges when omitting the optional post-exposure bake. The experiments were conducted with AZ 9260.

For a given film thickness, the exposure dose determined the size of the produced features. Below a threshold dose, no feature was produced, a feature of a high contrast resist. A higher volume of photoresist produces a thicker film and thus higher features, but also requires a higher energy dose for producing features of the same width. This mechanism is illustrated in Figure 4.14. As determined, a greater volume of photoresist produces a smaller line width for the same writing speed – but it is worth noting the minimum width (root) cannot be reduced by applying a greater volume of the resist.

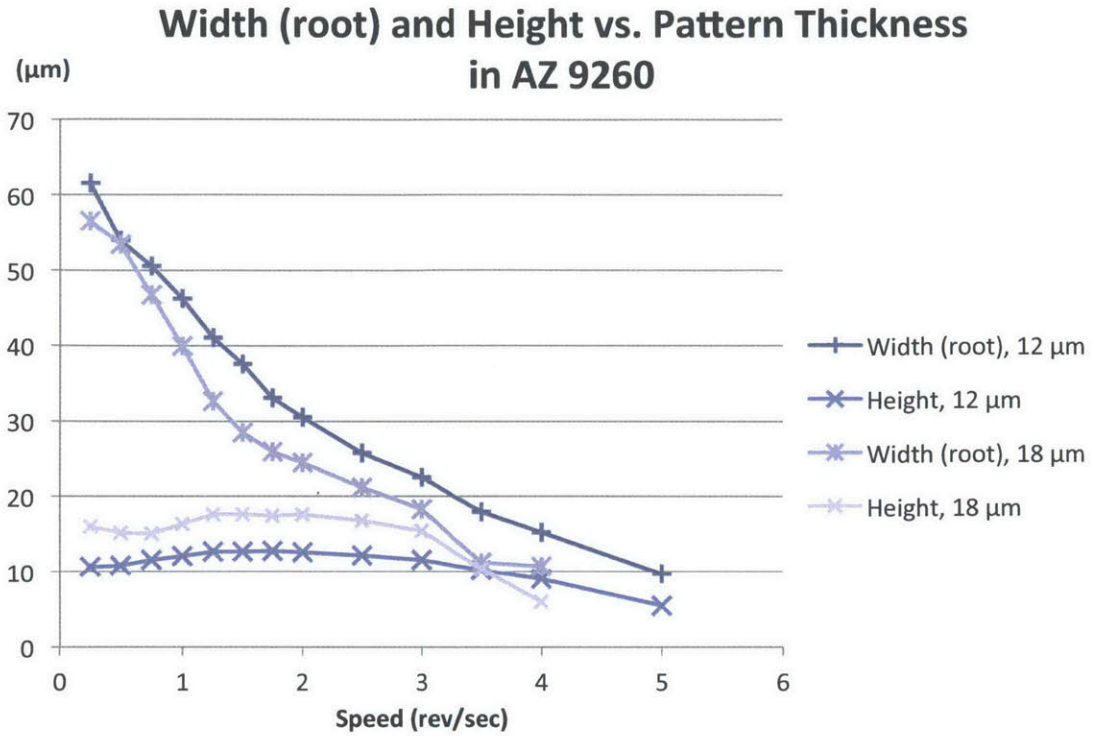


**Figure 4.14: Feature height and width comparison for different film thicknesses in AZ 9260.For an increase in speed and thus a decrease in energy dose delivered per unit of surface area, the width of the produced feature or line decreases as expected. By the height of the created feature or line, it can be seen that not only a lack in energy decreases effective feature height, but also an excess of energy.**

The observed reaction cutoff of AZ 9260 was very precise. If the exposure dose was below a certain threshold, no feature was produced, if it was above that threshold, the produced feature had a minimum width and height, and spanned the full film thickness.

Also evident from Figure 4.3 is that dose has a much stronger effect on width than height, which may be due to scattering from excessive energy delivered once the SU-8 layer is reached and to accumulating energy delivered by the less intense margins of the Gaussian beam. From an operational perspective this means that width can be modulated with dose and not just with beam width.

AZ 9260 did not exhibit any dual-tone effects. A higher exposure dose increased the feature width until adjacent features merged; a width range up to 100 µm could be observed in

thicknesses below 10 μm. In higher thicknesses, the resist "burnt" before the necessary exposure dose was reached to expand the reaction further to either side of the incoming beam.

The effect of the system accuracy can be seen in a series of images of the cross-section for a constant speed of 2 rev/sec for the 10 sections along the drum axis, displayed in Figure 4.15.

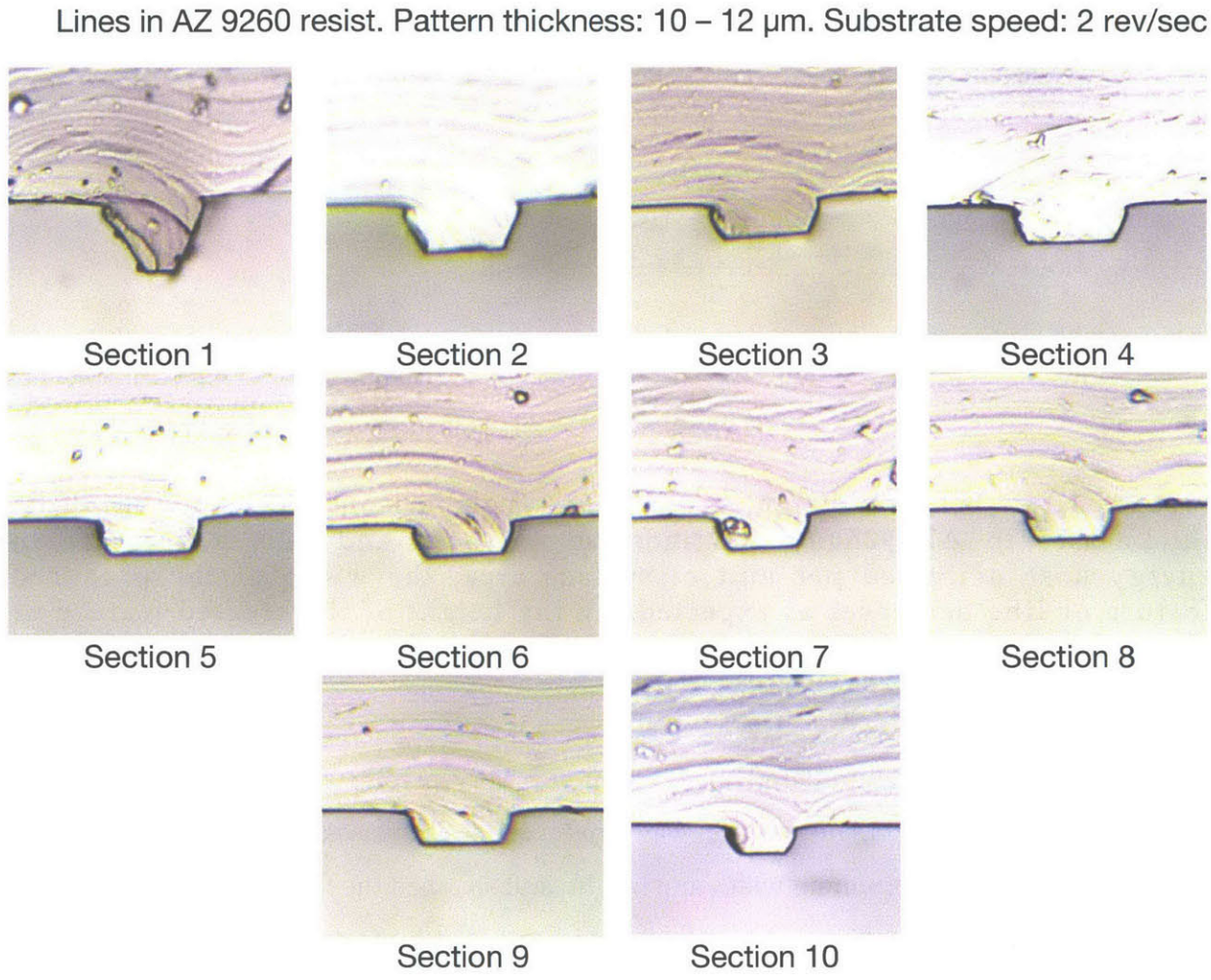


**Figure 4.15: Section comparison, fixed energy dose. The combined effect of focus (10) and film thickness (1, 2) produce an extended morphology for a common speed of 2 revolutions per second for 0.32 ml AZ9260.**

#### 4.4.2.1 Boundaries

For most features aspect ratios of 1:2 were achieved, which are considered high for this application. Figure 4.16 shows a feature cross-section with 11 µm feature height and 14.5 µm width on the top of the feature.

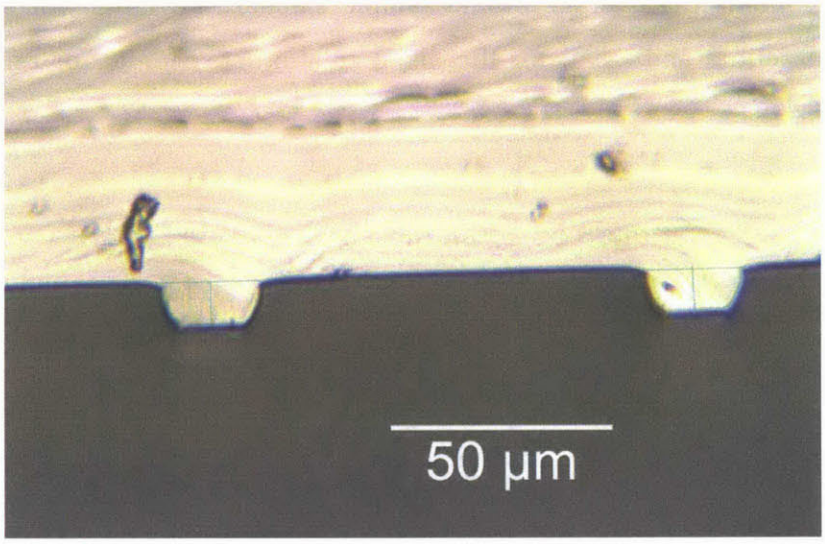


**Figure 4.16: Exemplary cross-section of features produced with AZ9260. The depicted geometry shows 14.5 µm top width for 11 µm height produced at 3 rev/sec.**

As shown in Figure 4.3, the width of the features shows a strong dependence on exposure energy. Furthermore, for both excessive and insufficient exposure energy, the process became prone to an increased variation. Different factors were identified as a reason for the observed variations for under- and over-exposure. In over-exposure (low speeds), the line width increases as a result of (i) irradiation by the less intensive part of the Gaussian beam outside its nominal radius, which are characterized by a low signal-to-noise ratio and (ii) reflections, which vary greatly in their effect. For under-exposure (high speeds), the resist is not fully saturated and the formation of a feature can vary greatly with subject to the contrast curve of the resist.

A range could be identified with medium to low variation, where the proportion of the standard deviation of the height and root width relative to the respective mean value was minimal and rose at an increasing rate to either side of this range. For each speed, the standard

deviation and mean value for both the width (root) and height was calculated for each section along the drum axis to account for a taper in the drum. For both width and height, the total relative error for each speed was derived as the mean of the relative error of all sections. For 0.32 ml (10 μm height), the range of least relative error for both the width and the height of the produced feature was identified as speeds between 1 rev/sec and 2 rev/sec (see Figure 4.17). In this figure each point is the average of the sample standard deviation for all measurement locations (circumferential and axial) for the given rotation speed, and for one film thickness (12 μm).

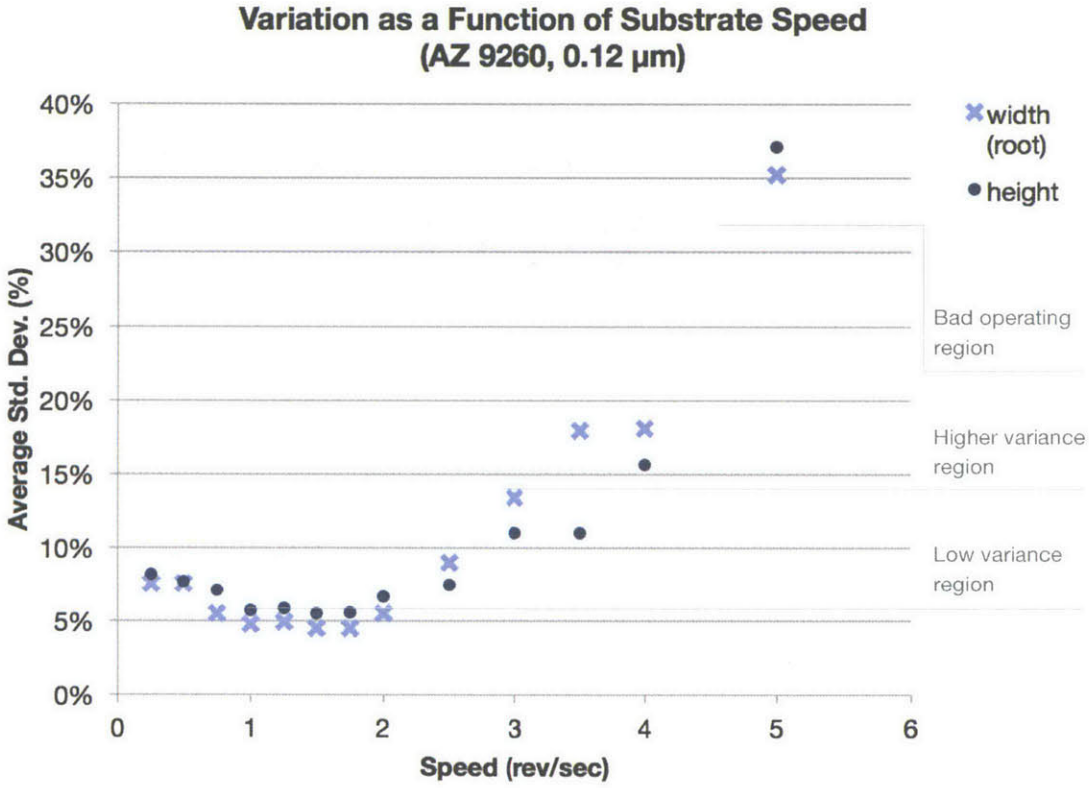


Figure 4.17: Optimum process parameters with regard to minimizing variation. The experiment with 12 μm AZ9260 showed minimum relative standard deviation (i.e. standard deviation per average value) for the width (root) and height of the formed features for speeds between 1 and 2 rev/sec, achieving 12 μm height and feature top widths between 17 μm for 2rev/sec and 35 μm for 1 rev/sec.

### 4.4.3 Comparison with Simulated Results

Contrasting the experimental results with the simulation (see 3.5), good conformity is seen for both types of photoresist. SPR 220, absorbing about twice the fraction of the incoming light as AZ9260, degrades faster in the top layers, resulting in a wide root width in the resulting PDMS stamp feature. AZ9260, a thick-film resist, absorbs a significantly smaller fraction of the incoming light, so that a greater fraction can penetrate the material and form a tall feature with steep sidewalls. Figure 4.18 contrasts the simulated and experimentally achieved feature cross-section of both resists.

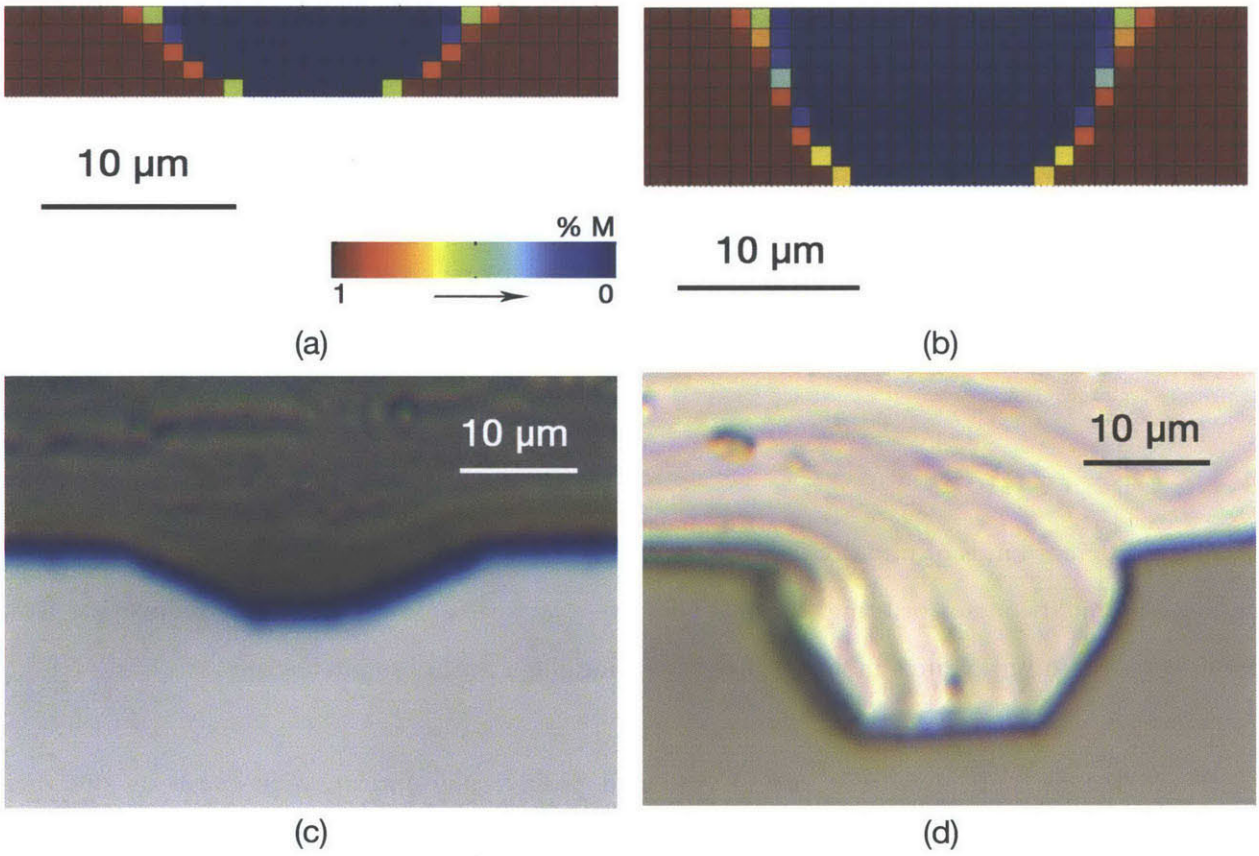


**Figure 4.18: Simulation versus experimental results for AZ9260 (a, c) and SPR 220 (b, d). Although the simulation (a, b) can not predict the required exposure dose, the achieved cross-sectional geometry (c, d) could be approximated.**

The experimental results can be can be reduced to a few important factors for contrasting AZ9260 and SPR 220. Table 4.1 lists characteristic distinctions that were found and could be confirmed.

**Table 4.1: Comparison between the two positive-tone photoresists**

| SPR 220 | AZ 9260 |
|---|---|
| *(i)* Higher concentration of photoactive compound necessitates less exposure dose | *(i)* Lower concentration of photoactive compound necessitates greater exposure dose |
| *(ii)* Finer achievable resolution | *(ii)* Less precise achievable resolution |
| *(iii)* If dose was insufficient to bleach through layer, produced features were round but similar in height | *(iii)* If dose was insufficient to bleach through layer, produced features were much smaller or nonexistent |
| *(iv)* Overexposure immediately burns material | *(iv)* Overexposure forms wider features |
| *(v)* Big sidewall angles | *(v)* Almost vertical sidewalls, small sidewall angles |

### 4.4.4 Observations

Two different kinds of photoresist were tested in their ability to present a patterning material for continuous microcontact printing stamps. They were compared in their capacity to provide for a robust process and to create a mold for high resolution, high fidelity stamp features.

Even though both photoresist are DNQ-based positive photoresists, their behavior and their feature formation boundaries showed distinct characteristics. In particular, SPR 220 exhibited a very narrow process window due to burning or possible dual-tone effects in the overexposed state. By contrast, a better resolution was achieved than with AZ 9260. A likely reason for this distinction was the higher density of photoactive compound in SPR 220, which reduces the necessary exposure dose, but increases the process' sensitivity to insufficient ambient water and other factors [64].

The series of experiments captured a variety of process correlations which can both be helpful in quantifying the ultimate limit of the system and point out factors causing those limits.

The following observations were made:

Focus is critical. A deviation in focus can not only affect sidewall angles, but also eliminate any flat surface capable of carrying ink in a controlled manner. For lower exposures, features exhibit a circular shape with a negative initial sidewall angle. For medium exposures commonly regarded stable, a triangular shape can be identified. High exposure doses create wide and round feature cross-sections for unsuitable focus.

Excessive exposure leads to burning and again a decline in dissolvability of the positive resist. If too much energy is introduced into the material, not enough water is available for the photo-initiated reaction to happen, and the material burns and develops bubbles. Bubbles are also seen as a result of disproportionally high pre-bake temperatures.

Lower exposure energies may be insufficient for the material to develop throughout the thickness of the photoresist layer and reach the underlying substrate. In this case, the top of the feature is not flat, but round. The radius and width largely depend on the width of the beam when it impinges on the substrate. Therefore, an in-process control and actuation system for the focal position (auto-focus), allows for a large numerical aperture (NA) and compensates for deficiencies in co-linearity between the exposure system trajectory and the substrate. Hence, it can contribute towards improving the feature size achievable by the system.

### 4.4.5 Optimum Parameters

A desirable outcome satisfies an ideal factor combination to produce a tool that is optimized for large-scale roll-based microcontact printing. Such a tool embodies the following characteristics:

*(i)* Reliable feature generation. To minimize undesired variation in the produced tool geometry, it is imperative that a given energy dose translate to a specific feature geometry.

*(ii)* Fine resolution. One of the strengths of microcontact printing is its achievable resolution, and in many applications, small line-widths increase the efficiency of a device or surface structure.

*(iii)* Large aspect ratio. Tall features increase the critical printing force that leads to roof collapse, creating a larger working range of the acceptable printing force.

*(iv)* Moderate sidewall angle. Where vertical sidewalls are prone to lateral feature displacement and buckling, a small sidewall angle provides additional mechanical stability without increasing the minimum feature size. A large sidewall angle negatively affects the ink deposition by acting as an extended reservoir and by greatly increasing the susceptibility to bulging.

*(v)* Small edge radius. As shown in 0, flat tops and small edge radii promote precise dosage of the deposited ink. Therefore, a minimum edge radius is recommended in tools for large-scale microcontact printing.

An optimum feasible feature is presented in the following. To satisfy *(iii)* and *(v)*, a photoresist needs to be optimized for a film thickness that exceeds the resolution achievable by the optical system. Accounting for possible misalignment in the apparatus, a small numerical aperture maximizes the depth of focus in the exposure system used, at the expense of minimum beam width and thus of achievable minimum line-width. Thus, to create steep sidewalls and a large aspect ratio, a high-contrast thick-film resist is preferred.

To satisfy *(i)*, favorable process parameters need to be chosen. As shown previously, minimum variation occurs between 1 rev/sec and 2 rev/sec for a photoresist volume of 0.32 ml. Within this range, the resolution is maximized with the highest substrate speed.

Leveraging the moderate variation in focus position and resist thickness (see Figure 4.15), favorable geometries can be identified. An example is depicted in Figure 4.19.

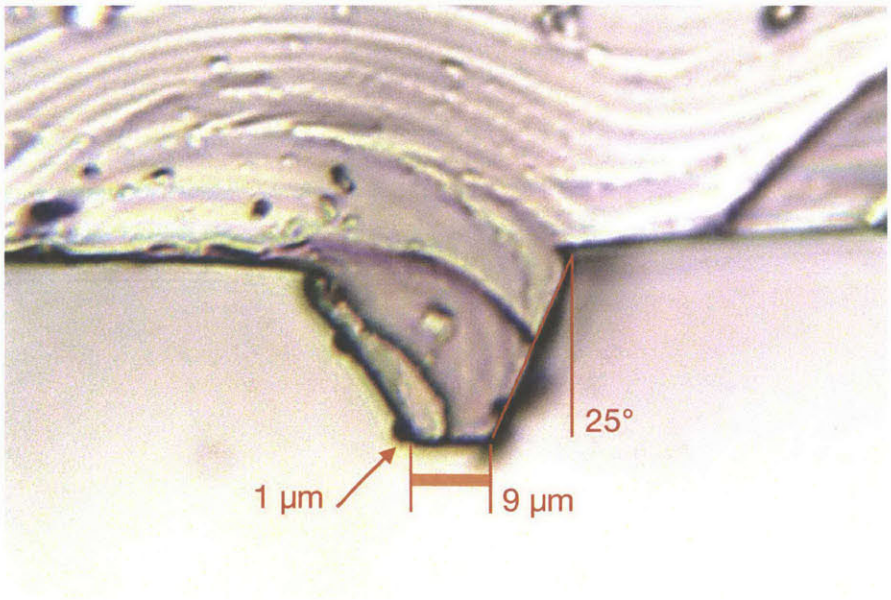


**Figure 4.19: Cross-sectional geometry optimized for large-scale microcontact printing. Tall features (25 µm) prevent ink dripping or roof collapse. With a tip width of 9 µm, an aspect ratio of ≈3:1 is achieved. A moderate sidewall angle of 25 ° stabilizes the feature laterally without affecting the ink deposition behavior. The edge radius of 1 µm is to be minimized to ensure optimal ink deposition.**

The feature shown in Figure 4.19 depicts the best aspect ratio achievable with the current systems, limited primarily by the laser beam width. If wider features are required, exposing adjacent and overlapping regions may, because of the high contrast of AZ 9200 resist, lead to wider features with similar sidewall angles.

## 4.5 Macroscopic System Characterization

As discussed in 4.3.3, the various dose level arrays (created by varying the rotation speed) in Figure 4.8 were repeated 10 times at different evenly spaced axial positions along the tool. This produced a total of 450 lines, which allowed for conclusions on the geometric layout of the system and variations in the instrument paths. Each created with identical input parameters for power and speed, the repeating experimental setup provides an extra dataset for drawing experimental conclusions on the drum and SU 8 geometry and topology. Figure 4.20 illustrates the locations on the inside of the drum, replicated as the exterior of the stamp, where the measurements were taken.

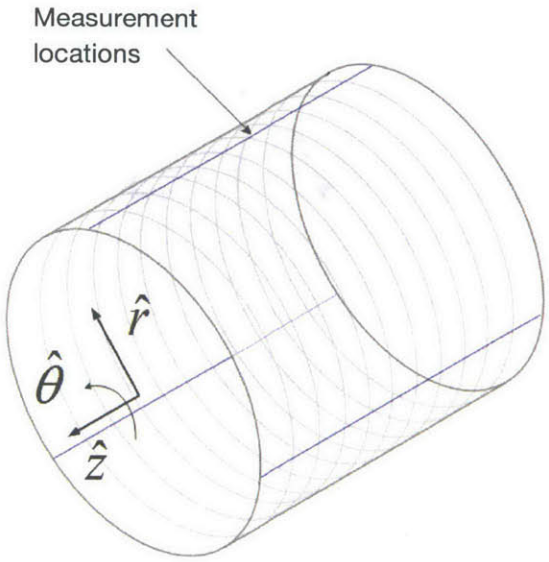


**Figure 4.20: Measurement locations. The cross-sections of the lines, which spanned the circumference of the drum, were measured at three different locations, 120° apart. This enabled to deduce the centricity and taper of the drum.**

### 4.5.1 Concentricity

A cylindrical centrifuge, centricity and parallelism play a major role in consistent feature formation. As the centrifugal force scales with the square of the distance to the axis of rotation, eccentricity causes uneven film thickness, which results in a variation not only in feature height, but also in the feature width produced, which (i) introduces a variation in stamp elasticity and thus required print force to the microcontact print process. The frequency of this variation can be greater than the bandwidth of the system above a certain line speed. Also, (ii) if the width of the created features deviates, the subsequent pattern may not produce an acceptable result. (iii) With a variation in film thickness or an eccentricity of the centrifuge, the focus may deviate, producing significantly different feature shapes and sizes that potentially deviate in inking and dynamic behavior, thus introducing variation to the microcontact printing process.

The centricity was measured by comparing the obtained series of values of the three locations 120° apart. For each angular location, the mean height was determined for each speed and axial section to account for the influence of both taper and energy dose. The minimum,

maximum and mean height was determined across all speeds for the separate sections. Trends were seen suggesting that the relation of the respective height values was consistent along the axis of the drum. Therefore, an average value was calculated for the mean, minimum and maximum deviation from the global mean for each angular location. Figure 4.22 illustrates the findings by mapping exaggerated values.

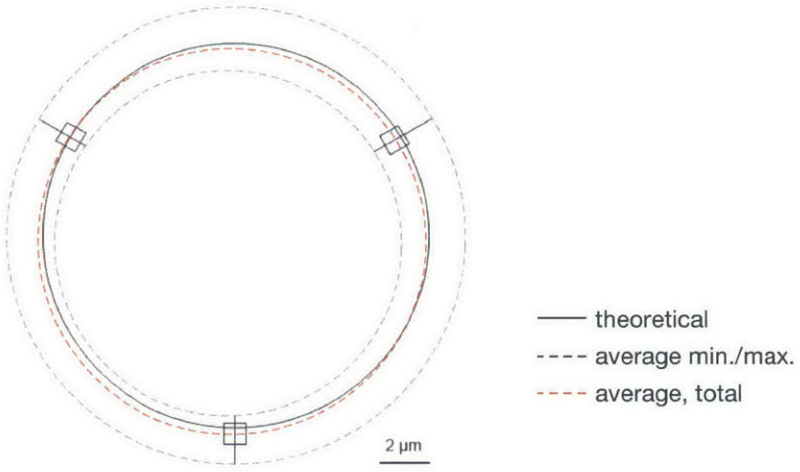


**Figure 4.21: Average concentricity as extracted from feature height values obtained. Illustration not to scale.**

To relate the angular variation in feature formation to the writing speed, the mean height was calculated over all axial sections. Figure 4.22 contrasts both the width (root) and height of the produced feature to the writing speed, separately for each angular location.

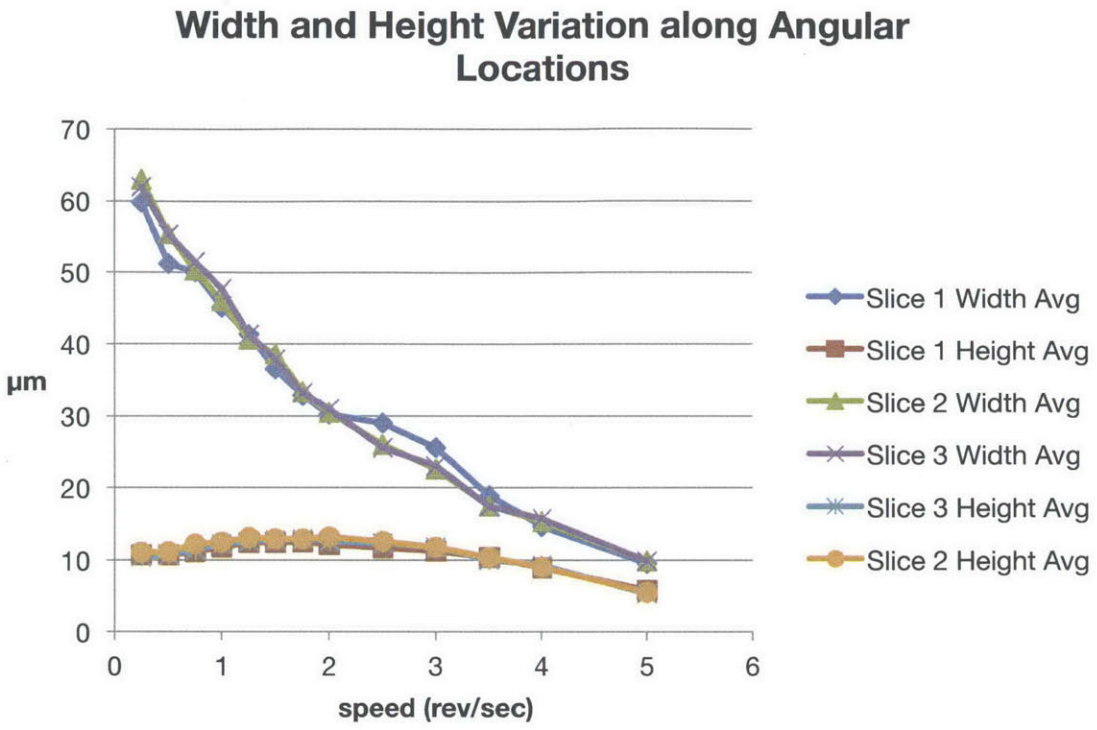


**Figure 4.22: Width and height along angular locations. Variation of width and height of formed lines for different substrate speeds at 3 different angular locations, 120° apart.**

### 4.5.2 Taper

Across the length of the centrifuge, a taper inside the drum or a deviation from the axis of rotation can cause a trend in the thickness of the resist. The variation in height amounts to almost 10 µm over 10 mm on the far end of the drum, and another 2.5 µm for the remaining 50 mm in length. An overview over height averages for each speed across the successive sections is given in Figure 4.23. The figure illustrates the effect of insufficient energy dosage, which can be observed for speeds of 4 – 5 rev/sec, and an excessive energy dose, which can be observed for speeds of 0.25 – 0.5 rev/sec.

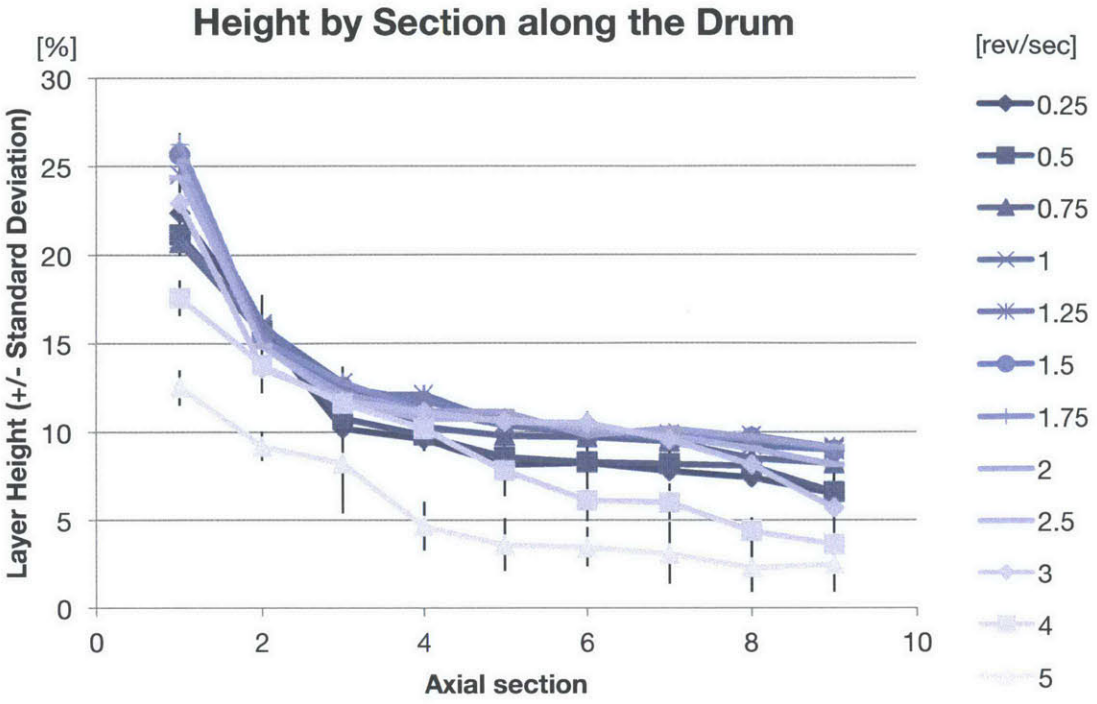


Figure 4.23: Taper measured by pattern thickness along the drum axis. Variation height of formed lines for various speeds, in 9 sections along the centrifuge drum axis.

## 4.6 Conclusion

The apparatus presented in chapter 2 served as a platform for verifying the model derived in chapter 3. Together, the analytical simulation could be compared against actual results formed by laser direct-write lithography. Moreover, it could be observed that the mechanisms of photolithography are applicable to this apparatus that is special by its nature, especially with regard to uneven Aluminum as a substrate. Further information gained from the conducted experiments helped verify the quality of the mechanical structure of the apparatus, and discovers potential for improvement.

# Chapter 5

# Composite Stamp Fabrication for Fluorescent Contact Imaging

The lack of a sensing technology inhibits the scale-up and process control of roll-based microcontact printing. Functionality can be added to the tool itself by creating fluorescent composite PDMS stamp. This allows the development of a technique for real-time contact visualization in microcontact printing.

## 5.1 Sensing Contact

Since SAMs are often transparent, visualizing the contact between the tool and the substrate is important for monitoring the microcontact printing process. Inspecting at the point of contact allows for minimizing defects when scaling the process to a roll-to-roll implementation. Few approaches exist for planar substrates. This work creates a technique for visualizing contact in a roll-to-roll process.

### 5.1.1 The Need for Contact Visualization

In microcontact printing, patterns of a high resolution are transferred from the inked tool, a PDMS stamp, to the substrate. Roll-to-toll microcontact printing allows for continuous printing, which holds great potential for better quality, higher speed and lower cost. Traditionally, clear thiol ink is transferred onto a metal-coated substrate, followed by an etching step to remove the metal layer in the areas not covered during the printing.

Alternatively, conductive ink can directly be transferred onto the non-conductive substrate, such as PET or glass.

With a resolution as fine as achievable in microcontact printing, and with materials as expensive as conductive inks or thiol, monitoring of the printing step is crucial. To scale up the microcontact printing process and transform it into a large-scale, roll-based production method, fast sensing is required to account for periodic errors. Moreover, since the print produced between the initial occurrence of an error and its detection is potentially erroneous and may destroy expensive constituents, it is desired to move the point of observation as close as possible to the printing region, i.e. the point of contact of the stamp with the substrate. By minimizing the distance between the occurrence of an error and its detection, the loss of material can be reduced. True real-time control allows for early detection of errors and can eliminate errors before they occur. Furthermore, since microcontact printing is mainly concerned with transparent inks such as thiols, visualization of the printed material may be a far bigger challenge than visualization of the stamp-substrate contact.

An illustration of state-of-the-art downstream print sensing techniques is presented in Figure 5.1.

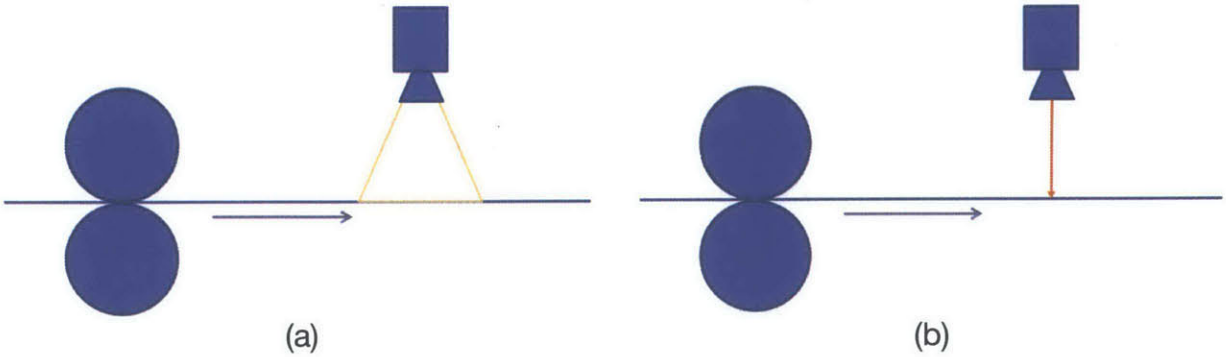


**Figure 5.1: In roll-based processes, the print is monitored down-stream. In graphics printing, a camera can capture the entire print (a). In micro-patterning processes with transparent thiols, one or more laser interferometers can show a trend, but not the entire picture (b). If an error occurs, the material produced until its detection is lost.**

### 5.1.2 Planar Contact Visualization

With planar substrates, such as plate-to-plate or roll-to-plate microcontact printing, the optical properties of the tool or ink present a solution for visualizing tool-substrate-contact.

The method of Total Internal Reflection (TIR) as a means of contact visualization emerged from efforts to automate fingerprint matching [86], where it was used to enhance the contrast of fingerprint imaging techniques at the time.

TIR describes the reflection at an interface between two media of different optical density, which happens if the angle of refraction in the target medium would be greater than 90 ° to satisfy the speed of light in that medium [87]. TIR happens when light travels to from optically dense material to optically less dense material, such as air. According to Snell's law, the critical angle $\theta_C$ that presents the maximum incoming angle for refraction can be calculated from the ratio of the refractive indices of the involved media, $n_1$ (source medium) and $n_2$ (target):

$$\theta_C = \arcsin\left(\frac{n_2}{n_1}\right) \tag{5.1}$$

Any angle greater than that causes reflection at the interface. Since the critical angle that determines whether TIR occurs depends on the ratio of the refractive indices of the media, a range can be identified where the incoming light refracts upon tool contact, whereas the light is refracted for media of a lower optical density. This results in a binary map of contact with great contrast. An implementation of TIR as a method of visualizing contact is illustrated in Figure 5.2. An implementation of TIR contact sensing in roll-to-plate microcontact printing is shown in Figure 5.3.

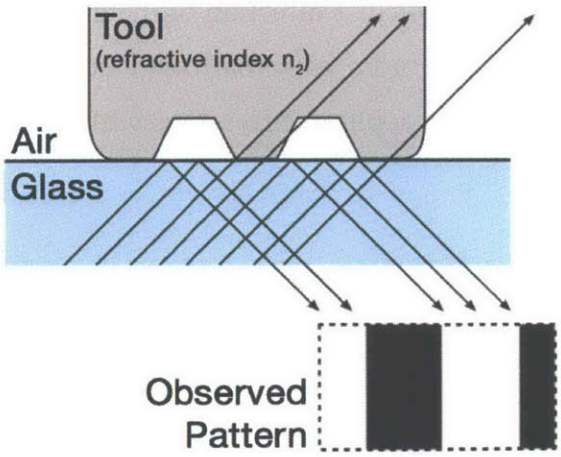


**Figure 5.2: TIR for contact measurement. Total Internal Reflection (TIR) occurs when the angle of incoming light is greater then a threshold value determined by the ratio of the refractive indices of the media and occurs when going to a less optically dense material, such as air. If the refractive index of the tool differs from that of air, a range of angles can be identified where TIR occurs**

depending on the presence contact.

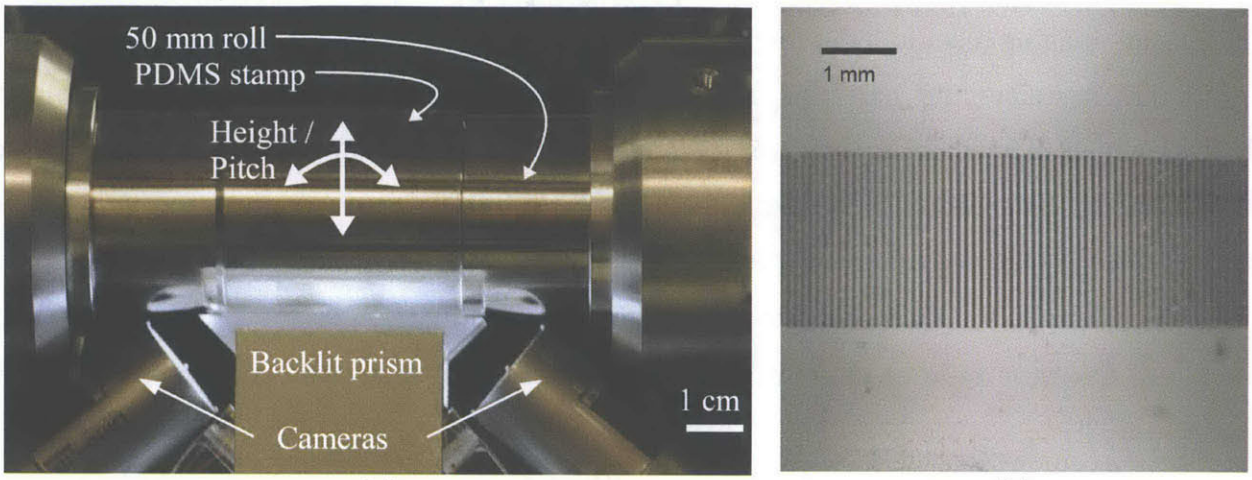


**Figure 5.3: TIR in roll-to-plate microcontact printing. (a) Implementation with a glass prism, LED illumination (left) and a camera (right). (b) Resulting contact image [19].**

By its nature, TIR as an imaging technique both distorts the aspect ratio of the contact image and is limited to substrates that allow enough space for illumination and inspection. A technique that overcomes these limitations can be found in Frustrated Total Internal Reflection (FTIR). It was was developed for finger print imaging and is still the most common method used for automated finger print scanning devices [87]. Moreover, it is used in certain touch-screen applications [88]. The perpendicular direction of the diffracted light presents FTIR as a relevant example for constructing a beam path that could exit a non-planar surface in radial direction. This example is eminently applicable to setups with optical paths as divergent as in roll-to-roll in-line contact imaging.

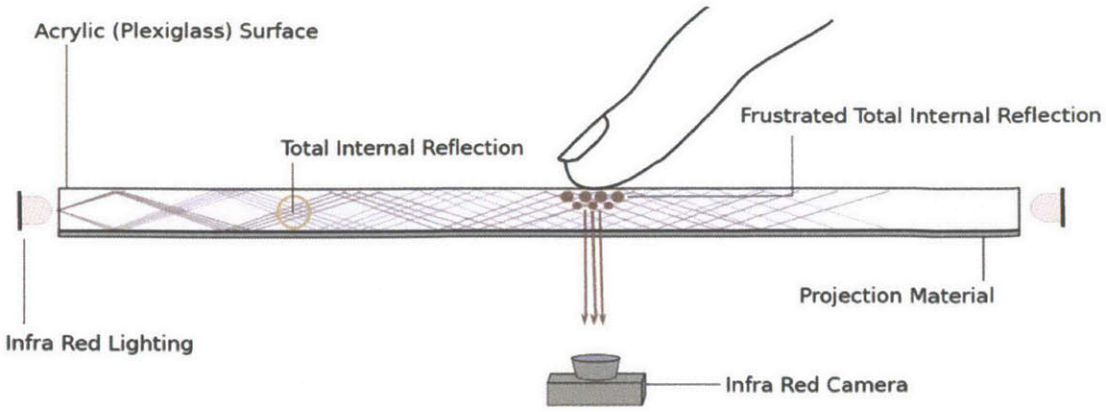


**Figure 5.4: Frustrated Total Internal Reflection (FTIR) is frequently used for imaging fingerprints [89].**

### 5.1.3 Implementing Contact Visualization in Continuous Patterning

The scale-up of microcontact printing is possible through a transformation of the technology to a roll-based continuous process. Therefore, the substrate backing is no longer a plate, but a cylinder. At the same time, high throughput requires a fast and precise sensing technology.

To tackle these challenges and create a metrology system that minimizes loss in case of an error, a method of observation was developed that operates directly at the point of contact, and thus allows for real-time control of the printing process. The print is visualized through the impression roll on the rear side of the substrate. The setup is displayed in Figure 5.10. A negative angle of engagement is chosen between the substrate and the tool to minimize distortion.

Integrating a passive light source directly into the stamp allows not only for uniform diffuse backlight illumination of the printing region, but also minimizes electrical and mechanical disturbance that arises from placing an active light source behind the rotating stamp. Through fluorescent particles, the excitation wavelength differs from the emission wavelength, reducing disturbances on the part of the imaging system and offering great flexibility in changing the incident vector of the excitation illumination without affecting the vision system.

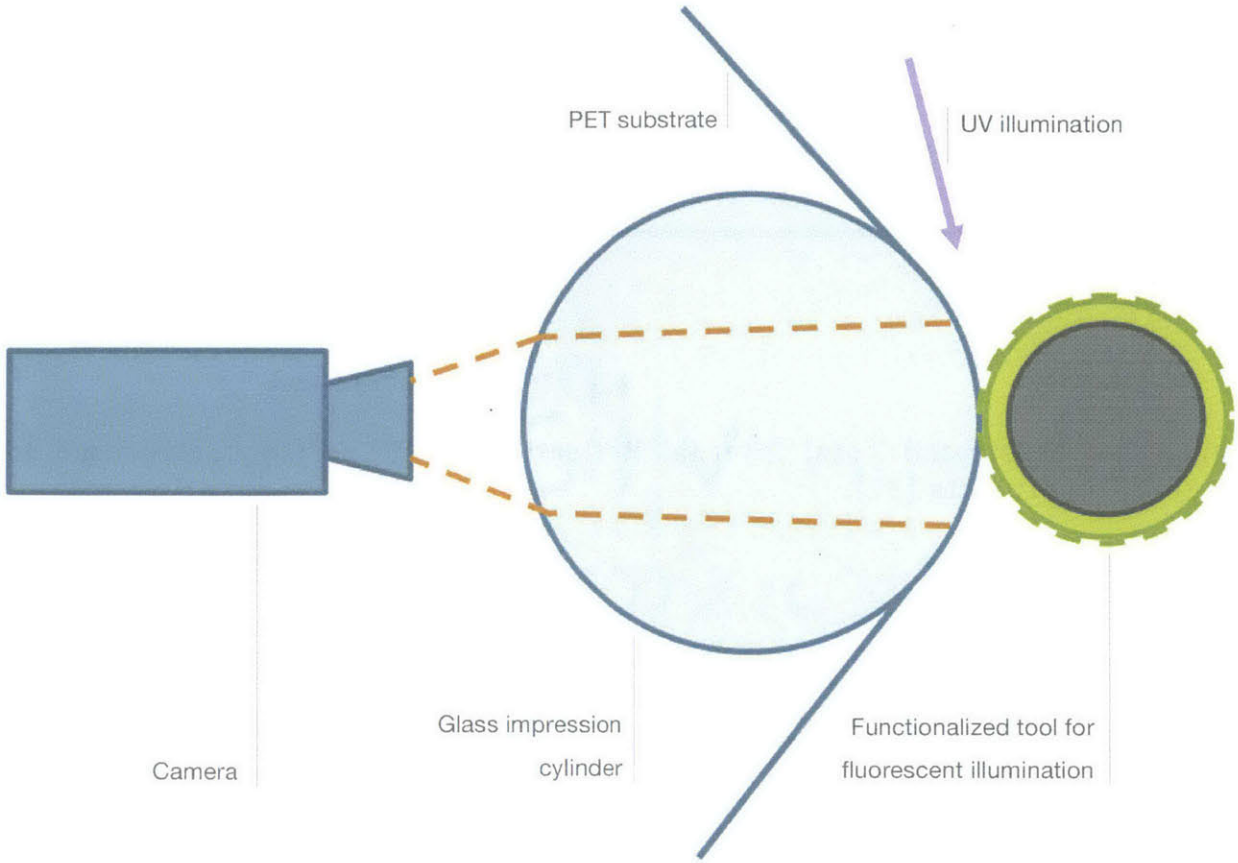


**Figure 5.5: Sensing setup. The contact is imaged through a transparent impression roll. Fluorescent loading functionalizes the tool to act as a passive source of illumination.**

## 5.2 Material Fundamentals

Characteristic for microcontact printing, tools are produced by casting highly compliant polydimethylsiloxane (PDMS) on the patterned layer of photoresist. Novel metrology is possible by expanding the range of materials and finding optically functional compositions that qualify as viable tooling material.

### 5.2.1 PDMS Processing

Polydimethylsiloxane (PDMS) is a silicon-based organic polymer with applications in a variety of fields. Its high elasticity and low surface energy allow PDMS to replicate a mold with

great fidelity and resolution [17]. Thus, PDMS is commonly used in microfluidics and soft lithography and it paved the way for microcontact printing as a high-resolution, low-cost surface patterning technique [26]. Furthermore, PDMS is relatively inexpensive (a stamp produced with the presented apparatus incurs a pure material cost on the order of $1). An additionally advantage, which shall be exploited by the work presented in this chapter, is its transparency over a wide range of wavelengths, which spans the UV spectrum.

Most commonly used is Sylgard 184 PDMS, available as resin and curing agent, which are mixed at a 1:10 ratio and thermally cured. It is highly viscoelastic and non-polar [25]. As a result, its great hydrophobicity poses a challenge in applications related to soft lithography. In biomedical micropatterning applications, plasmatic treatment and oxidization to render the surface hydrophilic [17]. From a conventional PDMS surface, the water contact angle drops from 111° to 40° during oxidization.

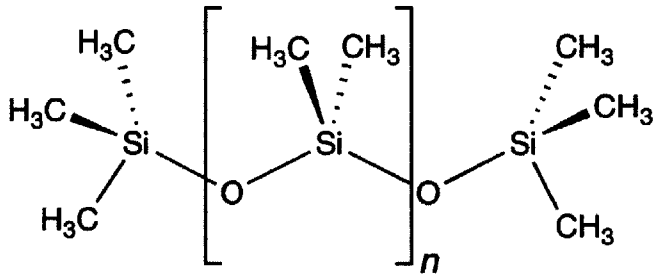


**Figure 5.6: Molecular structure of polydimethylsiloxane. (License: Smokefoot, CC).**

## 5.2.2 Fluorophore Processing

A fluorophore, such as fluorescein, is a substance that re-emits light at a wavelength longer than the wavelength of the absorbed light [90]. This makes fluorophores especially useful in metrological and indicative applications in biochemistry, healthcare and naval monitoring. Fluorescent materials see wide use as chemical indicators, markers and spectral filters.

In fluorescent microscopy, the ability to filter the detected wavelength and reduce the recoded image to the reflection produced by the specimen increases the signal-to-noise ratio allowing for higher quality filtering of the image and an improvement of the maximum

resolution [91]. Besides, multi-photon microscopy techniques allow a resolution past the diffraction limit of light [91].

Fluorescein, the most widely used fluorophore, absorbs wavelengths up to 494 nm and emits up to 521 nm. Other fluorescent dyes include derivatives of coumarin, naphthalene and rhodamine.

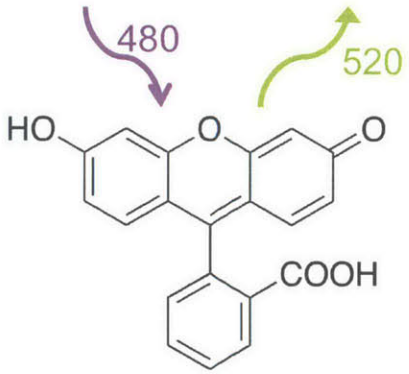


**Figure 5.7: Fluorescein, the most widely used fluorophore. It absorbs UV light up to a wavelength of 494 nm and re-emits light up to a wavelength of 521 nm. (License: Charlesy, CC; modified).**

The fluorescent behavior is possible as delocalized electrons jump bands excited by electromagnetic radiation. The energy required to exite an electron differs from the energy that is emitted upon relaxation of the electron to its ground state [91].

Typically, fluorophores consist of covalently bonded aromatic groups. In many cases, the performance and wavelength depends on the polarity of the environment. Chemically, fluorescein is a salt ($C_{20}H_{10}Na_2O_5$) [90]. It is soluble in water and other polar solvents.

## 5.3 Fluorescent Tool Fabrication

A method was developed to fabricate optically functional tools by creating material compositions of PDMS and fluorophore particles.

### 5.3.1 Initial Experiments of Fluorescein in PDMS

One of the big challenges in mixing fluorescent material with PDMS is the vastly different polarity property. A polar salt, fluorescein is soluble in water, ethanol, and other polar solvents. Non-polar PDMS does not usually dissolve in polar solvents.

To reduce the damage created from anticipated phase separation, dry fluorescent particles were mixed with PDMS without any intermediate solvent for the fabrication of a proof of concept. Yellow fluorescent salt (unknown formulation) was mixed with PDMS (Sylgard 184, 1:10). A high particle loading of 10% of the PDMS weight was chosen to observe a possible change in mechanical material properties. As expected, the composition produced an inhomogeneous suspension.

**Figure 5.8: Mixing of PDMS and fluorescent powder. They yield an inhomogeneous suspension.**

To qualify the material for its use, a preliminary tool had to be fabricated. Instead of a continuous cylindrical stamp with complex features, a flat stamp with a simple step profile was produced. Thick films of more than 1 mm thickness, even of materials as viscous as PDMS, are usually die-cast in heated molds. A layer of just one millimeter could be produced via spin coating. The 1:10 mixture of fluorescent particles and PDMS was prepared and dispensed on a

glass slide. Adhesive tape attached to the glass slide provided a 40 μm step to create an edge on the stamp to simulate a feature and allow to distinguish between contact and non-contact region in an experiment. The mixture was spun at 300 rpm for 30 seconds to create a layer of 0.6 mm [92]. Subsequently, the prototype was cured in an oven at 75 °C for 60 minutes.

After successful fabrication, the preliminary tool was qualified in its optical properties using an optical microscope. The heterogeneous nature was visible as the magnification revealed distinct fluorescent spots, see Figure 5.9.

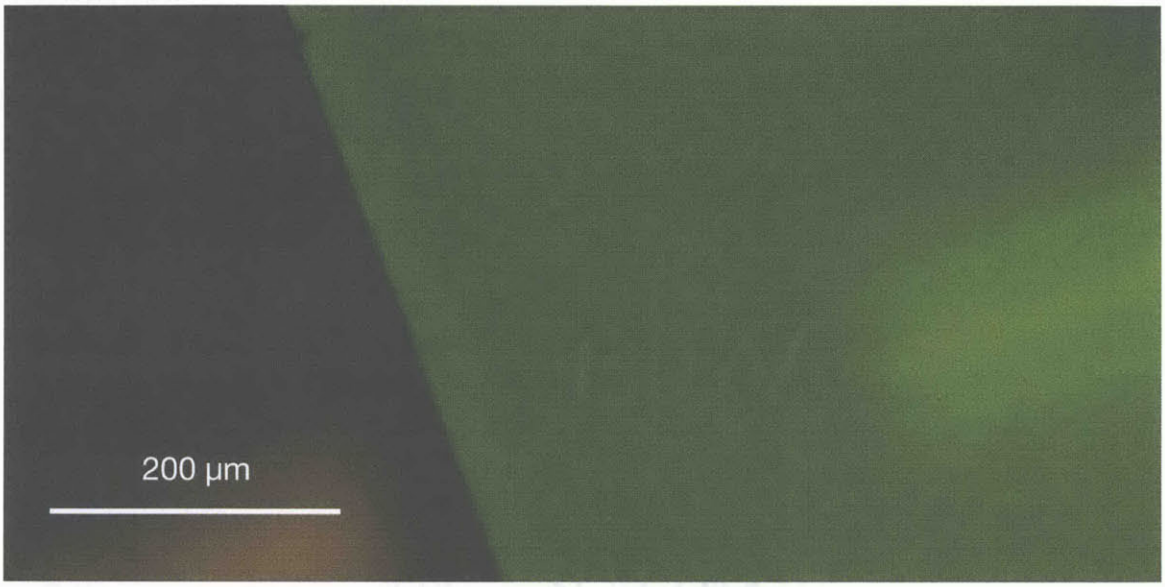


**Figure 5.9: The heterogeneity was visible when magnified in an optical microscope. The image above shows an edge of the initial feasibility study.**

The critical aspect for the metrology method under development was the intensity contrast of areas where the substrate was in contact with the stamp versus in those that were not. To detect this difference, the stamp was placed underneath the substrate, illuminated from different angles, and imaged through the microscope optics. In a first iteration, the contrast was measured between just the stamp and the glass slide. In a second iteration the PET substrate was introduced as an intermediary, to measure possible optical distortion. The setup is illustrated in Figure 5.10.

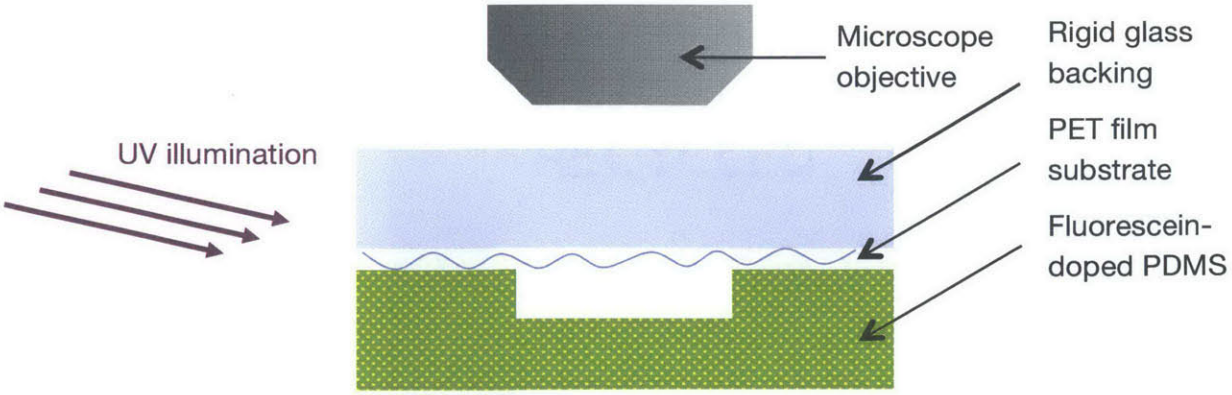


**Figure 5.10: The setup for preliminary optical tests. The stamp specimen contained fluorescent particles in a 1:10 weight ratio. Darkfield-illumination was found be optimal for creating fluorescent re-emittance upon contact when inspected vertically.**

With a UV illumination from an angle almost parallel to the substrate, the contrast in brightness of contact and non-contact regions in the fluorescent-doped material was greatly improved over white-light illumination lacking the UV region. The resulting images are shown in Figure 5.11 and Figure 5.12.

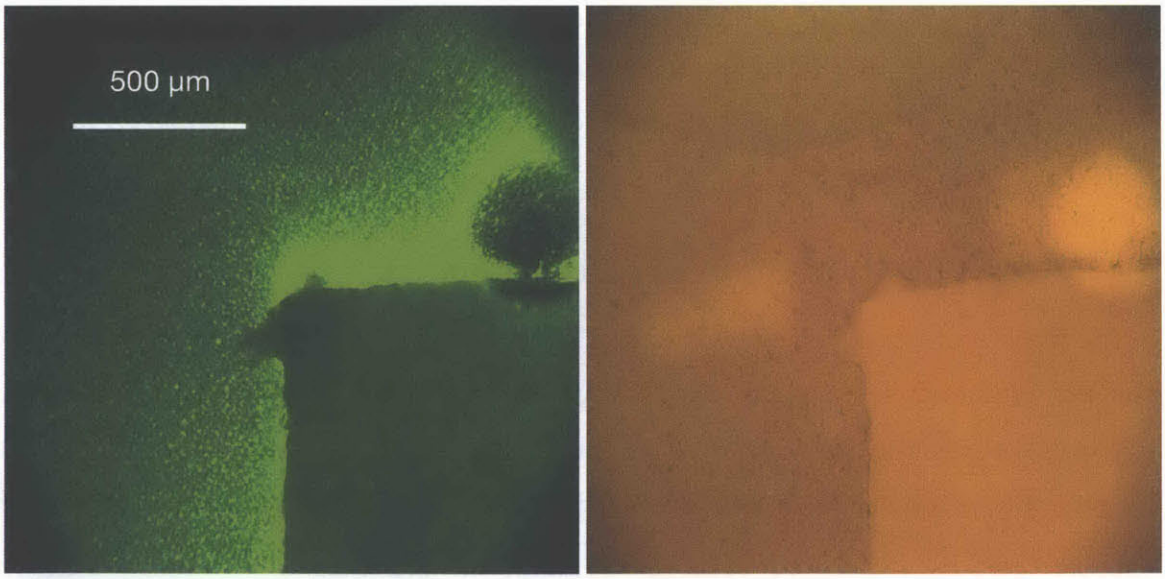


**Figure 5.11: Change of contact visibility with UV illumination of fluorescent-doped PDMS (composite stamp directly on glass, no PET).**

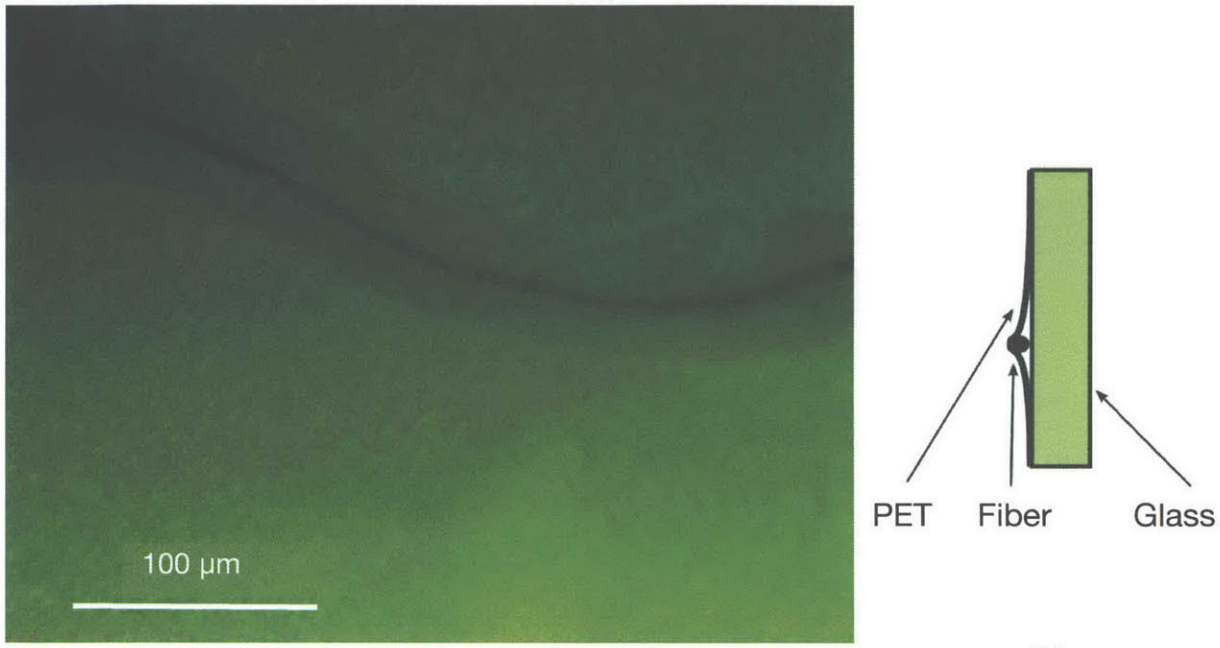


(a) (b)

**Figure 5.12: Contact visualization becomes apparent (a) around a fiber that was trapped between the tool and the glass substrate (b). The non-contact region is visibly darker than the in-contact region.**

The observed improvement could be applied to in-process control of microcontact printing and enable real-time imaging of the print contact with sufficient contrast for automated image processing. A robust tool fabrication process was to be generated following these successful feasibility investigations.

### 5.3.2 Fluorescent Stamp Process Development

Mixing fluorescent particles with PDMS showed promising results in initial experiments with a flat stamp spun on glass. To leverage the potential that was discovered, an investigation was undertaken whether this composite material can be processed in centrifugal casting on a photopolymer pattern created with photolithography, how material properties change, and where the process has to be adjusted.

### 5.3.2.1 Theoretical Process Design

To compare the composite tool with clear PDMS tools, the substrate had to be patterned in a similar fashion. The stamp material was a 1:10 weight-ratio mixture of yellow fluorescent particles and PDMS (Sylgard 184, 1:10).

No data were available on the particle density, thus making it impossible to calculate the fluid-dynamic behavior of the heterogeneous mixture when experiencing centripetal acceleration. A qualitative prediction could be given with the following approximations.

For a horizontal centrifuge, it can be shown that the body force of a point at an angle $\psi$ on the centrifuge spinning with speed $\omega$ can be described as [19]:

$$\boldsymbol{b} = \begin{bmatrix} b_\psi \\ b_r \end{bmatrix} = \begin{bmatrix} g\cos(\omega t + \psi) \\ g(\omega t + \psi) + \rho_f r\omega^2 \end{bmatrix} \tag{5.2}$$

where $\rho_f$ is the density of the fluid ($965.00\frac{kg}{m^3}$ for PDMS) and $\boldsymbol{b}$ are the body forces. For very high speeds $\omega$, as $\rho_f r\omega^2 \gg g$, this body force vector approaches $\boldsymbol{b} = [0, \rho_f r\omega^2]^{\mathrm{T}}$.

For a dynamic viscosity $\mu$, which is the product of kinematic viscosity and density, $\nu * \rho = \mu$, the vertical pressure gradient $\partial p/\partial y$ and velocity field $v$ then relate as follows:

$$0 = -\frac{\partial p}{\partial y} + \mu\left(\frac{\partial^2 v}{\partial x^2} + \frac{\partial^2 v}{\partial y^2}\right) - \rho_f r\omega^2 \tag{5.3}$$

As the pressure at the free surface is taken to be zero ( $p|_{y=h(x)} = 0$ ), the pressure $p$ can be described as a function of height $y$:

$$p(y) = \rho_f r\omega^2(h - y) \tag{5.4}$$

where $h$ is the height of the fluid (PDMS) at any given location.

If the particle surface area and density is known, Stokes law can be used to describe the force on particles in a viscous fluid that is subject only to gravity. For spherical particles, the surface area as a function of the sphere diameter $D_P$ is given as $\frac{1}{6}\pi D_P^3$. The force experienced by the particles becomes:

$$F = (\rho_p - \rho_f)g\frac{1}{6}\pi D_P^3 \tag{5.5}$$

where $\rho_f$ is the density of the fluid, $\rho_f$ is the density of the particles and $g$ is the acceleration of gravity. The terminal velocity of the particles is then subject to the dynamic viscosity of the fluid, $\mu_f$:

$$v_P = \frac{1}{18}\frac{\rho_p - \rho_f}{\mu_f} g D_P^2 \tag{5.6}$$

In a centrifugal field, the centrifugal force impinging on the particles is balanced by the buoyancy and drag forces. These are given by [93]:

$$F_{centrifugal} = \frac{\pi}{6}\rho_P D_P^3 \omega^2 r \tag{5.7}$$

$$F_{buoyancy} = \frac{\pi}{6}\rho_f D_P^3 \omega^2 r \tag{5.8}$$

$$F_{drag} = 3\pi\, \mu_f \rho_f D_P v_P \tag{5.9}$$

The radial velocity of the particles then becomes:

$$v_p = \frac{(\rho_P - \rho_f) D_P^2 \omega^2 r}{18\mu_f} \tag{5.10}$$

Given that the centrifugal process entails high speeds $\omega$ and the fluid's dynamic viscosity $\mu_f$ and drum radius $r$ are given nonzero values, this approximation of the particle velocity clarifies that consistent particle loading throughout the material can only truly be achieved if the density of the particles, $\rho_P$, is the same as the density of the fluid. But moreover it reveals that a reduction of the particle diameter can have a great impact on the particle distribution.

#### 5.3.2.2 Experimental Application

For conducting preliminary experiments, fluorescent particles of unknown density and particle geometry were used. 10 ml of PDMS were mixed with 1 g of particles. The mixture was stirred using a stirring rod and degassed for 10 minutes until all bubbles were gone. Like clear PDMS stamps, the mixture was inserted into the centrifuge at a speed of 10 rad/sec and then accelerated at 50 rad/sec$^2$ up to 300 rad/sec. The substance was allowed to spread out evenly for 5 minutes and then cured at 65 °C for 120 minutes.

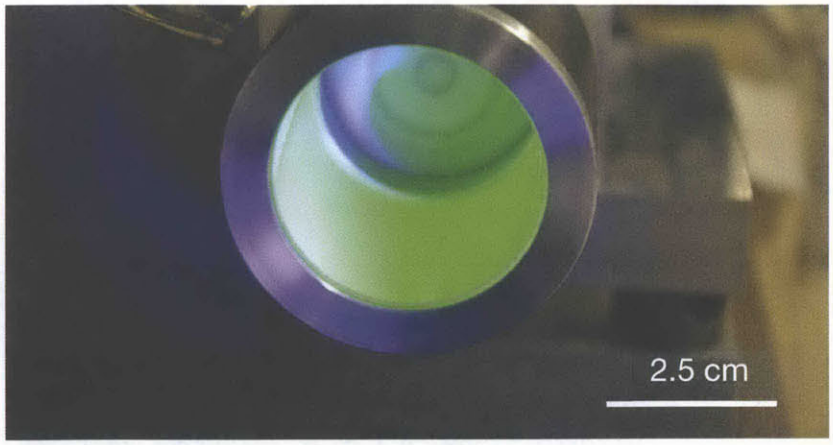


**Figure 5.13: Casting of fluorescent tools in the centrifugal drum.**

### 5.3.3 Results

Once cured, the stamp was removed from the drum and cut open to yield a flat specimen, which could be examined. It was first observed using a Zygo white-light interferometer. Then a thin slice was cut off the stamp, containing a profile of the length of the centrifuge, and observed under an optical microscope.

#### 5.3.3.1 Optical

The optical contrast properties in the full stamp prototype matched the performance seen in the preliminary experiment. Lines of 60 μm width (average value) were visible through an optical setup, consisting of a glass impression roll and an industrial camera. An image produced by the prototyped in-line imaging system is shown in Figure 5.14.

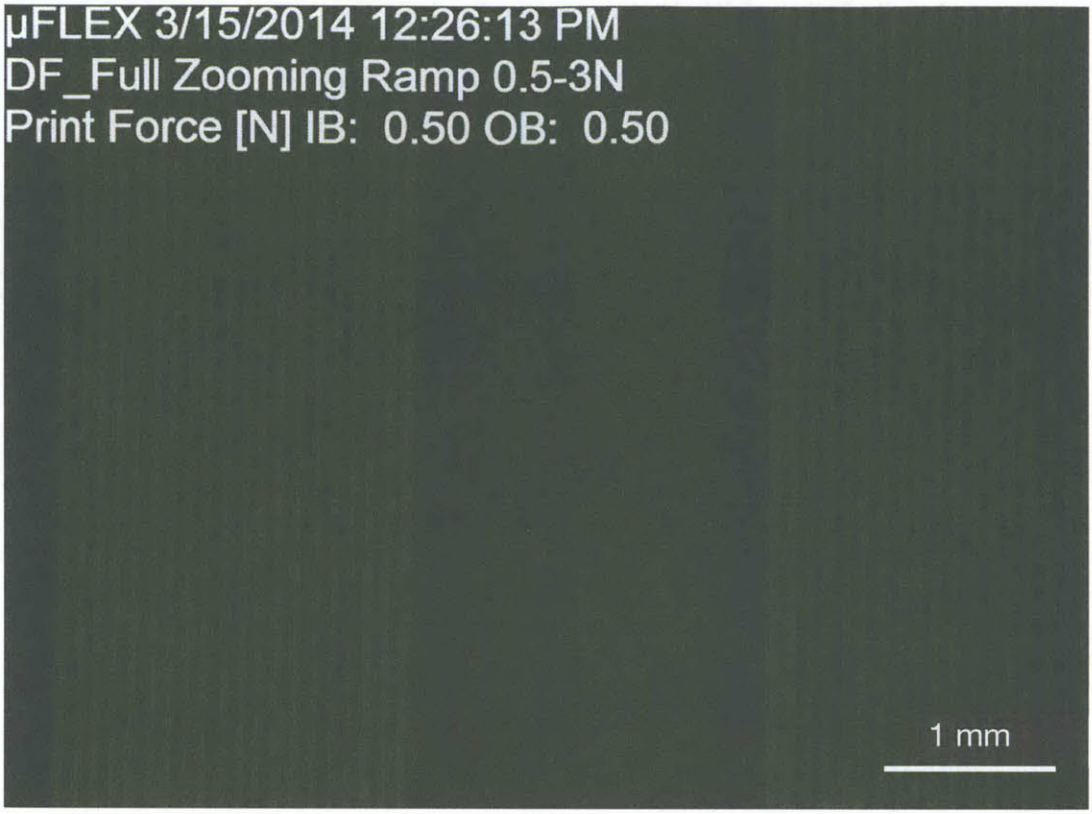


(a)

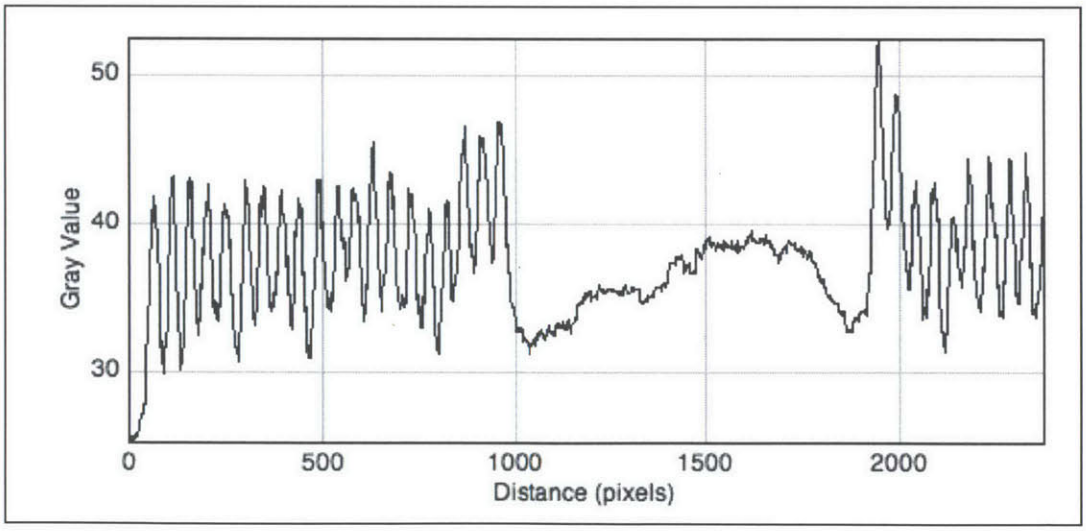


(b)

Figure 5.14: Fluorescent PDMS stamp as recorded through the glass cylinder (no PET). (a) Visible is a patterned region of 2 mm width, with lines spaced at 100 µm pitch. As the fluorescent particles re-emit the light at a wavelength that is in the visible spectrum, the pattern in contact is made visible through this novel technology. (b) Grayscale profile of the recorded image.

### 5.3.3.2 Topology

The patterned surface of the stamp was matte when initially observed. When placed in the Zygo white-light interferometer, only intermittent data-points could be acquired even at a compromising lighting and measurement range setting. These observations suggest that the centrifugal fabrication process produced a topology that is significantly rougher than in the case of clear PDMS stamps.

To support this hypothesis, a thin slice was extracted from the stamp to examine its cross-section using an optical microscope.

The result, shown in Figure 5.15, revealed that particles had indeed been pushed to the outside of the centrifuge, emerging from the PDMS suspension and pushing on the mold. It could be concluded that the density of the particles was higher than the density of PDMS and that the centrifugal force had pushed the particles into the photoresist, damaging its surface.

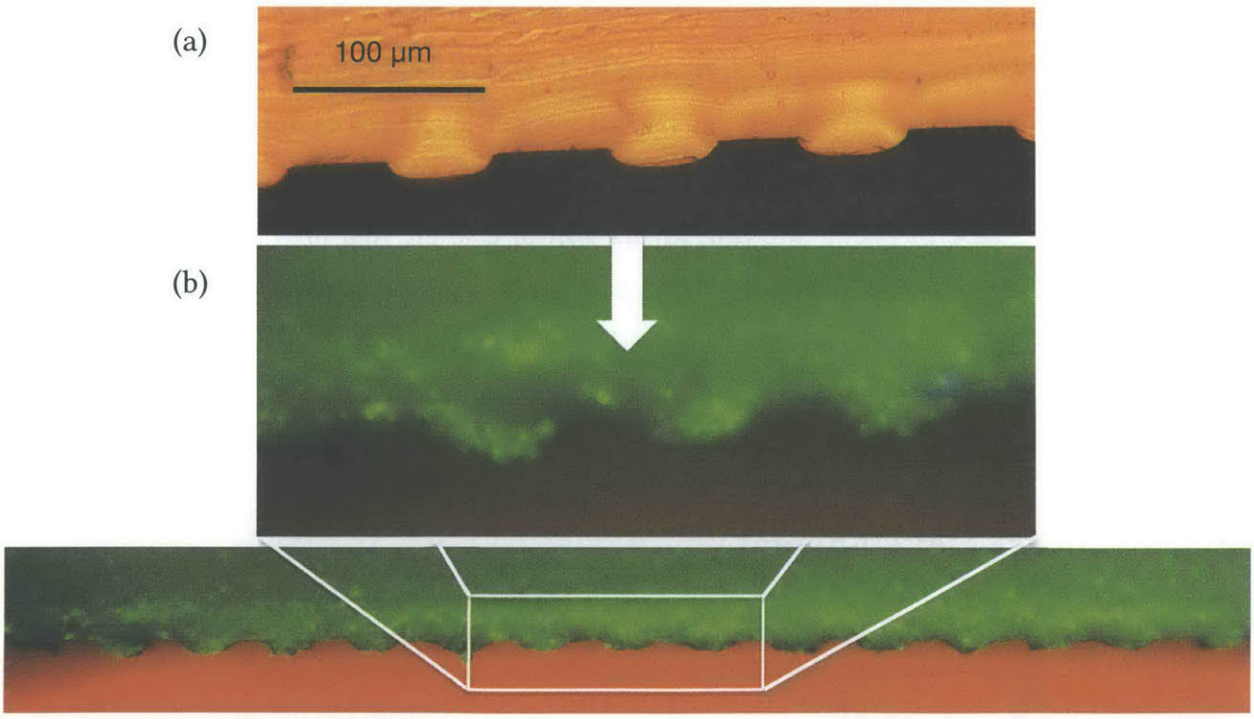


**Figure 5.15: Effect of particles on topology. (a) Clear stamp features. (b) Particle-filled stamp features. The centrifugal casting process created a centrifugal force pushing the particles at the mold. The clear PDMS stamp previously fabricated in the same master pattern presents a smooth topology.**

In conclusion, a consistent particle fill could not be easily obtained with the centrifugal method. As emerging particles distorted the topology of the stamp, which would limit the resolution when approaching the size of the particles or particle-clods, and as the mold was slightly damaged in the process, a solution had to be found to protect the mold and the patterned section of the stamp from the particles subject to centripetal acceleration.

## 5.4 Dual-layered Tool Fabrication

Blending the tool material, PDMS, with fluorescent particles set the stage for a novel imaging technique for in-line inspection of tool-substrate contact in roll-to-roll microcontact printing. Using the centrifugal casting technique presented in this thesis, which allows the fabrication of continuous tools with a large surface area for enabling a scale-up of microcontact printing, revealed a challenge posed by particles travelling to the features in the casting process, damaging the mold and distorting the high-resolution features. A possible solution to this challenge was the creation of multi-layer tools with a clear outer layer bearing the pattern and a fluorescent layer providing the optical properties required for the contact imaging technique. In similar geometries, PDMS has been successfully implemented as a light-guide [94]. Lastly, the ease of producing thin layers within a single tool provided by the centrifugal casting technology promoted the proposition to develop a process for a dual-layer stamp with a clear outer layer to replicate the photolithographic pattern and a particle-doped backing layer.

### 5.4.1 Process Development

The goal was to develop a process for creating a dual-layer stamp with a clear layer to replicate the photolithographic pattern and a particle-doped backing layer.

#### 5.4.1.1 Theoretical Process Design

A clear PDMS layer was to be cast into the pattern, backed by a layer containing fluorescent particles. The thickness of this layer had to satisfy a lower limit as the time

constant for the layer to reach its average height as a result of the centrifugal motion is subject to the volume of this fluid. As PDMS is applied without additional solvents and therefore has a relatively high viscosity, the lower boundary for PDMS is higher than that for the thinned photoresist.

To enhance adhesion between the two layers and prevent peeling under the directional and periodic stress resulting from the printing pressure, the clear layer was to be not fully cured, but still soft and partly monomeric at its backside when covered by the composite layer. Potentially, the layout of the thermal control system in the machine could be a favorable aspect in fulfilling this proposition, since the heat is introduced through the drum.

The acceleration of the centrifuge was reduced from the acceleration applied to pure PDMS, which had been 50 rad/sec$^2$. This action was taken to allow the suspension to spread more evenly before pushing the material to the underlying layer with high centrifugal force.

#### 5.4.1.2 Experimental Application

The following procedure was applied for creating a dual-layer composite stamp:

**Table 5.1: Procedure for Fabricating Dual-Layer Tools in the Laser-Lithographic Centrifuge.**

| |
|---|
| Create photoresist mold as discussed previously |
| Cast thin layer of clear PDMS<br>• Spin: 300 rad/sec for 5 minutes<br>• Crosslink: 15 to 30 minutes, depending on layer thickness, at 65 °C |
| Cast particle-loaded PDMS layer on top<br>• Spin: 80 rad/sec for 2 minutes, 300 rad/sec for 4 minutes<br>• Crosslink: 2h at 65 °C |

For about 3 ml of clear PDMS and 3 ml particle-loaded composite PDMS, each translating to a layer of 300 μm height, a baking time of 30 minutes was chosen to partly crosslink the first layer at 65 °C. A clear layer of about 150 μm was baked for 15 minutes before introducing the composite layer.

### 5.4.2 Results

The produced stamps were examined in their cross-sectional geometry and their functionality using an optical microscope, and in their topology using a Zygo white-light interferometer.

As predicted, the PDMS served as a light-guide and transmitted the light emitted by the fluorescent material through the clear-PDMS layer, including the features. This behavior can be seen in Figure 5.16.

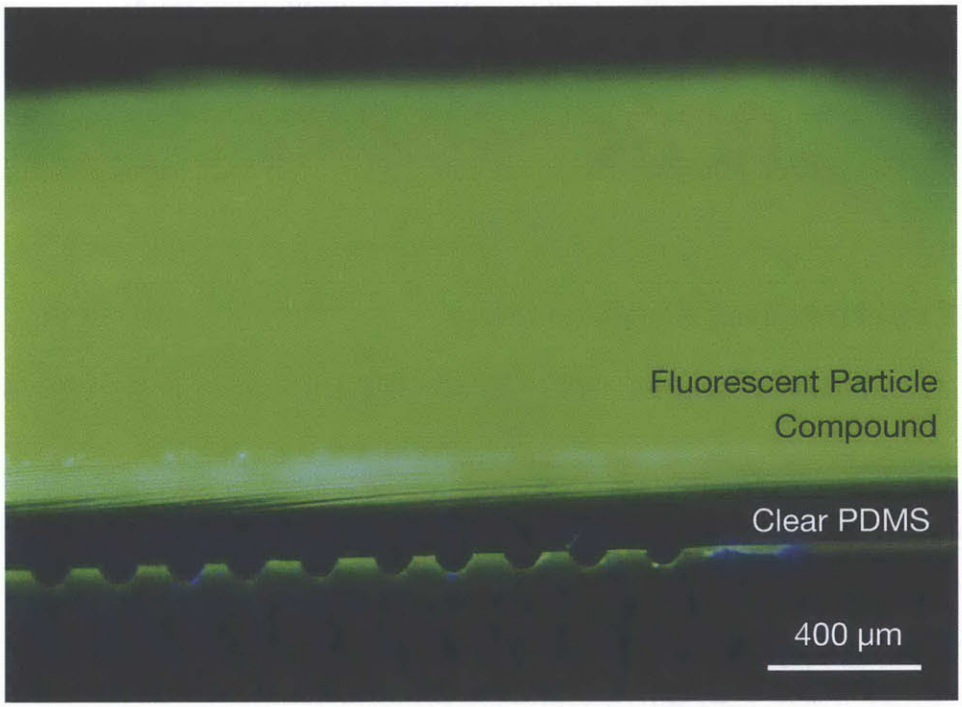


**Figure 5.16: Composite dual-layer stamp showing fluorescence and demonstrating the light-guiding behavior of PDMS by the glow beyond the clear, patterned layer.**

As a result of this light-guiding characteristic, the ability of the material to visualize contrast through illumination is preserved even through a clear layer. This is demonstrated in Figure 5.17.

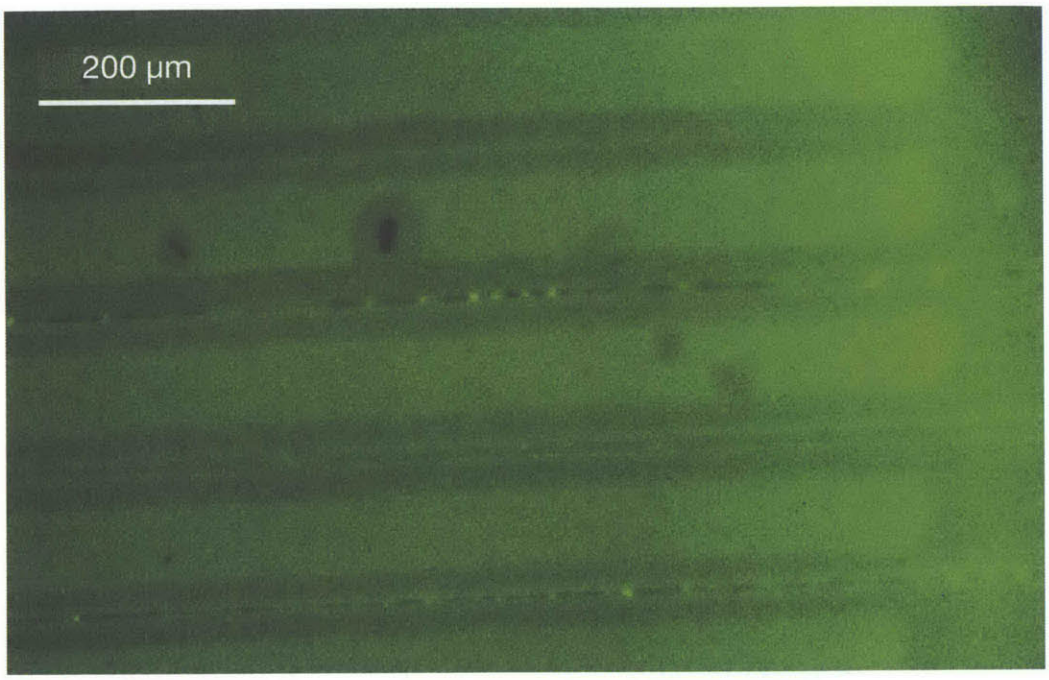


**Figure 5.17: Contrast visualization with a layered stamp. Even though the fluorescent material is 320 µm below and smooth throughout, it is still capable to visualize the contact between the pattern on the clear layer and the substrate, a glass slide. Regions that are in contact with the substrate can be distinguished from those that are not through a high-contrast difference in brightness. At this scale, the resolution is limited only by the imaging system.**

The topology of the clear layer was as smooth for the layered stamp as for a comparable 100% PDMS stamp. Results are shown in Figure 5.18 and Figure 5.20.

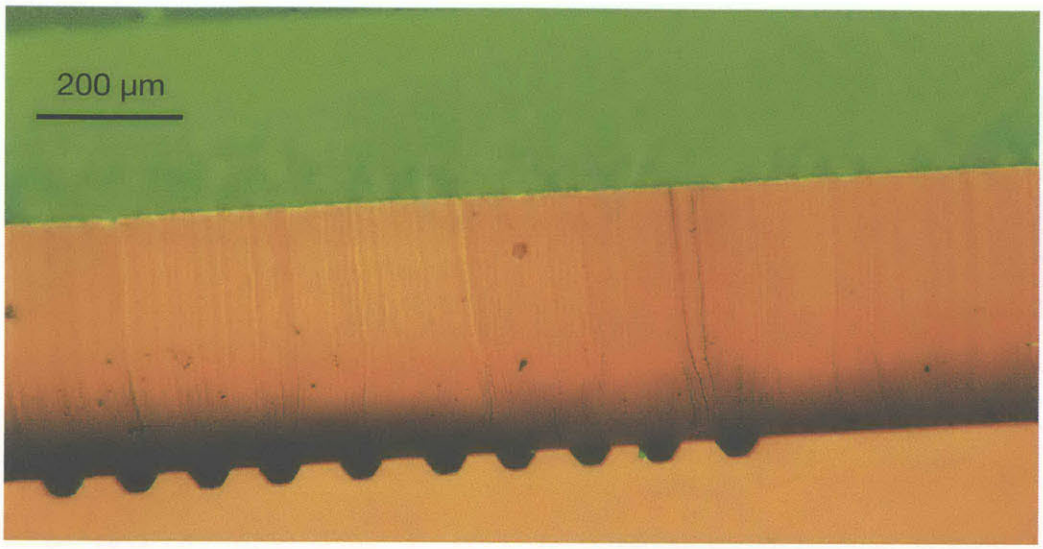


Figure 5.18: Microscope image of the cross-section of the first fluorescent dual-layer stamp created. The layer thickness of clear PDMS and fluorescent PDMS composite was 320 µm and 230 µm respectively, adding to a total stamp thickness of 550 µm.

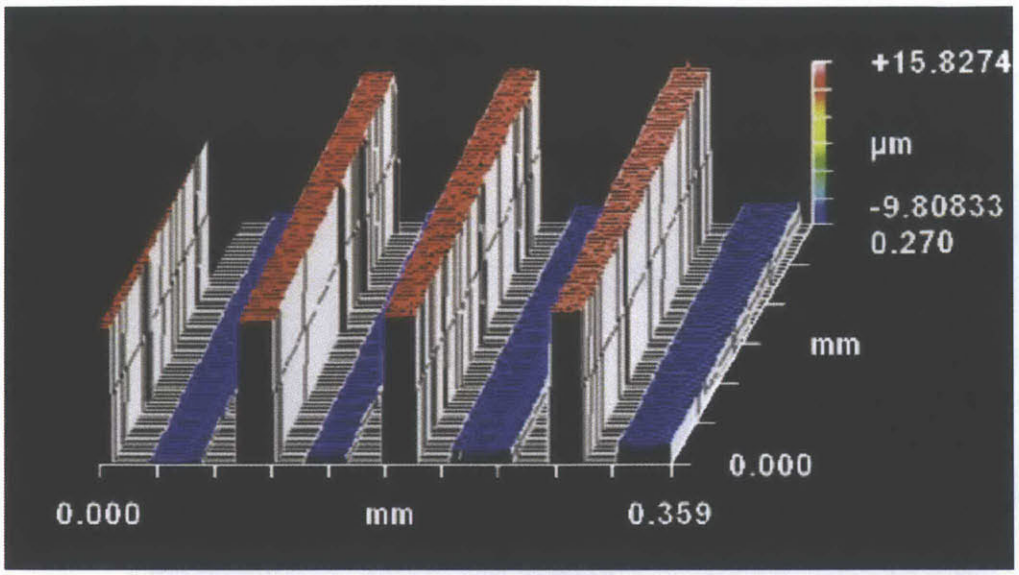


(a)

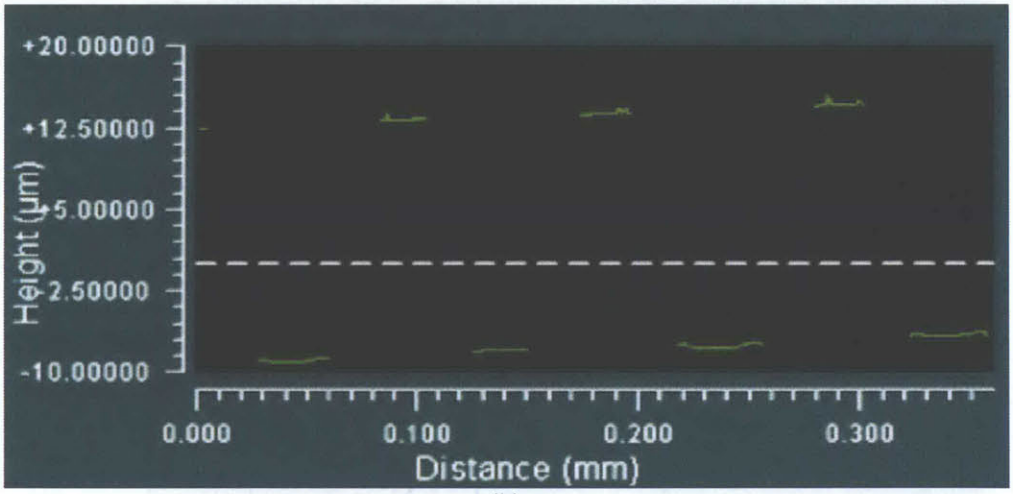


(b)

**Figure 5.19: Measurement of topology using white-light interferometry. (a) Volume view of a 0.36 mm by 0.27 mm section of the stamp. Lines produced are smooth and of equal height and width. (b) Surface profile plot.**

#### 5.4.2.1 Stiffness characterization

The stiffness of the experimental tools could be characterized using the impedance controlled force and displacement monitoring of the print-head in the µFLEX roll-to-toll printing machine. The results of the experiments are shown in Figure 5.20. In summary, the

composite material presents itself significantly more elastic than the pure PDMS, but the change in elasticity cannot be explained by a proportional reduction in Young's modulus alone.

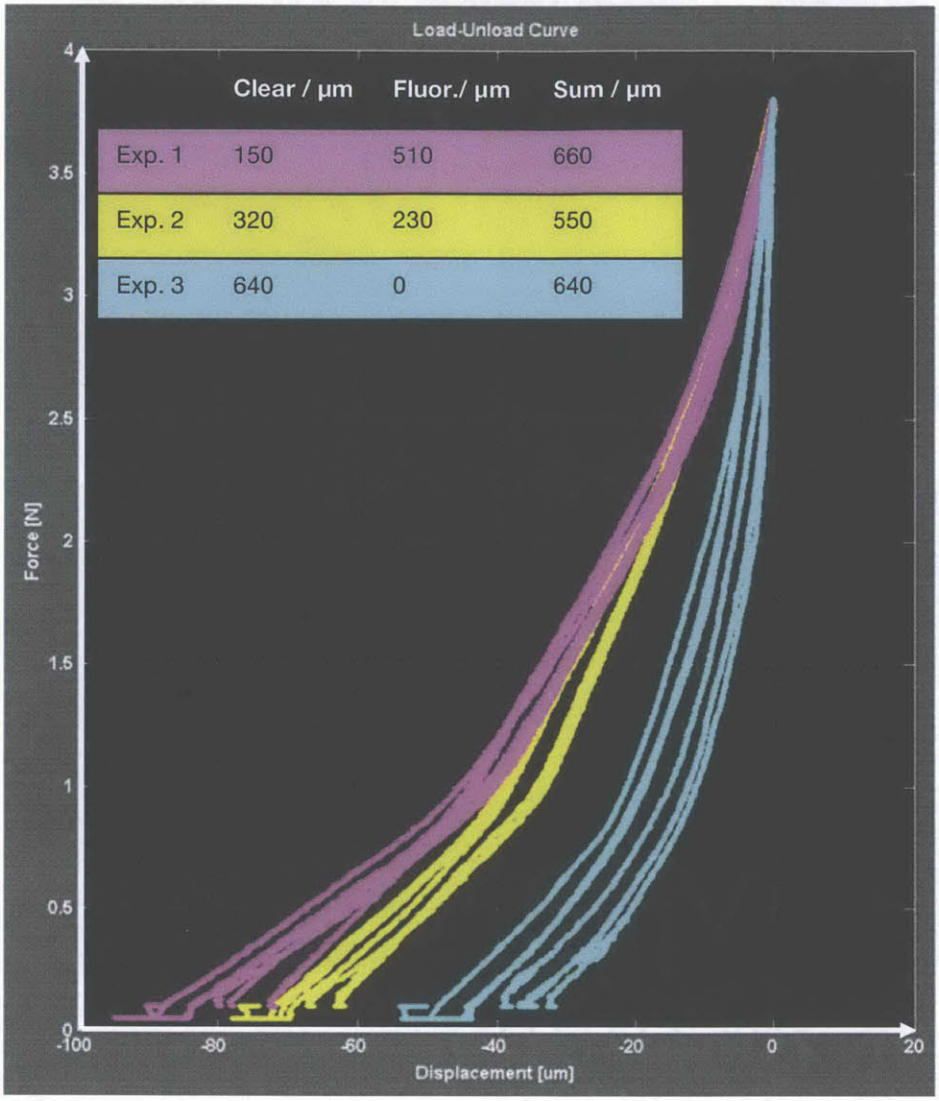


**Figure 5.20: Results of preliminary stiffness characterization of clear and layered stamps with varying layer thickness combinations. Thicker composite layers yield greater displacement per force and thus exhibit a higher compliance.**

### 5.4.3 Pushing Layer Thickness Boundaries

The thickness of the layers has a lower boundary introduced by the fluid viscosity, given time constraints, and its surface energy.

In a first iteration, experiments were conducted to investigate the minimum layer thickness without the addition of any possible solvents. As limits became apparent, Toluene was examined as a solvent for PDMS and in its ability to reduce the layer thickness.

Using pure PDMS for the thin, clear layer and centrifuging it at a speed of 300 rev/sec, a layer thickness of 25 µm – about as high as the features for thick films of resist – could not be achieved. In two separate experiments, regions of the photoresist pattern remained uncovered. A detailed cross-section is displayed in Figure 5.22. Thicker films, such as 100 µm, could be achieved, as documented in Figure 5.21.

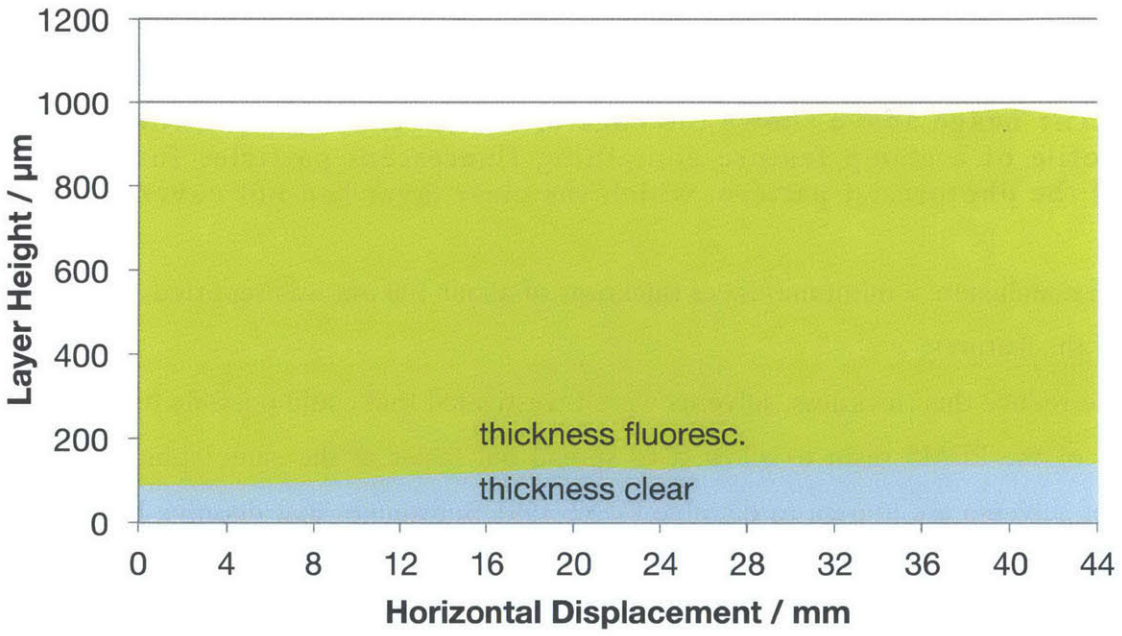


**Figure 5.21: A clear layer of 100 µm thickness was produced within a tolerance of ± 30 µm.**

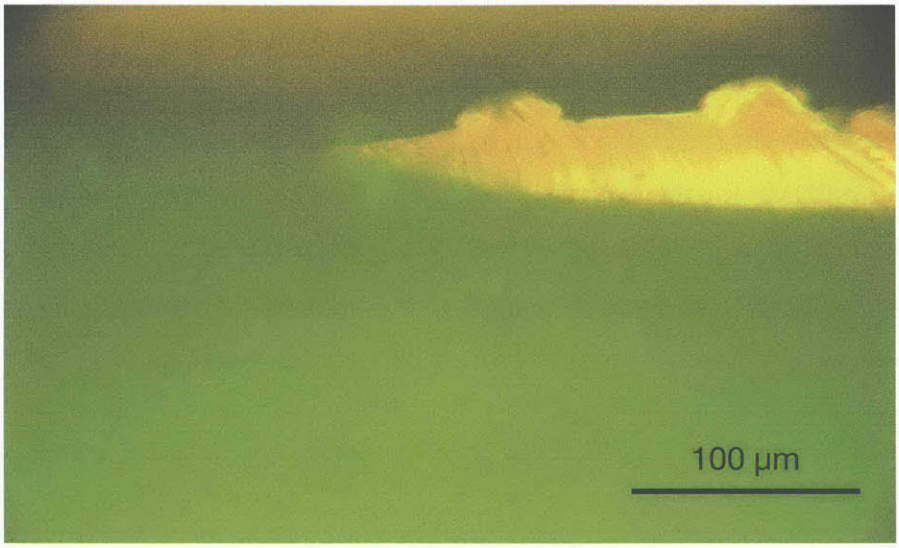


**Figure 5.22: 0.25 ml of PDMS could not entirely cover the surface of the drum. The image above shows the edge of the covered area. On the far left is the profile of a stamp feature containing fluorescent particles formed in an area of the photoresist pattern, which the clear layer had not covered.**

In conclusion, a minimum layer thickness of about 100 µm was reported, excluding the height of the features.

To reduce this thickness, solvents were investigated that could possible help reduce the viscosity of the PDMS resin to allow it to spread out faster at the same spinning speed. A variety of solvents are known to dissolve PDMS [95]. Substances that dissolve PDMS include acyclic and cyclic hydrocarbons, aromatic hydrocarbons, halogenated compounds and ethers. Toluene was shown to increase the length of a solid piece of PDMS by 30 %. Swelling and de-swelling did not influence the ability of the polymer to make conformal contact with smooth surfaces.

An initial experiment was conducted to examine timing parameters in the solubility and subsequent separation of PDMS and Toluene. In this experiment 7.6 g (7.9 ml) of PDMS (6.5 g base resin, 1.1 g curing agent) were mixed with 2.25 g (2.6 ml) of Toluene, creating a volume ratio of 3:1. The substances were mixed with a stirring rod for 2 minutes, yielding a homogeneous, medium-viscosity clear solution. The latter was dispensed in a shallow aluminum vessel and baked at 150 °F (65 °C) for 30 minutes and at 300 °F (150°C) for 60 minutes. The weight of the substance was reduced from 9.1 g to 7.2 g, indicating small dispensing loss and no Toluene residual. The resulting cross-linked PDMS exhibited mechanical and optical

properties identical to conventional PDMS. The experiment confirmed that Toluene could be used to reduce the viscosity of PDMS without inhibiting it in its functions.

Following this successful investigation, the performance of Toluene as a solvent in centrifugal stamp casting was examined. For this purpose, 0.25 ml (0.24 g) PDMS (10:1 weight ratio of base to curing agent) were dissolved in 0.1 ml (0.087 g) Toluene, creating a volume ratio of 5:2 and weight ratio of 3:1. The mixture was dispensed in the patterned drum and spun at 350 rad/sec for 5 minutes. Still spinning, the drum was heated to 95 °C for 30 minutes.

Then 6 ml of PDMS (10:1) were mixed with a suspension of 2 ml Toluene and 0.6 g fluorescent particles. When letting the Toluene-particle suspension rest for 30 minutes, significant phase-separation could be observed. This particle-doped toluene and PDMS solution was inserted into the drum, and spun at only 50 rad/sec for 5 minutes. Then the system was heated to 95 °C for 60 minutes.

The result of this experiment shows a very uneven boundary between the two layers, as shown in Figure 5.23. It can be assumed that the toluene had not been fully evaporated from the clear layer by the time the fluorescent layer was introduced, and therefore could not resist the forces generated when spinning the particle-doped layer in obtaining even distribution. Figure 5.24 shows that this deficiency rendered the stamp unusable for providing a darkfield backlight to the printing process.

A different caveat with Toluene is illustrated in Figure 5.25. If PDMS crosslinking occurs inside the patterned master, before the Toluene has been evaporated, material cracking can occur.

In summary, the addition of Toluene to PDMS could reduce the minimum layer thickness over pure PDMS from about 100 μm to less than 30 μm. It could be noted, however, that this process modification adds extra time to evaporate the solvent from the material, and requires precise temperature control for fabricating such a thin layer.

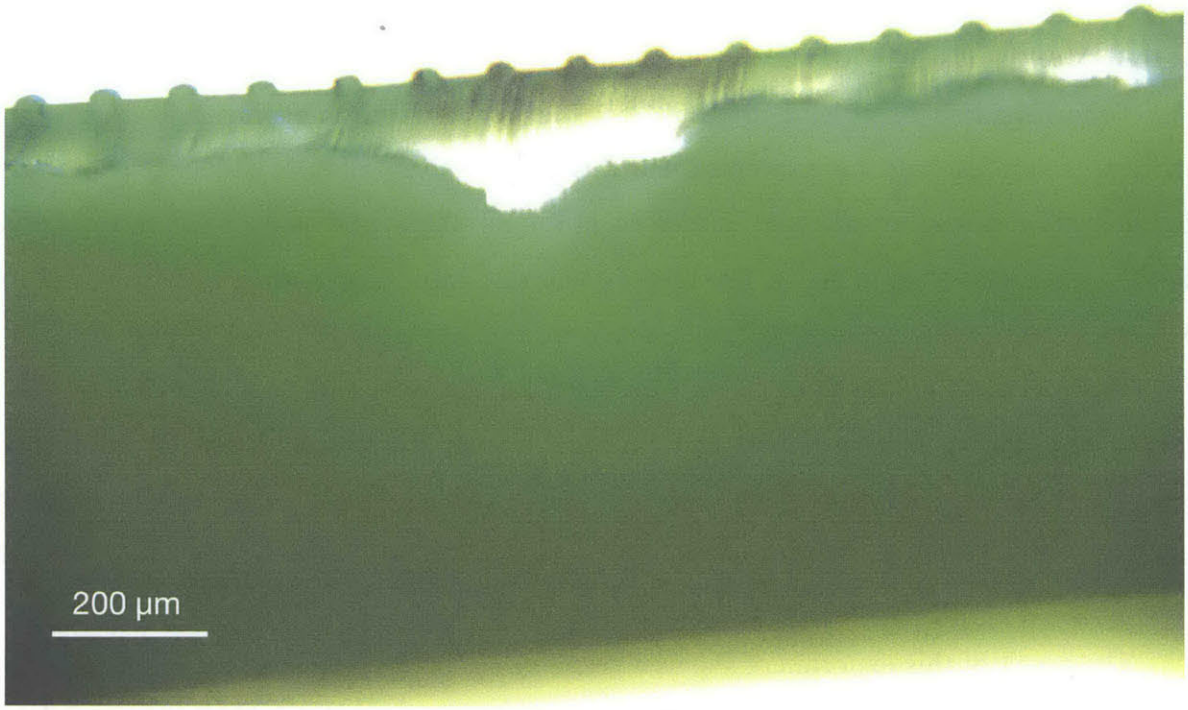


Figure 5.23: Due to Toluene content, the first layer was still soft after the first bake and could not withstand the centrifuging of the particle-doped backing layer.

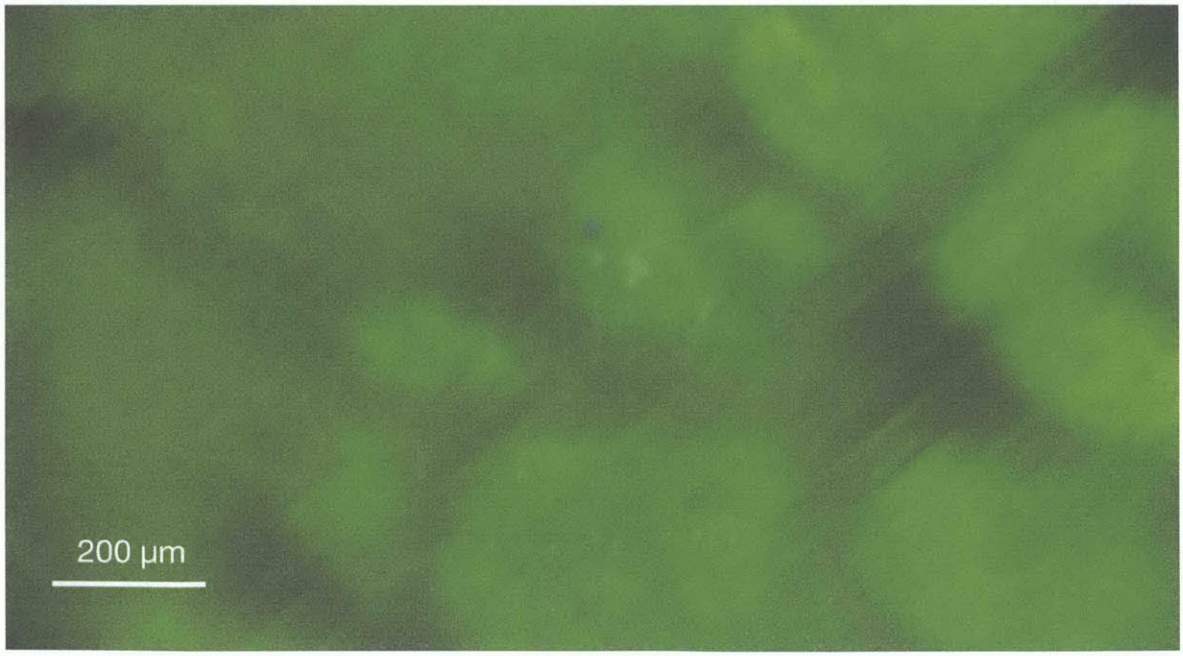


Figure 5.24: The Topology of the fluorescent layer inhibited the optical functionality of the dual-layer stamp.

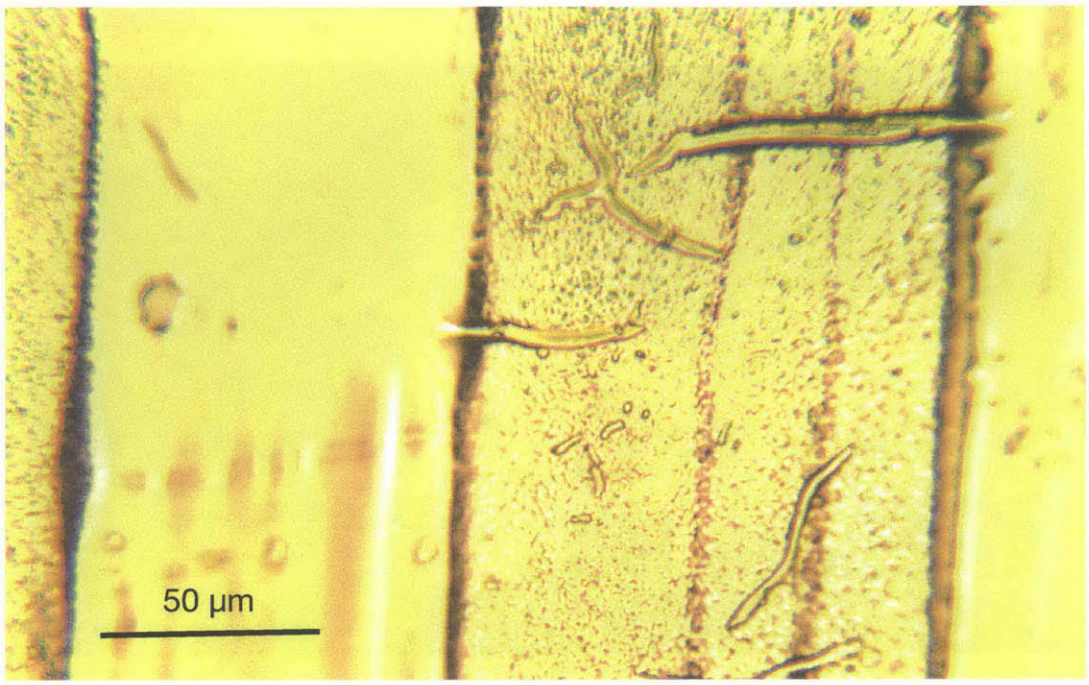


**Figure 5.25: Breakage of material as a result of incomplete toluene evaporation upon PDMS cure.**

## 5.5 Impact

A novel contact sensing technology was developed for roll-to-roll microcontact printing. Moreover, a manufacturing process was developed to produce optically functional, continuous stamps for microcontact printing.

It was possible, for the first time, to visualize the full contact area between the tool and the substrate in a roll-to-roll lithographic process. This method was implemented and a real-time closed loop control system could be created that actively controls the microcontact printing process in a continuous, roll-to-toll implementation (see [96] for complete details). Not only the contact could be visualized, but also the lateral force balance along the contact line.

To develop novel process control and prove the scale-up of microcontact printing, a lab-scale production machine was built on the basis of this novel metrology system. With an actuated print head, the contact region was successfully controlled in real-time. An optical resolution of 7.7 µm was achieved with a pixel size of 5 µm, and the bandwidth of the system allows for further scale-up, presenting the novel metrology system based on a functional tool as an enabler for large-scale continuous microcontact printing.

The sensing process with the functional tool is depicted in Figure 5.26.

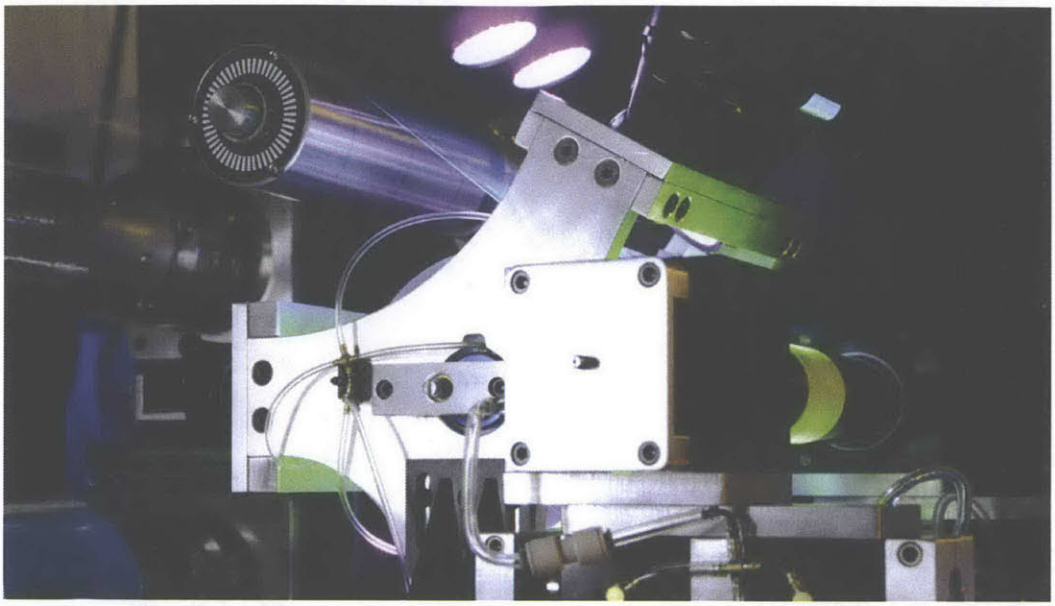

(a)

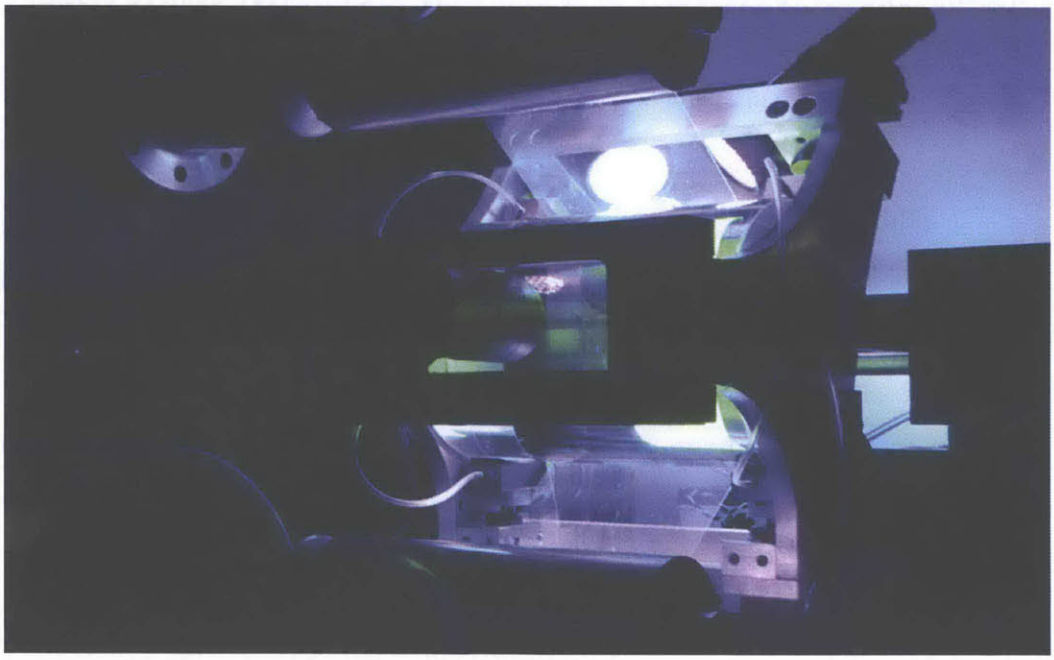

(b)

Figure 5.26: Sensing process with tool. (a) The composite stamp is backlit with ultraviolet light. A higher wavelength is re-emitted upon excitation. (b) Through a lens-quality glass impression cylinder, the contact image is recorded and processed in real-time [96], [97].

## 5.6 Future Work

### 5.6.1 Contact Sensing

In experimenting with different illumination techniques, it could be seen that the new method presented not only visualizes contact region with a great contrast, which is favorable for automated image processing. But also, parts of the tool can be imaged that are not in contact with the substrate. This happens in two ways: (i) front- and side-illumination make the topology of the stamp visible through the glass impression cylinder, (ii) for a small distance, interference patterns are visible. Combined with the high-contrast contact imaging, an unprecedented wealth of information is available that allows to investigate stamp contact mechanics in great complexity.

Furthermore, a process control system is conceivable, which leverages the various aspects of obtainable contact status detection. For instance, the system developed in the presented work allows to not only monitor the areas on the substrate in contact with the tool, but also, through (i), which part of the tool is in contact with respective areas, and through (ii), the angle of disengagement between the tool and the substrate.

This opens new pathways for the study of contact mechanics, stamp pattern geometry optimization, and precision surface patterning control such as closed-loop control for microcontact printing.

### 5.6.2 Homogenous Composite Material

In experimental use, it becomes apparent that the intermediate layer of clear PDMS can limit the range of possible optical setups, such as lighting and viewing angle. Therefore, it remains desirable to create a homogeneous composite material of PDMS and a fluorescent molecular group.

Zhang et. al. create fluorescent PDMS surfaces by diffusing thiols into the PDMS as a primer [98]. Lee et. al. analyzed mixture compatibility of PDMS and fluorescent compounds as a function of the solubility of each component in a variety of solvents and PDMS. Solvents considered were water, propylene carbonate, nitromethane and acetonitrile [95]. In 2011, Seiffert et.al. presented microfluidic devices based on synthesized fluorescent nanoparticles

that were directly mixed with PDMS [99]. A solvent combination compatible with both fluorescent particles and PDMS, or a process combining both, is still to be found.

# Chapter 6

# Machine Design for Scale-Up

The technique investigated in this work promises scalability far beyond the limits seen in similar but wafer-based processes. Leveraging this potential, a scaled-up revision of the machine is envisioned to prove the scale-up of R2R microcontact printing.

Following the investigations into the manufacturing processes, critical parameters are mapped to the desired outcome. Design characteristics are mapped to these critical parameters to determine machine elements to focus on for scaling up the design. General guidelines are given for designing a machine for seamless μCP tool fabrication via centrifugal, cylindrical direct write.

The system, as described earlier, is depicted in Figure 6.1. It comprises the velocity controlled centrifuge, a position controlled linear motion stage, an 80 mW diode laser and optics mounted on a 3-ball kinematic coupling.

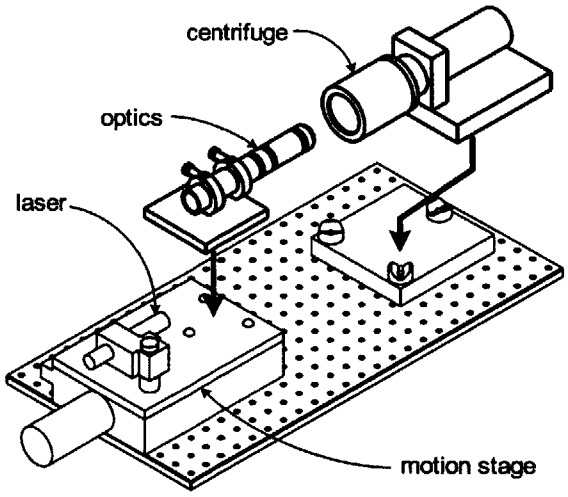


**Figure 6.1: Current machine layout.The assembly includes a position controlled linear motion stage, the laser, optics mounted on a kinematic coupling, and the centrifuge powered by a velocity controlled DC brush motor (reproduced from Figure 2.5 for convenience) [41].**

## 6.1 Gauging Machine Performance

Using the process map generated in Chapters 3 and 4, priorities are determined for process parameters to inform machine design requirements. These are used to investigate strategies for and concrete solutions.

Important process steps and their machine design dependencies are presented in Figure 6.2. The diagram suggests that a good control of the manufacturing process depends on the mechanical quality of the centrifuge motion and exposure system alignment, the substrate reflectivity and exposure optics, and to a certain extent on the thermal control accuracy and additional components that help with handling and timing. These machine design factors determine the process parameters in the centrifugal casting and photolithographic process, and thus the robustness of these processes. Thereby, these machine design factors determine the geometry and functional characteristics of the produced stamp.

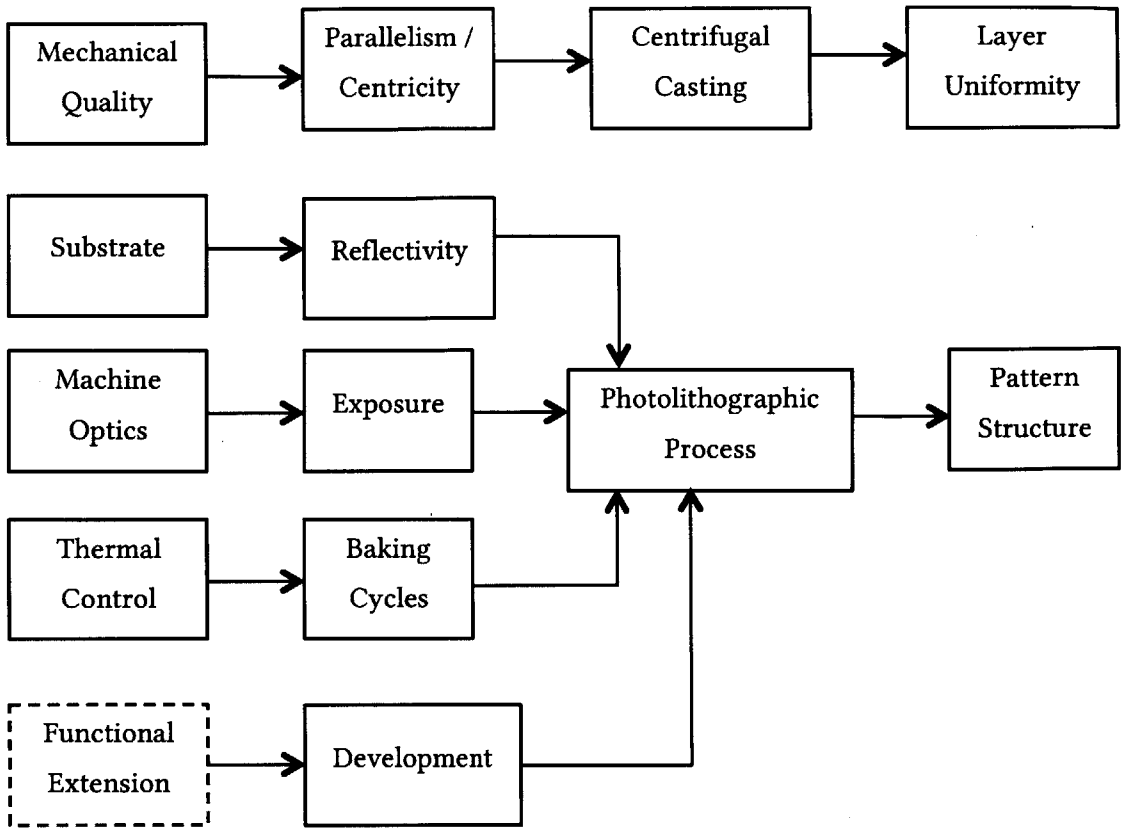


**Figure 6.2: Correlation between machine design factors and fabricated stamp geometry. The mechanical quality, substrate, machine optics, thermal control and additional functionality determine the parameters of the centrifugal casting and photolithographic process. These, in turn, govern the produced stamp geometry, which critically influences the inking and elasticity behavior of the stamp during its use.**

## 6.2 Derivation of Design Principles

One of the unique advantages of the technology discussed in this work is its unprecedented suitability for scale-up and process control. Not limited by the size of silicon wafers as existing tool-fabrication techniques for microcontact printing, this novel technique can provide for the production of stamps as large as common flexography plates, approaching several feet in width and diameter. Yet, rigorous design requirements need to be satisfied in order to maintain micron-scale accuracy.

The following design principles can be derived from the knowledge gained in investigating the limits and dependencies within the process:

*A Fast and Powerful Laser*

The laser sets the limit for feature sizes created. The profile of diode lasers is fundamentally asymmetrical, but suitable optics are capable of shaping the beam to show an almost circular profile. The wavelength of the laser needs to be matched with the resist sensitivity. Commonly, a smaller wavelength will improve the resolution, since the beam waist linearly depends on the wavelength of the focused beam.

*Precise and Actuated Optics*

The shape of the stamp features depends on the size and shape of the beam exposing the photoresist, and on the position of the focal point relative to the resist. The exposure optics need to ensure that the beam is focused on the substrate level and that the depth of focus is sufficient to cover variations in the photoresist topology and radial misalignment of the centrifuge and laser optics. With the centrifugal casting, a smooth surface can be assumed, but deviations in machine alignment also have to be accommodated by providing a depth of focus that can span the substrate. As the technology undergoes scale-up, variations may increase. Figure 6.3 relates the depth of focus and the minimum spot diameter, i.e. the waist of the Gaussian beam, to the focal length in the current system.

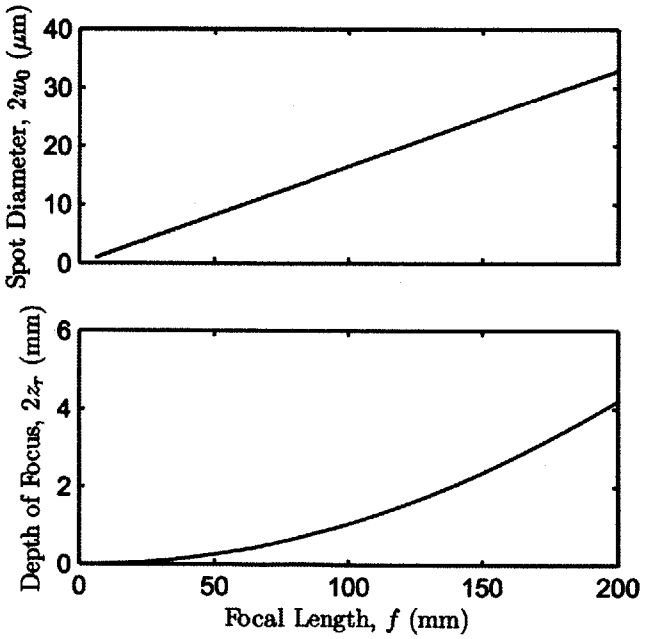


**Figure 6.3: Trade-off between spot size and depth of focus [19] for different focal lengths in the current system.**

*Precise Positioning Elements*

In maskless laser lithography the resolution of the rasterized pattern, even in the case of simple lines, is determined by the accuracy of the positioning system. Generally, machine design faces a trade-off in balancing precision versus range. Even though piezoelectric positioners are a ubiquitous means of improving the scanning accuracy of lithography systems, magnetic linear stages offer a far wider range of motion while achieving accuracy on the order of nanometers. A detailed discussion follows in 6.4.2.

Replacing rolling contact bearings supporting the centrifuge with air bearings can significantly contribute to improving the stiffness and reducing friction of those points that are otherwise prone to introducing disturbance into the process.

*Low-Reflectivity Substrate*

Even with the layer of SU-8, the reflectivity of the substrate can lead to unwanted dispersion or standing waves, causing unwanted photoresist conversion and rippled sidewalls. This can be reduced by ensuring that the substrate absorbs the excess irradiation, as ARCs do.

*Fast and Precise Thermal Control*

The chemical processes in the photoresist are largely influenced by the temperature at which they happen. Therefore, the temperature must be controlled within a tight window. Active heating (or cooling) elements, sensing and components with low thermal capacity and resistance can contribute towards this goal.

*Volumetric Metering*

The volume of fluid introduced into the machine determines the height of the created pattern, as all fluid solidifies inside the centrifuge. The high viscosity of thick-film photoresists in particular makes precise volumetric metering difficult. Also, as photoresists are usually developed for use with spin coaters, the final thickness depends on the resist's viscosity, not its initial volume. As a result, solvent content and volume shrinkage are often not known and not published by photoresist vendors.

These principles, referring to the laser, optics, positioning, substrate, thermal control and volume metering, form a holistic picture, which can be used to develop an idea of what the next generation equipment for this application may look like.

## 6.3 Design Strategy Development

Having determined the weak spots and the key elements in machine design for this application, the current problems are analyzed and common approaches from similar applications are investigated to improve these elements. Different strategies and suitable machine components are compared to derive concrete suggestions and design principles.

As addressed in 4.2, alignment between elements in the casting and patterning processes crucially determines the quality and repeatability of the produced result. The laser-patterning step, in particular, is sensitive to deviations in parallelism between the drum and the exposure system, as displayed in Figure 6.4.

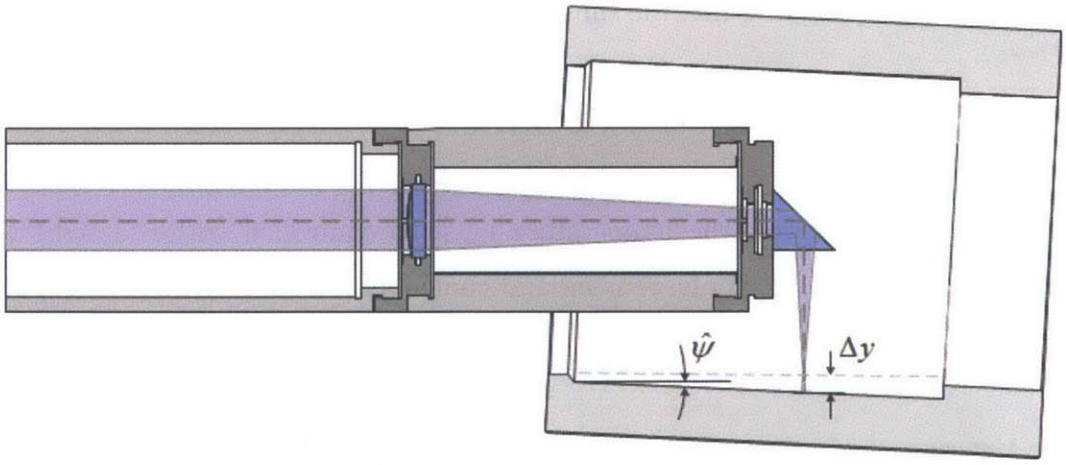


**Figure 6.4: The position of the laser focal spot relative to the substrate fundamentally determines the result of the exposure process. A deviation in the drum position can affect the focal point to the beam relative to the layer of resist inside the drum, as shown above (reproduced from Figure 4.4 for convenience).**

The significance of deviations in the focal position become apparent from the experimental results gained from the patterning process investigation described in Chapter 3. The mean feature width (root) of all measured features is determined for any given substrate

speed and for 9 evenly spaced axial sections. The plot in Figure 6.5 indicates a trend in root width for varying positions along the machine, which applies for all speeds. The mean pattern height is also decreasing in axial direction for the same experiment (see Figure 4.23). Since the root width for a given substrate speed decreases for thicker patterns, the trend seen in Figure 6.5 can not be explained with thickness-related power dose requirements, but may indicate the effect of a change in beam intensity as a result of a deviation from the focal plane.

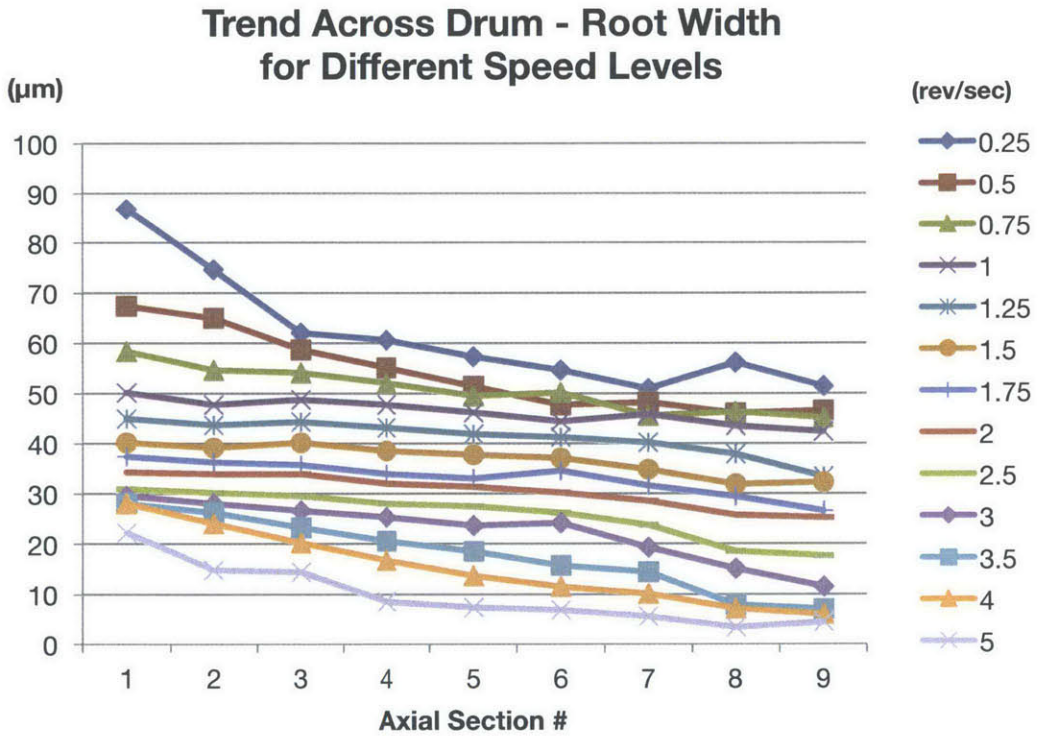


**Figure 6.5: The mean root width decreases as a function of the axial position. This may be an indicator for a deviation in the parallelism of the stage trajectory and drum axis, which results in a change in focus along the drum. The plot shows width values achieved with a mean pattern thickness of 12 µm.**

Figure 6.9 shows two exemplary cross-sections for different axial locations. A complete series of changing cross-section is given in Figure 4.15 for a speed of 2 rev/sec.

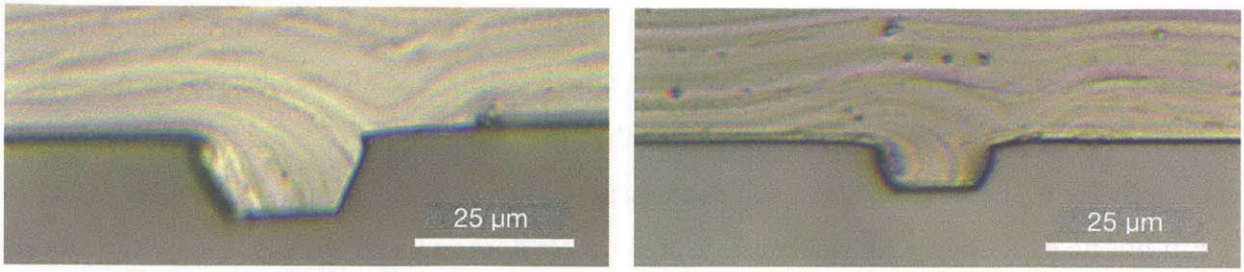


**Figure 6.6: Cross-section of a line written with 2.5 rev/sec substrate speed in (a) section 2 and (b) section 9.**

Many lithography systems overcome this problem by adding auto-focus systems. These may be reused from CD-players [100]. While this is certainly recommended for the system presented, a significant contribution to the precision of the machine can be provided by ensuring repeatable motion and optimal alignment.

To provide a better picture for the great source of error introduced by elastic deformation and imperfectly aligned interfaces, Figure 6.7 again displays the structural loop of the system, which was briefly addressed above.

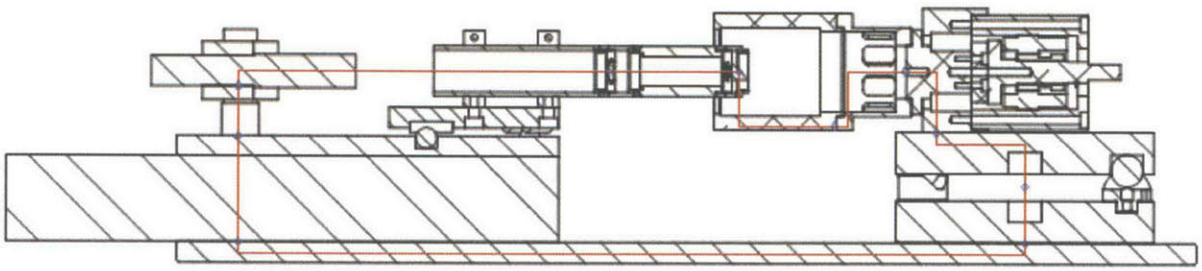

**Figure 6.7: The structural loop of the current apparatus. Interfaces (illustrated above) present eminent sources of variation (reproduced from Figure 4.3 for convenience).**

Though not impacted by an additional force during the process, the cantilevered support of the drum is prone to deflection when envisioning a larger version of this machine. The use of roller bearings is limited in accuracy and adds heat and thus deformation in the process. For ultimate scale-up, air bearings should be considered due to their great stiffness.

The static alignment of the machine is determined during assembly. In essence, the linear stage trajectory and centrifuge axis need to be stringently parallel.

To ensure a high lateral resolution in the creation of the pattern in the photoresist, the positioning of both the brush DC motor of the centrifuge and the linear motion stage is imperative. For true high-resolution fabrication of continuous stamps it is therefore necessary that the machine actuation satisfy certain accuracy criteria, namely in its repeatability.

Thin film processing requires exact temperature control to prevent over- and underdevelopment during endotherm processing steps. An overshoot in baking temperature may cause a shift in linewidth [101], burn the resist [102] or lead to a cracked film due to uneven solvent evaporation.

The current control system is depicted in Figure 6.8. The centrifuge drum is heated using a heat gun. Cooling is provided mainly by convection and a cooling fan. The temperature is monitored using an infrared (IR) sensor. Closed-loop control is achieved with a pulse-width-modulator (PWM) regulating the intensity of the heat gun based on the difference of a given target temperature and the temperature measured by the IR sensor. A low-pass filter prevents undesired variation resulting from the response time of the system.

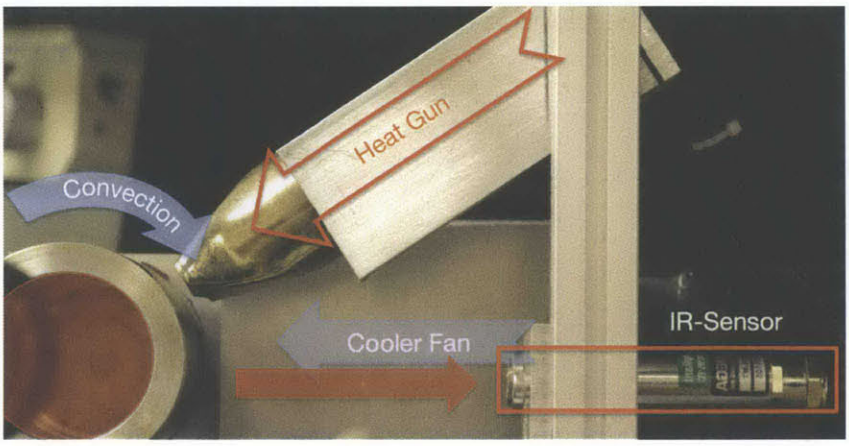


**Figure 6.8: Thermal control system.**

The performance of the thermal control system is fundamentally determined by the thermal dynamic characteristics of the drum and the ability to monitor its temperature. In the current design, the thickness of the drum wall exceeds 5 mm. While this provides excellent stiffness, it may not be required and unnecessarily slow down the change in temperature in the system and limit the bandwidth of the thermal control system. Reducing the drum thickness to a minimum value may greatly accelerate the thermal system.

Lab-scale photolithography sees two forms of equipment for photoresist baking: ovens and hot plates. Convection ovens are common in thick-film processing because they allow for batch processing [66]. However, hot plates are usually preferred because they provide the best temperature control (within ± 0.2 °C of the set point) and because the resist is heated through the substrate, promoting solvent evaporation. Heating the centrifuge through the drum follows the same mechanism, and it is recommended that a revised heating system be heated through the drum.

Using infrared (IR) to detect the temperature of the rotating drum appears highly suitable. Tactile temperature sensing techniques are deemed inappropriate for such rotating equipment. Since IR sensing relies on emissive surfaces to detect temperature, the reflective aluminum drum must be coated or anodized to be accurately monitored. Figure 6.9 illustrates this relation. Photoresist has a high emissivity, but controlling the temperature through the outside of the drum provides more a higher quality in the resist film. As discussed in 6.3, heating through the substrate creates a more homogenous layer of photoresist. The temperature should be measured close to where it is introduced to provide a fast thermal control system.

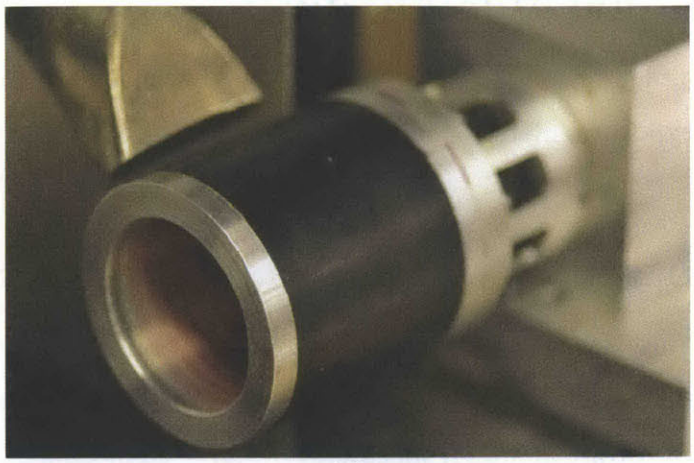

(a)

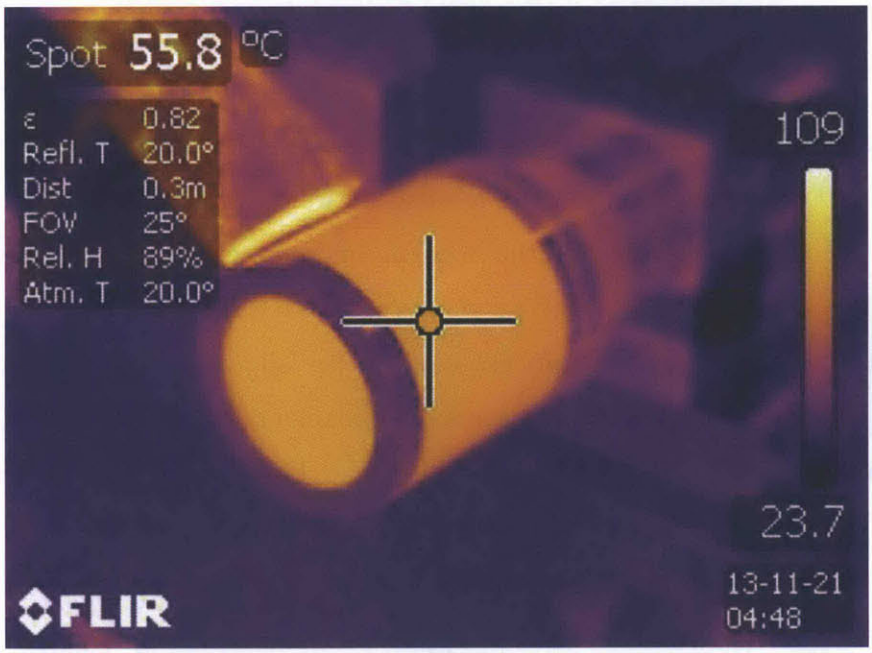


(b)

**Figure 6.9: The centrifuge temperature is monitored with an IR-sensor. It is sensitive to the emissivity of a material. Since the emissivity of bare aluminum is insufficient, the drum can either be anodized or coated black (a). The emissivity of the coated region is much higher as seen on the thermal image (b). The photoresist inside the drum also has a high emissivity.**

## 6.4 Proposed Machine Layout

From these guidelines, a second revision of the machine can be derived, with modifications for the exposure, motion and thermal system.

### 6.4.1 Laser and Optics

A more powerful laser can speed up the patterning process. A fast rise time and high bandwidth will reduce the additional taper that is created when the pattern is written while the laser moves along the substrate at a high speed.

As shown in the preceding sections, the beam distribution, subject to the focal position of the beam, has a great impact on the created feature cross-section. Therefore, it is necessary that the focal point of the beam be at a defined position relative to the photoresist film. Furthermore, not only can variation be prevented by confining the focal position, but active control of the focal region can be leveraged to create features geometries of desired dimensions optimized for the subsequent use of the tool in micropatterning applications on various substrates.

To avoid the necessity of in-process control, the alignment between stage trajectory and centrifuge axis must be ensured by means of fundamental machine design. In the current design, alignment is performed when mounting the kinematic coupling that allows for disassembly of the centrifuge from the machine frame. To permit fine adjustment of the components, a manual positioner, such as a set micrometer, a goniometer or an optics-grade tilt platform, or a combination of such manual positioners, can be integrated into the centrifuge mount. Alignment can be improved with a simple, detachable focusing system, comprising a beam splitter, a plano-convex lens, a CCD and a tubing or cage system to mount these components. Such a system is drafted in Figure 6.10

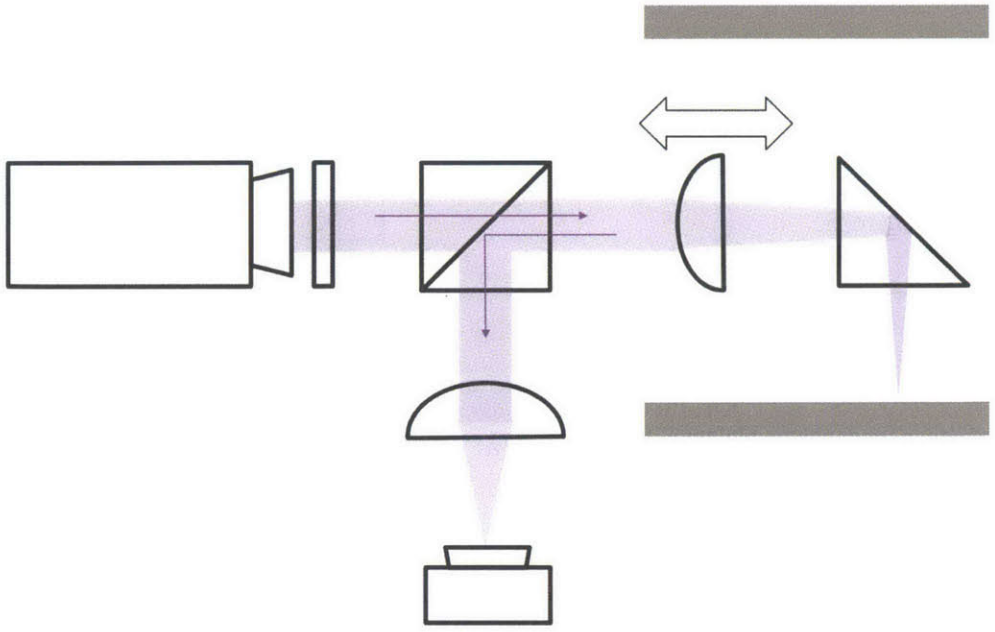

**Figure 6.10: Possible realization of a simple focus system. The beam-splitter and CCD can be mounted on a separate device to make a detachable focusing system. Alternatively, the system can be integrated into a closed-loop control system.**

If implemented into the exposure process, an autofocus system can compensate for topological variation and allow for a high numerical aperture, which will focus the beam to a smaller spot with a lower depth of focus. For drum diameters as small as the existing model, there is little space for optical components near the point of focus. Also, optical components could weigh the cantilevered optics assembly down, threatening the precision of the machine, especially as possible vibrations reduce the obtainable speed of the control system.

Instead, the beam could be split close to the centrifuge to reduce overlap on the optical path and guided to a sensor, which is positioned outside the centrifuge. For large widths, resulting in a long cantilevered optics system, the reflected beam and sensor could be attached and guided in parallel to the active beam.

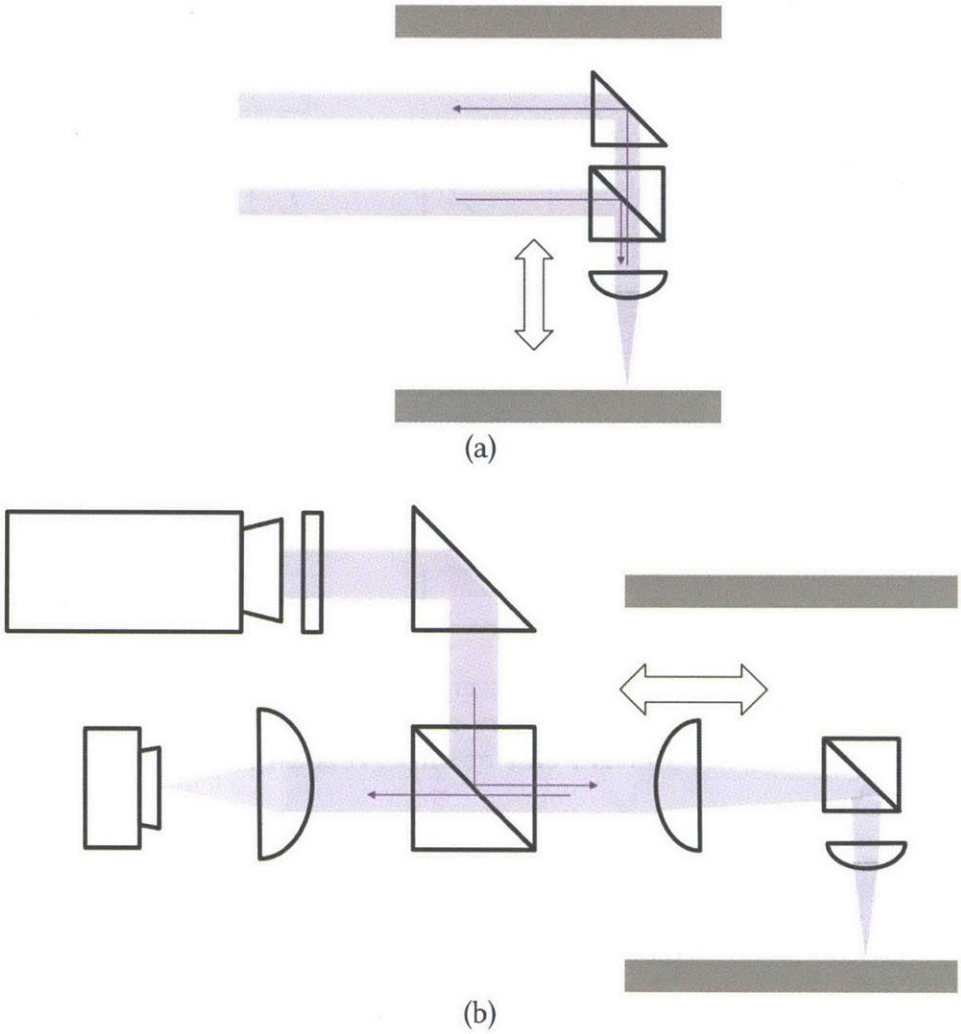


**Figure 6.11: Possible next steps for the focusing system. (a) Parallel beams in tube (b) Adjustment via second lens.**

### 6.4.2 Scanning Motion System

The accuracy of the scanning system is critical for the lateral resolution and repeatability of the pattern inscribed into the photoresist. High-precision actuation allows for the creation arbitrary patterns (rasterizing). As shown in Chapter 4, the cross-sectional geometry depends on the exposure dose, so controlling the writing speed is critical for controlling the overall feature dimension.

Good precision can be achieved with piezoelectric actuation. Such systems see wide application in lithography systems [103], [100], [104]. Owing to their short range, the most

common application of piezoelectric actuators is in wafer positioning [100]. For large range applications in lithography, they can be combined with linear magnetic actuation [105]. Magnetic linear stages have been shown to achieve positioning accuracies on the order of nanometers [106], [107]. Not limited in range such as piezoelectric actuators, magnetic actuation is eminently suitable for a large-scale implementation of the discussed technology.

To optimize the positioning accuracy of the system, a simple revision could consist in replacing the linear motion stage with an air-bearing supported linear magnetic actuator, supporting the centrifuge in air bearings, and equipping the brushed DC motor that drives the centrifuge with a more precise optical encoder.

To enable the scale-up of the system beyond 6 inch tool widths, the cantilevered design could be exchanged for a gantry design where the drum solely supported by a set of enclosing air bearings. The centrifuge could be driven through an exterior coupling. This way, two different drives can be used to satisfy both the need for high speed and precise positioning. In this design, the importance of the SU-8 planarizing layer is especially obvious, since an eccentricity in the drum cylinder can not be compensated by manual adjustments, such as inserting shim.

As for enhancing the precision of the lateral optics positioning stage, a separate compensation element could allow for a large-range, medium-resolution linear actuation mechanism that can span a range multiple orders of magnitude larger than the desired precision of the system.

### 6.4.3 Thermal Control

Thus far, the temperature of the centrifuge is detected on its exterior surface using an infrared (IR) sensor, and manipulated with a high-power heat gun and a cooling fan. Combined with a drum wall thickness in excess of 5 mm, a potential for creating a more dynamic thermal system can easily be seen.

Various methods come to mind in how thermal energy could be introduced into the drum. One example is a hinged encapsulation. Since the drum is moving during the process, radiation is an efficient form of introducing heat.

It is also important to note that such a heating system must provide for sufficiently rapid discharge of energy to provide for a low throughput time in the process, thus incorporating heating elements into the drum is not optimal.

For example, imagine a hinged shell mechanism, encapsulating the drum and irradiating the exterior of the drum. Alternatively, such a module may be introduced inside the drum and irradiating the material directly. However, as discussed in 6.3, any overshoot in temperature must be avoided. Thus, it is advised to measure the temperature at a point that is not separated from where the heat is introduced into the system.

## 6.5 Conclusion

The critical parameters in the process of fabricating tools for soft lithography were identified and related to machine components. Suggestions were given for future machine design iterations. Machine components were designed for a scaled up revision of the apparatus, which may provide a key to continuous roll-based microcontact printing.

# Chapter 7

# Conclusions and Future Work

A new technique was examined to produce seamless cylindrical tools for soft lithography using laser-based maskless lithography for micro-patterning. The development of a fluorescent contact imaging method for the print region was enabled by the creation of a process for the fabrication of layered, fluorescent composite PDMS stamps. A machine design was suggested for a scalable implementation of the examined technique.

Using two different thick-film positive photoresists, SPR 220 and AZ 9260, this work investigated the resulting feature shape fidelity, repeatability and sensitivity to parametric changes at close to threshold (resolution limit) conditions. It examined the process' capabilities to create structures optimized for the subsequent microcontact printing process in both mechanical resistance and ink control, for a low-cost machine design. Structural properties included high aspect ratios, flat-top topography and small sidewall angles. Ideal geometries for a pattern thickness of 15 μm were achieved with AZ 9260, also offering wide stable process window for this operating point. A simulation created on the basis of analytical data was compared with the experimental results, verifying the suitability of the novel setup for photolithographic patterning methods.

A fluorescent contact imaging technique was presented on the basis of fluorescent composite PDMS image carriers. A process was developed to fabricate dual-layer stamps that are independent of particle eruption using the centrifugal tool fabrication technique. It was confirmed that precise thermal control is important to realize the latter. Also, the thickness of the layers was reduced by adding Toluene to PDMS to reduce its viscosity.

## 7.1 Contribution

This work performed extensive development on a laser-lithographic process capable of fabricating seamless, cylindrical tools for microcontact patterning. The technology was contrasted to existing implementations and continuous, scalable tools fill a need in a rapidly growing market. In providing a technology that is not constrained in size or cost by silicon wafers, yet achieves a resolution on the order of single micrometers, the technology brings large-area micropatterning within reach.

Moreover, the process development presented herein contributes towards the process robustness and thus precision of such a production process. The laser-lithographic system, which substantially determines the feature geometry of the produced stamps and thus the inking an elasticity behavior of the consequent microcontact printing process, was investigated. A model was created to simulate this process and it could be noted that characteristics in sidewall geometry could be approximated with this model. With such, the foundation was laid for controlling the feature formation process and giving microcontact printing the ability to tune feature geometries and tailor inking and elastic tool behavior for an optimum patterning result on various surfaces. An enhanced consistency in the feature geometry, enabled by more accurate control over the process, provides the microcontact printing process with additional robustness.

Finally, optically functional tools were created to enable novel metrology in the microcontact patterning process. New implementations of composite PDMS stamps were realized. Providing a passive illumination system through the tool, the process development performed as part of this work not only minimized disturbance during the microcontact printing process but plays a role in its active control system.

The significance of this work is illustrated in Figure 7.1.

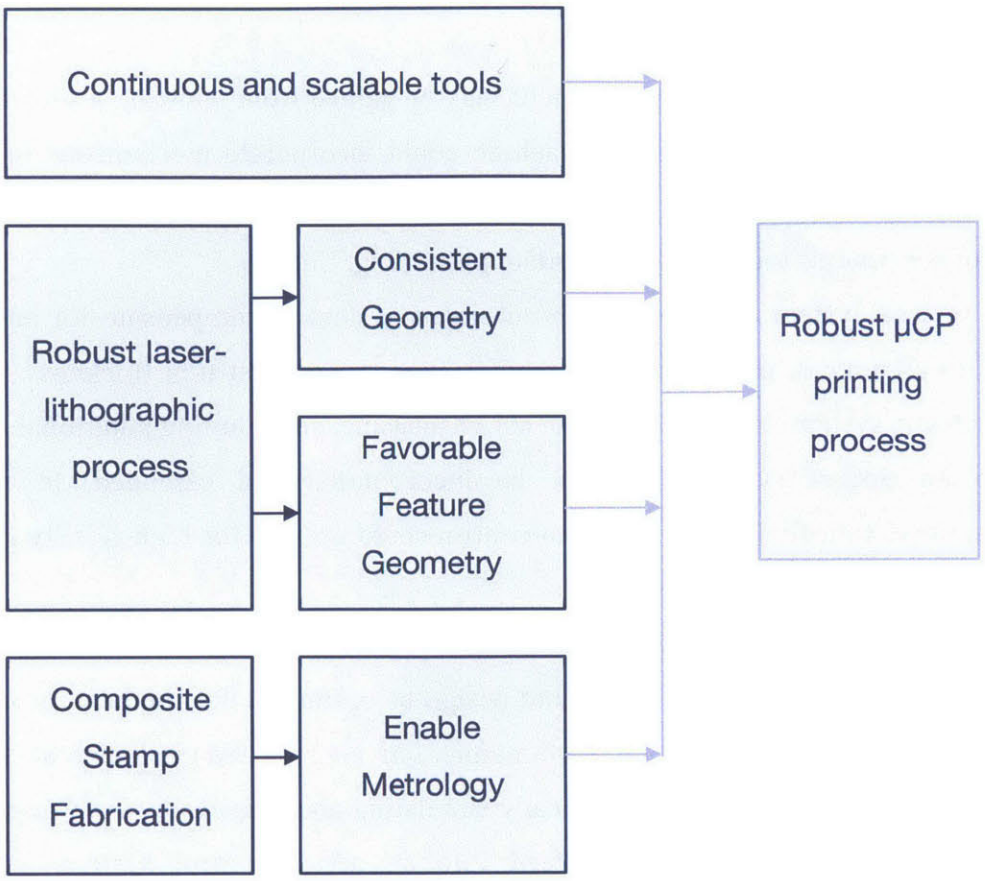


**Figure 7.1: Contributions of this work. By providing scalable tools, this work allows microcontact printing to exceed wafer-induced limitation. Through a robust and predictable laser-lithographic process, consistent and optimized feature geometries can be created. With functional stamps, the tool plays an active role in controlling the microcontact patterning process.**

## 7.2 Future Work

The investigations presented and the conclusions drawn from the results allow for specific steps forward in further developing this process and equipment. The following highlights implications for machine design and stamp materials.

### 7.2.1 Machine Scale-Up

Through the preceding chapter, benefit may be gained from realizing a second revision of the apparatus. This next generation machine could incorporate mechanisms to meet the requirements derived earlier and provide for a more robust, controlled and automated fabrication of continuous tools for microcontact patterning.

The revised system may include an autofocus system to compensate for any possible deficiencies in alignment, parallelism and regular changes in resist film thickness. Moreover, such an autofocus system may automate the act of focusing, contributing additional degrees of freedom to an optical system that can be incorporated and extended. In rasterizing applications, novel thin-film monitoring and control could provide for high-fidelity geometries even with varying substrate conditions.

Furthermore, alterations can be made to improve the thermal control system of the machine. Not only can the drum material and design be optimized but the heating system can be fundamentally modified towards a more dynamic, actively actuated implementation.

The knowledge gained from analytically simulating and empirically verifying the laser-lithographically created feature shapes feed into an active control system, which may potentially close the loop around generating features of a pre-determined shape. Through an interference-based imaging system, the effective depth of the exposed material could be monitored to control the generation of the features with a variable temporal resolution as the exposure progresses.

### 7.2.2 Exploit Stamp Material

PDMS has been very popular in microcontact printing. It has three unique advantages: (1) Its large ratio of elasticity to surface energy enable it to obtain conformal contact even with non-planar substrates. (2) PDMS is transparent to a wide range of wavelengths. (3) It is relatively inexpensive (one stamp cast in the apparatus used for the experiments in Chapter 4 incurred a cost of material on the order of $1). The high elasticity and low surface energy of PDMS however result in a trade-off: at high aspect ratios, features tend to stick to each other, and especially for small feature sizes < 100 nm, stiffer materials are required [44]. Partly glass-filled 'hard-PDMS' is an alternative, but problems arise in separating the stamp from the mold

without breaking it, and in achieving conformal contact during the microcontact printing process. Further, efforts were undertaken in plate-to-plate microcontact printing to produce composite stamps with a stiff patterned layer and an elastic PDMS backing layer [108]. Rigid stamp materials that were previously implemented include PMMA, PMMS, PS, PFPE and epoxy resin. Furthermore, polyolefins and hydrogels found application in microcontact printing, in particular in biomedical applications where hydrophilicity is paramount. To solve the same problem, PDMS stamps with porous surfaces, fabricated by a phase separation process, were shown to provide a reservoir for proteins and reduce the re-inking required to print multiple times in a row.

Poly-urethane has also been proven as a stamp material in microcontact printing [109]. A group at UMass Lowell used injection molding to produce urethane stamps on a silicon micromold. Although defects are visible, the resolution approaches 1 μm. Urethane can be considered as an alternative material for use in continuous stamps fabricated in the centrifugal lithography apparatus which is investigated in this work. Depending on its formulation, its Young's modulus amounts to 2 – 10 MPa, compared to 2.4 MPa for PDMS. A problem in its application with microcontact printing may arise from its degradation under UV light.

To reduce the risk of distortion as the stamp dislocates on the printhead roll, a thin layer of a stiffer material may be added to the backside of the stamp as it is fabricated in the centrifugal process. Such a layer may be bendable to ensure ease of handling, namely to remove it from the master after production, but stiff along its plane, comparable to a thin sheet or film of PET.

### 7.2.3 Open for Scope of Applications

The presented technique was proven to be suitable for the creation of arbitrary patterns. Geometric characteristics, such as the sidewall angle or edge radius, was modulated and shown to represent a model, which can be simulated prior to exposure. This opens applications for the technique in other fields of soft lithography, such as nanoimprint lithography and other hybrid micro-patterning processes.

If scaled up in speed and substrate size, soft lithography can revolutionize a number of applications, including water purification, desalination, surface patterning of moving vehicles for

drag reduction, functional textiles, organic photovoltaic, and many other areas in sustainable generation of energy.

# References


[1] A. Kumar and G. Whitesides, "Features of Gold Having Micrometer to Centimeter Dimensions Can Be Formed Through a Combination of Stamping with an Elastomeric Stamp and an Alkanethiol Ink Followed by Chemical Etching," *Appl. Phys. Lett.*, vol. 63, no. 14, pp. 2002–2004, Oct. 1993.

[2] A. Kumar, H. A. Biebuyck, and G. M. Whitesides, "Patterning Self-Assembled Monolayers: Applications in Materials Science," *Langmuir*, vol. 10, no. 5, pp. 1498–1511, May 1994.

[3] H. A. Biebuyck, N. B. Larsen, E. Delamarche, and B. Michel, "Lithography beyond light: Microcontact printing with monolayer resists," *IBM J. Res. Dev.*, vol. 41, no. 1.2, pp. 159–170, Jan. 1997.

[4] A. Perl, D. N. Reinhoudt, and J. Huskens, "Microcontact Printing: Limitations and Achievements," *Adv. Mater.*, vol. 21, no. 22, pp. 2257–2268, 2009.

[5] A. P. Quist, E. Pavlovic, and S. Oscarsson, "Recent advances in microcontact printing," *Anal. Bioanal. Chem.*, vol. 381, no. 3, pp. 591–600, Feb. 2005.

[6] C. D. Bain, E. B. Troughton, Y. T. Tao, J. Evall, G. M. Whitesides, and R. G. Nuzzo, "Formation of monolayer films by the spontaneous assembly of organic thiols from solution onto gold," *J. Am. Chem. Soc.*, vol. 111, no. 1, pp. 321–335, Jan. 1989.

[7] J. A. Helmuth, H. Schmid, R. Stutz, A. Stemmer, and H. Wolf, "High-Speed Microcontact Printing," *J. Am. Chem. Soc.*, vol. 128, no. 29, pp. 9296–9297, Jul. 2006.

[8] T. E. Balmer, H. Schmid, R. Stutz, E. Delamarche, B. Michel, N. D. Spencer, and H. Wolf, "Diffusion of Alkanethiols in PDMS and Its Implications on Microcontact Printing (μCP)," *Langmuir*, vol. 21, no. 2, pp. 622–632, Jan. 2005.

[9] M. Geissler, H. Wolf, R. Stutz, E. Delamarche, U.-W. Grummt, B. Michel, and A. Bietsch, "Fabrication of Metal Nanowires Using Microcontact Printing," *Langmuir*, vol. 19, no. 15, pp. 6301–6311, Jul. 2003.

[10] A. G. Lopez and H. G. Craighead, "Subwavelength Surface-Relief Gratings Fabricated by Microcontact Printing of Self-Assembled Monolayers," *Appl. Opt.*, vol. 40, no. 13, pp. 2068–2075, May 2001.

[11] E. Delamarche, J. Vichiconti, S. A. Hall, M. Geissler, W. Graham, B. Michel, and R. Nunes, "Electroless Deposition of Cu on Glass and Patterning with Microcontact Printing," *Langmuir*, vol. 19, no. 17, pp. 6567–6569, Aug. 2003.

[12] N. L. Jeon, R. G. Nuzzo, Y. Xia, M. Mrksich, and G. M. Whitesides, "Patterned self-assembled monolayers formed by microcontact printing direct selective metalization by chemical vapor deposition on planar and nonplanar substrates," *Langmuir*, vol. 11, no. 8, pp. 3024–3026, Aug. 1995.

[13] Tae Hyun Park, Young Min Kim, Young Wook Park, Jin Hwan Choi, Jin-Wook Jeong, Kyung Cheol Choi, and Byeong-Kwon Ju, "Self-assembled microarray of organic light-emitting diodes using a self-assembled monolayer by microcontact printing," *Appl. Phys. Lett.*, vol. 95, no. 11, p. 113310, Sep. 2009.

[14] L. B. Goetting, T. Deng, and G. M. Whitesides, "Microcontact Printing of Alkanephosphonic Acids on Aluminum: Pattern Transfer by Wet Chemical Etching," *Langmuir*, vol. 15, no. 4, pp. 1182–1191, Feb. 1999.

[15] A. G. Koutsioubas, N. Spiliopoulos, D. L. Anastassopoulos, A. A. Vradis, and G. D. Priftis, "Formation of alkane-phosphonic acid self-assembled monolayers on alumina: an in situ SPR study," *Surf. Interface Anal.*, vol. 41, no. 11, pp. 897–903, Nov. 2009.

[16] J. C. Love, L. A. Estroff, J. K. Kriebel, R. G. Nuzzo, and G. M. Whitesides, "Self-Assembled Monolayers of Thiolates on Metals as a Form of Nanotechnology," *Chem. Rev.*, vol. 105, no. 4, pp. 1103–1170, Apr. 2005.

[17] T. Kaufmann and B. J. Ravoo, "Stamps, inks and substrates: polymers in microcontact printing," *Polym. Chem.*, vol. 1, no. 4, pp. 371–387, May 2010.

[18] M. Hale, *Manufacturing conductive patterns on polymeric substrates: development of a microcontact printing process / by Melinda Hale.* c2013., 2013.

[19] J. E. Petrzelka, "Contact region fidelity, sensitivity, and control in roll-based soft lithography," Thesis, Massachusetts Institute of Technology, 2012.

[20] C. Y. Hui, A. Jagota, Y. Y. Lin, and E. J. Kramer, "Constraints on Microcontact Printing Imposed by Stamp Deformation," *Langmuir*, vol. 18, no. 4, pp. 1394–1407, Feb. 2002.

[21] J. N. Lee, C. Park, and G. M. Whitesides, "Solvent Compatibility of Poly(dimethylsiloxane)-Based Microfluidic Devices," *Anal. Chem.*, vol. 75, no. 23, pp. 6544–6554, Dec. 2003.

[22] E. Delamarche, H. Schmid, B. Michel, and H. Biebuyck, "Stability of molded polydimethylsiloxane microstructures," *Adv. Mater.*, vol. 9, no. 9, pp. 741–746, Jan. 1997.

[23] P. Roca-Cusachs, F. Rico, E. Martínez, J. Toset, R. Farré, and D. Navajas, "Stability of Microfabricated High Aspect Ratio Structures in Poly(dimethylsiloxane)," *Langmuir*, vol. 21, no. 12, pp. 5542–5548, Jun. 2005.

[24] K. G. Sharp, G. S. Blackman, N. J. Glassmaker, A. Jagota, and C.-Y. Hui, "Effect of Stamp Deformation on the Quality of Microcontact Printing: Theory and Experiment," *Langmuir*, vol. 20, no. 15, pp. 6430–6438, Jul. 2004.

[25] H. Schmid and B. Michel, "Siloxane Polymers for High-Resolution, High-Accuracy Soft Lithography," *Macromolecules*, vol. 33, no. 8, pp. 3042–3049, Apr. 2000.

[26] K. M. Choi and J. A. Rogers, "A Photocurable Poly(dimethylsiloxane) Chemistry Designed for Soft Lithographic Molding and Printing in the Nanometer Regime," *J. Am. Chem. Soc.*, vol. 125, no. 14, pp. 4060–4061, Apr. 2003.

[27] D. Trimbach, K. Feldman, N. D. Spencer, D. J. Broer, and C. W. M. Bastiaansen, "Block Copolymer Thermoplastic Elastomers for Microcontact Printing," *Langmuir*, vol. 19, no. 26, pp. 10957–10961, Dec. 2003.

[28] Y. Xia, D. Qin, and G. M. Whitesides, "Microcontact printing with a cylindrical rolling stamp: A practical step toward automatic manufacturing of patterns with submicrometer-sized features," *Adv. Mater.*, vol. 8, no. 12, pp. 1015–1017, 1996.

[29] J. A. Rogers, Z. Bao, A. Makhija, and P. Braun, "Printing Process Suitable for Reel-to-Reel Production of High-Performance Organic Transistors and Circuits," *Adv. Mater.*, vol. 11, no. 9, pp. 741–745, Jun. 1999.

[30] Z. Bao, A. Makhjita, and J. A. Rogers, "High-resolution method for patterning a substrate with micro-printing," US6736985 B1, 18-May-2004.

[31] H. H. Lee, E. Menard, N. G. Tassi, J. A. Rogers, and G. B. Blanchet, "Large Area Microcontact Printing Presses for Plastic Electronics," *MRS Online Proc. Libr.*, vol. 846, p. null–null, 2004.

[32] A. Stagnaro, *Design and development of a roll-to-roll machine for continuous high-speed microcontact printing / by Adam Stagnaro.* c2008., 2008.

[33] C. A. Datar, *Design and development of high precision elastomeric-stamp wrapping system for roll-to-roll multi-layer microcontact printing / by Charudatta Achyut Datar.* c2009., 2009.

[34] A. M. Kendale, *Automation of soft lithographic microcontact printing / by Amar Maruti Kendale.* c2002., 2002.

[35] T. Burgin, V.-E. Choong, and G. Maracas, "Large Area Submicrometer Contact Printing Using a Contact Aligner," *Langmuir*, vol. 16, no. 12, pp. 5371–5375, Jun. 2000.

[36] A. M. Kendale and D. L. Trumper, "Microcontact printing," US7665983 B2, 23-Feb-2010.

[37] A. M. Kendale and D. L. Trumper, "Microcontact printing," US7117790 B2, 10-Oct-2006.

[38] P. Baldesi, *Design and development of high precision five-axis positioning system for roll-to-roll multi-layer microcontact printing / by Paolo Baldesi.* c2009., 2009.

[39] D. J. C. Herr, *Alternative lithographic technologies II [electronic resource]: 23-25 February 2010, San Jose, California, United States / Daniel J.C. Herr, editor; sponsored and published by SPIE; cooperating organization, SEMATECH Inc.* Bellingham, Wash.: SPIE, c2010., 2010.

[40] E. Menard and J. A. Rogers, "Stamping Techniques for Micro-and Nanofabrication," in *Springer Handbook of Nanotechnology*, Springer, 2010, pp. 313–332.

[41] J. E. Petrzelka and D. E. Hardt, "Laser direct write system for fabricating seamless roll-to-roll lithography tools," 2013, p. 861205.

[42] L. Du, Q. Wang, and X. Zhang, "Reduction of internal stress in SU-8 photoresist layer by ultrasonic treatment," *Sci. China Technol. Sci.*, vol. 53, no. 11, pp. 3006–3013, 2010.

[43] P. Abgrall and N.-T. Nguyen, *Nanofluidics.* Artech House, 2009.

[44] D. j. Lipomi, R. v. Martinez, L. Cademartiri, and G. m. Whitesides, "7.11: Soft Lithographic Approaches to Nanofabrication," *Polym. Sci. Compr. Ref. 10 Vol. Set*, pp. 211–231, Jan. 2012.

[45] T. Claypole, "Improving the Accuracy of Flexo Printing for Flexible Electronics," in *FlexTech Alliance 2013 Flexible & Printed Electronics Conference & Exhibition Proceedings*, Phoenix, Arizona.

[46] K. Charlesworth, "Flexo turns to flat-top dots," *PrintWeek*, pp. 29–30, Feb. 2008.

[47] J. H. Bruning, "Optical lithography: 40 years and holding," 2007, vol. 6520, pp. 652004–652004–13.

[48] F. Su, "Microlithography: from contact printing to projection systems," *SPIE Newsroom*, 1997.

[49] L. Chi, *Nanotechnology: Volume 8: Nanostructured Surfaces*. John Wiley & Sons, 2010.

[50] L. M. Minsk, "Light sensitive unsaturated esters of polyvinyl alcohol," US2725372 A, 29-Nov-1955.

[51] D. M. P. Schmidt and D. O. Sues, "Aus Schichttraeger und lichtempfindlicher, wasserloeslicher oder wasserquellbarer Kolloidschicht bestehendes Material fuer die Herstellung von Gerbbildern," DE1003576 B, 28-Feb-1957.

[52] M. Cipolloni, P. L. Gentili, F. Ortica, R. S. Becker, and G. Favaro, "Effects of solvent, excitation wavelength, and concentration on the photobehavior of some diazonaphthoquinones," *Ark. Online J. Org. Chem.*, pp. 205–220, Jan. 2011.

[53] B. J. Lin, *Optical Lithography*. 1000 20th Street, Bellingham, WA 98227-0010 USA: SPIE, 2010.

[54] "A History Of The Laser: A Trip Through The Light Fantastic." [Online]. Available: http://www.photonics.com/Article.aspx?AID=42279. [Accessed: 24-Mar-2014].

[55] D. Basting and G. Marowsky, *Excimer laser technology / edited by D. Basting and G. Marowsky*. Berlin; New York: Springer/Praxis, c2005., 2005.

[56] K. Jain and C. G. Willson, "High resolution optical lithography method and apparatus having excimer laser light source and stimulated Raman shifting," US4458994 A, 10-Jul-1984.

[57] M. Endo and R. F. Walter, *Gas Lasers*. CRC Press, 2006.

[58] J. Hecht, "History of Gas Lasers, Part 1 - Continuous Wave Gas Lasers," *Opt. Photonics News*, vol. 21, no. 1, p. 16, Jan. 2010.

[59] O. Kumagai, M. Ikeda, and M. Yamamoto, "Application of Laser Diodes to Optical Disk Systems: The History of Laser Diode Development and Mass Production in Three Generations of Optical Disk Systems," *Proc. IEEE*, vol. 101, no. 10, pp. 2243–2254, Oct. 2013.

[60] A. Schilling, H. P. Herzig, L. Stauffer, U. Vokinger, and M. Rossi, "Efficient Beam Shaping of Linear, High-Power Diode Lasers by Use of Micro-Optics," *Appl. Opt.*, vol. 40, no. 32, pp. 5852–5859, Nov. 2001.

[61] "Passively Q-Switched Nd:YAG Lasers and Their Use in UV Light Generation." [Online]. Available: http://lib.tkk.fi/Diss/2009/isbn9789522480743/. [Accessed: 27-Mar-2014].

[62] "Heidelberg Instruments Mikrotechnik GmbH • Technology • Laser Lithography." [Online]. Available: http://www.himt.de/en/technology/laserlithography.php. [Accessed: 24-Mar-2014].

[63] "Thick Resist Processing - MicroChemicals GmbH." 07-Nov-2013.

[64] C. A. Mack, *Fundamental principles of optical lithography: the science of microfabrication / Chris Mack*. Chichester, West Sussex, England; Hoboken, NJ, USA: Wiley, c2007., 2007.

[65] C.-H. Liu, P. C. W. . Ng, Y.-T. Shen, S.-W. Chien, and K.-Y. Tsai, "Impacts of point spread function accuracy on patterning prediction and proximity effect correction in low-voltage electron-beam-direct-write lithography," *J. Vac. Sci. Technol. Part B-Nanotechnol. Microelectron.*, vol. 31, no. 2, pp. 021605–021605–18, Mar. 2013.

[66] H. J. Levinson, *Principles of lithography / Harry J. Levinson.* Bellingham, WA: SPIE Press, c2005., 2005.

[67] F. M. Dickey, S. C. Holswade, and D. L. Shealy, *Laser Beam Shaping Applications.* CRC Press, 2005.

[68] M. Rothschild, T. m. Bloomstein, T. h. Fedynyshyn, R. r. Kunz, V. Liberman, M. Switkes, N. N. Efremow Jr., S. t. Palmacci, J. h. c. Sedlacek, D. e. Hardy, and A. Grenville, "Recent trends in optical lithography," *Lincoln Laboratory Journal*, vol. 14, no. 2, pp. 221–236, 01-Jan-2003.

[69] Z. Gan, Y. Cao, R. A. Evans, and M. Gu, "Three-dimensional deep sub-diffraction optical beam lithography with 9 nm feature size," *Nat. Commun.*, vol. 4, Jun. 2013.

[70] "Anti reflective Coatings Improve Photoresist Profile | AZ Electronic Materials." [Online]. Available: http://www.azem.com/en/About-AZ/Glossary/Anti%20reflective%20coating.aspx. [Accessed: 15-May-2014].

[71] S. Franssila, *Introduction to microfabrication / Sami Franssila.* Chichester, U.K.; Hoboken, N.J.: John Wiley & Sons, 2010., 2010.

[72] "Photoresist Developers in Litho technology | AZ Electronic Materials." [Online]. Available: http://www.azem.com/en/Products/Litho-technology/Photoresist%20Developers.aspx. [Accessed: 23-Apr-2014].

[73] "Semiconductor Lithography (Photolithograph) - The Basic Process - Chris Mack." [Online]. Available: http://www.lithoguru.com/scientist/lithobasics.html. [Accessed: 23-Apr-2014].

[74] M. Pitchumani, "Additive lithography fabrication and integration of micro optics," University of Central Florida Orlando, Florida USA, 2006.

[75] M. C. Hakey, S. J. Holmes, D. V. Horak, A. D. Katnani, N. M. Patel, and P. A. Rabidoux, "Preparing a film forming photoresist composition used in manufacture of integrated circuit chips," US6114082 A, 05-Sep-2000.

[76] M. J. Madou, *Manufacturing Techniques for Microfabrication and Nanotechnology.* CRC Press, 2011.

[77] W.-L. K. Jen, "Materials and processes for advanced lithography applications," 2011.

[78] F. H. Dill, W. P. Hornberger, P. S. Hauge, and J. M. Shaw, "Characterization of positive photoresist," *IEEE Trans. Electron Devices*, vol. 22, no. 7, pp. 445–452, Jul. 1975.

[79] D. F. Swinehart, "The beer-lambert law," *J. Chem. Educ.*, vol. 39, no. 7, p. 333, 1962.

[80] S. Nonogaki, U. Takumi, and T. Ito, *Microlithography Fundamentals in Semiconductor Devices and Fabrication Technology.* CRC Press, 1998.

[81] C. A. Mack, "Modeling solvent effects in optical lithography," University of Texas at Austin, 1998.

[82] H. Sun, *Laser diode beam basics, manipulations and characterizations [electronic resource] / Haiyin Sun.* Dordrecht; New York: Springer, c2012., 2012.

[83] "Encyclopedia of Laser Physics and Technology - M2 factor, laser beam, quality factor, beam divergence, caustic, ISO Standard 11146." [Online]. Available: http://www.rp-photonics.com/m2_factor.html. [Accessed: 29-Mar-2014].

[84] "SPR220 Series Resist Datasheet." Rohm and Haas Electronic Materials.

[85] "AZ 9200 Photoresist Product Data Sheet." Clariant GmbH.

[86] P. Komarinski, *Automated Fingerprint Identification Systems (AFIS).* Academic Press, 2005.

[87] O. K. Ersoy, *Diffraction, Fourier Optics, and Imaging.* Hoboken, N.J.: Wiley-Interscience, 2007.

[88] "Frustrated Total Internal Reflection | Seth Sandler." [Online]. Available: http://sethsandler.com/multitouch/ftir/. [Accessed: 17-May-2014].

[89] "Fluorescein Fundamentals - Ophthalmic Photographers' Society." [Online]. Available: http://www.opsweb.org/?page=FA. [Accessed: 14-Apr-2014].

[90] A. Diaspro, *Optical fluorescence microscopy [electronic resource]: from the spectral to the nano dimension / Alberto Diaspro, editor.* Heidelberg; New York: Springer-Verlag Berlin Heidelberg, c2011., 2011.

[91] B. Valeur and M. N. Berberan-Santos, *Molecular fluorescence: principles and applications.* Weinheim [Germany]: Wiley-VCH; [Chichester, England: Wiley, distributor], c2012., 2012.

[92] H. Sundani, V. Devabhaktuni, C. Melkonian, and M. Alam, "Design and fabrication of a micromachined free-floating membrane on a flexible substrate," *J. MicroNanolithography MEMS MOEMS*, vol. 12, no. 1, pp. 013002–013002, 2013.

[93] J. J. H. Brouwers, "Phase separation in centrifugal fields with emphasis on the rotational particle separator," *Exp. Therm. Fluid Sci.*, vol. 26, no. 2, pp. 325–334, 2002.

[94] J.-H. Lee, H.-S. Lee, B.-K. Lee, W.-S. Choi, H.-Y. Choi, and J.-B. Yoon, "Simple liquid crystal display backlight unit comprising only a single-sheet micropatterned polydimethylsiloxane (PDMS) light-guide plate," *Opt. Lett.*, vol. 32, no. 18, pp. 2665–2667, Sep. 2007.

[95] J. N. Lee, C. Park, and G. M. Whitesides, "Solvent Compatibility of Poly(dimethylsiloxane)-Based Microfluidic Devices," *Anal. Chem.*, vol. 75, no. 23, pp. 6544–6554, Dec. 2003.

[96] S. Nill, "Integrated Hardware, Software, and Sensor Design for Control of a Scalable, Continuous Roll-to-Roll Microcontact Printing Process," Master of Science, Massachusetts Institute of Technology, Cambridge, MA, 2014.

[97] A. Libert, "Precision Control of Cylindrical Stamp Contact in a Continuous Roll-to-Roll Microcontact Printing Machine," Master of Science, Massachusetts Institute of Technology, Cambridge, MA, 2014.

[98] J. Zhang, Y. Chen, and M. A. Brook, "Facile Functionalization of PDMS Elastomer Surfaces Using Thiol–Ene Click Chemistry," *Langmuir*, vol. 29, no. 40, pp. 12432–12442, Oct. 2013.

[99] S. Seiffert, J. Dubbert, W. Richtering, and D. A. Weitz, "Reduced UV light scattering in PDMS microfluidic devices," *Lab. Chip*, vol. 11, no. 5, pp. 966–968, Mar. 2011.

[100] H. Becker, R. Caspary, C. Toepfer, M. V. Schickfus, and S. Hunklinger, "Low-cost direct writing lithography system for the sub-micron range," *J. Mod. Opt.*, vol. 44, no. 9, pp. 1715–1723, 1997.

[101] O. D. Crisalle, C. L. Bickerstaff, D. E. Seborg, and D. A. Mellichamp, "Improvements In Photolithography Performance By Controlled Baking," 1988, vol. 0921, pp. 317–325.

[102] "Lithography Trouble Shooter - Questions and Answers Around the Most Common Problems in Micro-Structuring - MicroChemicals GmbH." 2012.

[103] D. L. White and O. R. W. Ii, "Novel alignment system for imprint lithography," *J. Vac. Sci. Technol. B*, vol. 18, no. 6, pp. 3552–3556, Nov. 2000.

[104] S.-H. Chang, C. K. Tseng, and H. C. Chien, "An ultra-precision XY/spl theta//sub Z/ piezo-micropositioner. I. Design and analysis," *IEEE Trans. Ultrason. Ferroelectr. Freq. Control*, vol. 46, no. 4, pp. 897–905, Jul. 1999.

[105] W. Kim and D. L. Trumper, "High-precision magnetic levitation stage for photolithography," *Precis. Eng.*, vol. 22, no. 2, pp. 66–77, 1998.

[106] T.-T. Chung, C.-H. Chu, K.-C. Fan, J.-Y. Yen, and K.-I. Szu, "Development of a nano-positioning planar motion stage," in *2010 2nd International Conference on Mechanical and Electronics Engineering (ICMEE)*, 2010, vol. 1, pp. V1–122–V1–126.

[107] J. Lei, X. Chen, and X. Luo, "Electromagnetic analysis of a novel Lorentz-force-driven planar motor via 3D FEM calculation and experimental verification," in *2011 Second International Conference on Mechanic Automation and Control Engineering (MACE)*, 2011, pp. 1285–1288.

[108] B. Michel, A. Bernard, A. Bietsch, E. Delamarche, M. Geissler, D. Juncker, H. Kind, J.-P. Renault, H. Rothuizen, H. Schmid, P. Schmidt-Winkel, R. Stutz, and H. Wolf, "Printing meets lithography: Soft approaches to high-resolution patterning," *IBM J. Res. Dev.*, vol. 45, no. 5, pp. 697–719, Sep. 2001.

[109] A. Chandekar, M. Alabran, S. K. Sengupta, J. S. Lee, J. L. Mead, C. M. F. Barry, J. E. Whitten, S. Somu, and A. A. Busnaina, "Fabrication of stamps for microcontact printing by injection molding," *Microelectron. Eng.*, vol. 85, no. 1, pp. 187–194, Jan. 2008.

# A

# Experimental Procedures

## A.1 Experimental Protocol (SPR 220)

The general operating procedure for SPR 220 is conducted as follows:

(1) Clean surface using acetone and dry.

(2) Insert solution of photoresist (SPR 220) and solvent (ethyl lactate and anisole, 2:1) and spin at 300 rad/s. Allow one minute for the liquid to spin out evenly.

(3) Still spinning, evaporate solvent and softbake at 115 °C for at least 120 seconds. A ventilating module consisting of a fan and a tube is mounted on the linear stage and moved inside the centrifuge to create a high-velocity air flow surpassing the resist film.

(4) Cool down and allow for at least 60 minutes required for rehydration.

(5) Expose the photoresist selectively using aforementioned laser and optics (see A.2 *Exposure Dose Calculation*).

(6) Post-exposure bake at 115 °C for 120 seconds.

(7) Develop for 120 seconds under a stream of MF24-A developer. Exchange for DI water immediately. Agitate in DI water for 120 seconds. Use compressed air to dry.

(8) Cast PDMS by inserting a volume of 10 mL (degassed). Spin at 300 rev/s for 5 minutes before heating to 65°C for 60 minutes.

## A.2 Exposure Dose Calculation

Planarizing Layer (SU-8)

Thickness given 0.5 mL volume, 9953 $mm^3$ drum surface:

Before solvent evaporation: 50 μm

After solvent evaporation 31.5 μm

Specified nominal energy (for 26 – 40 μm thickness):

150 – 160 $mJ/cm^2$

Relative dose (Aluminum): 1.5 – 2x

→ Required exposure dose at 365 nm:

150 $mJ/cm^2$ * 2 * 99.53 $cm^2$

= 29.86 J

Patterning Layer (SPR 220)

Thickness given 0.1 mL volume, 9953 $mm^3$ drum surface:

Before solvent evaporation: 10 μm

After solvent evaporation 4 μm

Specified nominal energy

(for 3 μm): 320 $mJ/cm^2$

(for 7 μm): 470 $mJ/cm^2$

→ interpolate: 360 $mJ/cm^2$ for 4 μm thickness absorption transmission photoresist

Required writing speed given 80 mW laser power, 12μm focused beam width:

80 mW / (360 $mJ/cm^2$ * 12 * $10^{-4}$ cm)

= 1852 mm/s

Given 52.8 mm drum diameter:

1852 mm/s / (52.8 mm * π) = 11 rev/sec = 670 rpm

## A.3 Photolithography Resources

The propagation of the energy in the material is governed both by the bell-shape of the laser beam, and by the proportional absorption and transmission in the material. The resist's absorbance decreases as the resist is bleached. A typical absorbance spectrum is shown in Figure . The resulting propagation is simulated in Figure A.1.

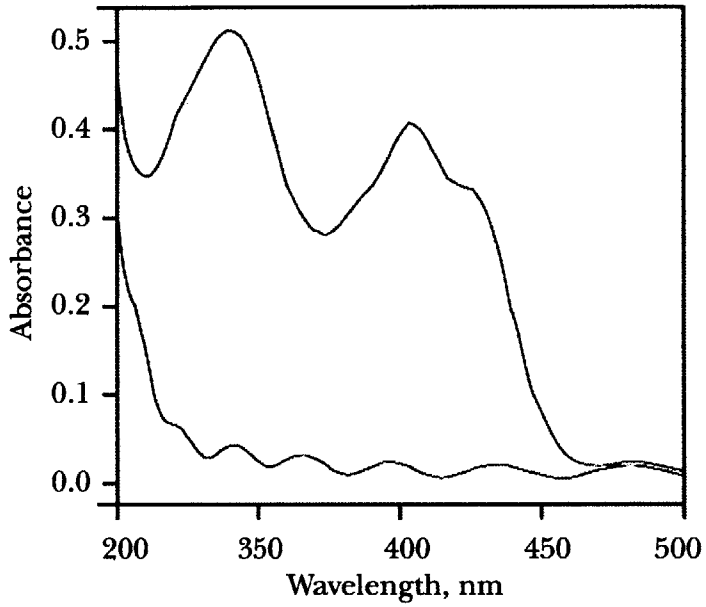


**Figure A.1: Broadband sensitivity of a typical DNQ-based photoresist (SPR 220). The unexposed resist exhibits greater absorbance than the bleached resist [84]**

Appendix

# B

# Experimental Procedures

## B.1 Experimental Protocol: AZ 9260

Positive thickfilm-resist AZ 9260 is to be used in the setup which comprises a centrifugal caster (cylinder with Ø 52.8mm and length 60mm) and a linear stage with a 60mW, 400-700nm laser (to be operated at 405nm) and simple optical tools for focusing and directing the laser beam (NA = 0.08).

AZ series photoresist is a DQN resist dissolved in the flammable organic solvent PGMEA, 1-Methoxy-2-propyl acetate (CAS: 108-65-6); 58 % [iii].

- AZ series resist causes irritation to skin, eyes, nose, and respiratory tract. It is readily absorbed through the skin. Prolonged, repeated contact, inhalation, ingestion, or absorption through the skin, may cause toxic effects to internal organ systems.
- AZ series resists are flammable and should be kept away from ignition sources. Baking spun resist on a hotplate is, however, acceptable.

Nitrile gloves and eye protection required for all procedures.

### Outline

(1) Clean SU-8 surface using Acetone, following air drying and a quick dehydration bake.
(2) Insert blend of AZ 9260 and 5 ml PGMEA.
5 μm: 0.13 ml
10 μm: 0.25 ml
15 μm: 0.38 ml

[iii] AZ Series Photoresist Processing SOP, Tufts University

25 μm: 0.63 ml

(given 58% solvent content and 10 μm initial film thickness per 0.1 ml liquid).

(3) Evaporate solvent at 60°C for at least 30 minutes.

(4) Softbake

5 μm: 110°C for 120 seconds

10 μm: 110°C for 165 seconds

15 μm: 110°C for 200 seconds

25 μm: 110°C for 240 seconds

(5) Cool down slowly.

(6) Expose (sets of lines) of fixed drum speed each. Pitch 100μm, 20 revolutions each speed, at 100% laser power.
Speeds: 0.1 rev/sec, 0.25 rev/sec, 0.5 rev/sec, 0.75 rev/sec, 1 rev/sec, 1.25 rev/sec, 1.5 rev/sec, 1.75 rev/sec, 2 rev/sec, 2.5 rev/sec, 3 rev/sec.

(7) Do NOT post-exposure bake. Record temperature for developing.

(8) Develop with AZ 400K 1:4 developer.

5 μm: 120 seconds

10 μm: 180 seconds

15 μm: 220 seconds

25 μm: 260 seconds

Exchange for DI water immediately when the time limit is reached.

(9) Agitate in DI water for 60 seconds.

(10) Cast PDMS (5ml, degassed, heat to 90° for 60 minutes)